Digitized Theses   Digitized Special Collections

2010

EVALUATING THE MECHANISMS OF UNCONJUGATED BILIRUBIN TOXICITY THROUGH ANALYSIS OF THE DISULFIDE PROTEOME

Abudi Awaysheh
Western University

Follow this and additional works at: https://ir.lib.uwo.ca/digitizedtheses

EVALUATING THE MECHANISMS OF UNCONJUGATED BILIRUBIN TOXICITY THROUGH ANALYSIS OF THE DISULFIDE PROTEOME

(Spine title: Unconjugated Bilirubin Toxicity)

(Thesis format: Monograph)

by

Abudi Awaysheh

Graduate Program in Pathology

A thesis submitted in partial fulfillment
of the requirements for the degree of
Master of Science

The School of Graduate and Postdoctoral Studies
The University of Western Ontario
London, Ontario, Canada

© Abudi Awaysheh 2010

THE UNIVERSITY OF WESTERN ONTARIO
School of Graduate and Postdoctoral Studies

CERTIFICATE OF EXAMINATION

Supervisor

_____
Dr. Jack R. Bend

Supervisory Committee

_____
Dr. Subrata Chakrabarti

_____
Dr. Chandan Chakraborty

Examiners

_____
Dr. Robert C. Cumming

_____
Dr. Zia A. Khan

_____
Dr. Michael Rieder

The thesis by

Abudi Awaysheh

entitled:

**Evaluating the Mechanisms of Unconjugated Bilirubin Toxicity
through Analysis of the Disulfide Proteome**

is accepted in partial fulfillment of the
requirements for the degree of
Master of Science

Date_____

_____
Chair of the Thesis Examination Board

ABSTRACT

Unconjugated bilirubin (UCB), the end product of heme catabolism, is an important physiological antioxidant at nMolar concentrations, but becomes a pro-oxidant at µMolar concentrations by causing the release of reactive oxygen species (ROS) from mitochondria. We employed diagonal redox two-dimensional polyacrylamide gel electrophoresis (R2D-PAGE), to separate and identify specific proteins by mass spectrometry and determined the proteomic signature of the disulfide proteome in different subcellular fractions of Hepa 1c1c7 cells treated with pro-oxidant (50 µM) or antioxidant (70 nM) concentrations of UCB in Hepa 1c1c7 cells. Our results demonstrate that treating cells with pro-oxidant or antioxidant concentrations of UCB had a significant and different change on disulfide bonded proteins in the cytosol, with notable effects on peroxiredins (Prx). Pro-oxidant concentrations of UCB led to the irreversible oxidation of Prx1 with no effect on Prx2, whereas antioxidant concentrations led to an enhanced reduction in Prx2 with no effect on Prx1.

Keywords: Diagonal redox two-dimensional polyacrylamide gel electrophoresis, disulfide proteome, protein disulfide binding, reactive oxygen species, reversible and irreversible oxidation

CO-AUTHORSHIP STATEMENT

All work in this thesis was performed in full by Abudi Awaysheh, with the following exceptions. Figure 4.3 and data were provided by Dr. Garth Oakes, then a PhD student in Pharmacology and Toxicology (University of Western Ontario) under the supervision of Dr. Jack Bend. Data points for the mass spectrum found in Fig. 4.7 were obtained from Kristina Jurcic at the MALDI Mass Spectrometry Facility at the University of Western Ontario, London, Ontario.

DEDICATION

To Dr. Bend

Thank you for all of the opportunities you have given me

AKNOWLEDGEMENTS

TABLE OF CONTENTS

LIST OF TABLES

LIST OF FIGURES

LIST OF APPENDICES

LIST OF ABBREVIATIONS

AD	- Alzheimer's disease
ALS	- amyotrophic lateral sclerosis
APS	- ammonium persulfate
BBB	- blood-brain barrier
BE	- baicalein
B_f	- free or unbound unconjugated bilirubin
BSA	- bovine serum albumin
cm	- centimeter(s)
CO	- carbon monoxide
Cys	- cysteine
DTT	- dithiothreitol
ER	- endoplasmic reticulum
FBS	- fetal bovine serum
G6PD	- glucose-6-phosphate dehydrogenase
GAPDH	- glyceraldehyde 3-phosphate dehydrogenase
Grx	- glutaredoxin
GSH	- glutathione
GSH-Px	- glutathione peroxidase
GSH-Rx	- glutathione reductase
GSSG	- glutathione disulfide
GST	- glutathione S-transferase
h	- hour(s)
H_2O_2	- hydrogen peroxide
Hb	- hemoglobin
HCl	- hydrochloric acid
HD	- Huntington's disease
HEK 293	- human embryonic kidney
Hepa 1c1c7	- murine hepatoma cell line
HO	- heme oxygenase
HO^-	- hydroxyl radical
HSP	- heat shock proteins
IA	- iodoacetamide
$K_{A\text{-}UCB}$	- albumin-UCB binding constant
kDa	- kilodalton
Keap1	- Kelch-like ECH-associated protein 1
KP	- sodium phosphate
mA	- milliamps
MALDI	- matrix assisted laser desorption/ionization
MDR	- multidrug resistance P-glycoproteins
min	- minute(s)
mL	- milliliter(s)
mm	- millimeter(s)
MRP	- multidrug resistance protein
MS	- mass spectrometry

MS PMF	- mass spectrometry peptide mass fingerprinting
NADPH	- nicotinamide adenine dinucleotide phosphate
Nrf2	- nuclear factor 2
O_2^-	- superoxide anion
OATP2	- organic acid transporter 2
$(PSSP)_n$	- oligomeric protein disulfide
P^1SSP^1	- homodimeric protein disulfide
P^1SSP^2	- heterodimeric protein disulfide
PBS	- phosphate-buffered saline
PCS	- protein confidence score
PD	- Parkinson's disease
PDI	- protein disulfide isomerase
Prx	- peroxiredoxin
PS^-	- reactive (oxidized) protein thiol
PSH	- protein cysteine thiol
PSO_2H	- protein sulfinic acid
PSO_3H	- protein sulphonic acid
PSOH	- protein sulfenic acid
PSS	- intramolecular protein disulfide
PSSG	- protein glutathione disulfide
PSSP	- protein disulfide
qRT-PCR	- real-time reverse-transcription polymerase chain reaction
R1D-PAGE	- redox one-dimensional polyacrylamide gel electrophoresis
R2D-PAGE	- redox two-dimensional polyacrylamide gel electrophoresis
RNS	- reactive nitrogen species
roGFP2	- mutated redox green fluorescent protein
ROH	- alcohol formed from the reduction of hydroperoxide
ROOH	- hydroperoxide
ROS	- reactive oxygen species
s	- second(s)
SDS	- sodium dodecyl sulfate
SOD	- superoxide dismutase
Srx	- sulfaredoxin
TBHP	- tert-butyl hydroperoxide
TEMED	- tetramethylethylenediamine
Trx	- thioredoxin
Trx-Rx	- thioredoxin reductase
TSB	- total serum bilirubin
TTR	- transthyretin
UCB	- unconjugated bilirubin
UGT 1A1	- UDP-glucuronosyltransferase 1A1
WT	- wild type

CHAPTER 1: INTRODUCTION

1.1 Bilirubin

1.1.1 Biosynthesis of Bilirubin

Unconjugated bilirubin (UCB) is the end product generated by the oxidation of the iron-containing porphyrin ring of heme in mammals (from heme proteins such as hemoglobin and cytochrome P450). UCB has very limited solubility in aqueous medium (70 nM at physiological pH). UCB is also neurotoxic in some babies that suffer from hyperbilirubinemia (1). Heme oxygenase (HO) which is localized within the endoplasmic reticulum (ER), enzymatically cleaves the tetrapyrrole ring of heme to produce equimolar amounts of three biologically active products: biliverdin, ferrous iron, and carbon monoxide (CO) (2, 3). HO exists as three different isoforms, an inducible form known as HO-1, and two constitutively expressed isoforms, HO-2, and HO-3 (4). HO-1 is rapidly induced by diverse cytotoxic stimuli including UV radiation, hydrogen peroxide (H_2O_2), heavy metal exposure, and nitric oxide (5, 6). HO-1 is most abundant in the spleen and is considered a heat shock protein (HSP 32), whereas the constitutively expressed HO-2 is most concentrated in the brain and testes (7).

Biliverdin exists at extremely low concentrations as it is rapidly reduced to UCB by the high tissue densities of biliverdin reductase (8). UCB is normally predominantly (>99.9%) bound to albumin in the blood serum to become water soluble where it is transported to the liver via circulation for further metabolism (2). The barely water soluble form of UCB is not bound to albumin. It is termed free UCB (B_f) and exists in water solution at concentrations up to 70 nM at physiological pH. B_f is of pathological

significance as it is the only form of UCB that is able to cross the intact blood-brain barrier (BBB), enter and damage the basal nuclei of the brain (9). This rare, though devastating complication may result in UCB-induced irreversible brain damage in neonates (whose BBB has yet to mature), a condition termed kernicterus (10). Albumin-bound UCB is only capable of entering the brain if the BBB is disrupted (1).

Ferrous iron, itself toxic is excreted from cells by an ATP dependent iron transport pump, stored in ferritin, or oxidized by the Fenton Reaction into ferric iron and subsequently stored in ferritin (11-14). CO preferentially binds to hemoglobin forming carboxyhemoglobin, and its presence in large quantities causes death due to carboxyhemoglobinemia or CO poisoning whereas a concentration of less than 2.5% CO is considered safe with little or no observable effects (15). Low concentrations of CO can exert biological functions as diverse as neurotransmission, protection against cell death by an anti-apoptotic mechanism, and protection against oxidative injury (16, 17).

The presence of two double bonds between the pyrrole rings in UCB leads to conformational changes in its structure enabling this compound to exist as different isomers. The predominate form of UCB in neonates is ZZ-bilirubin, whose structure mirrors the closed ring structure of the original heme molecule (2). ZE-bilirubin and EZ-bilirubin which account for ~14% and >1% of UCB respectively, have a more open configuration that exposes more reactive groups and enables albumin to bind to them more readily than ZZ-bilirubin (2). UCB is light sensitive, and exposure to UV light affects the conformational structure of ZZ-bilirubin, converting it into water soluble EZ-cyclobilirubin and EE-cyclobilirubin (18). Phototherapy utilizes this knowledge to effectively lower the concentration of circulating UCB or to prevent it from increasing.

This form of therapy which utilizes light energy to change the shape and structure of UCB, converting it to molecules that can be excreted even when normal conjugation is deficient, is used to effectively treat infants with elevated levels of circulating UCB at or below 220 μM (19).

1.1.2 Pathological Significance of Bilirubin

Hyperbilirubinemia develops when UCB production exceeds the body's capacity to metabolize and excrete it, in clinical terms this is known as UCB encephalopathy (9). Approximately 60% of normal newborns become clinically jaundiced sometime during the first week of life (19). Neonatal hyperbilirubinemia occurs as a result of excessive UCB formation due to an increased breakdown of fetal erythrocytes, ineffective hepatic conjugation because of delayed expression of UDP-glucuronosyltransferase 1A1 (UGT 1A1), the enzyme that normally eliminates UCB by reaction with one or two molecules of glucuronic acid. As a result of this developmental deficiency of UGT 1A1 the neonatal liver cannot clear UCB rapidly enough from the blood and it accumulates (20, 21).

The clinical features of UCB encephalopathy range from deafness and severe cerebral palsy, seizures, or death from kernicterus, to mild retardation and subtle cognitive disturbances (1). In adults, neurotoxic levels of UCB are rarely encountered because UCB does not cross the mature BBB. In adults with severe hyperbilirubinemia, as in some individuals with severe Criger-Najjar Type I disease, a recessively inherited condition involving the virtual absence of UGT 1A1, the enzyme required for conjugation of UCB prior to hepatic excretion of bilirubin via the bile, hepatotoxicity results (22).

Kernicterus is a devastating but rare disease with an incidence that ranges from 0.4 to 2.9 per 100,000 live births (23). It is most prevalent in population groups from the Mediterranean area and in the Middle East, where glucose-6-phosphate dehydrogenase (G6PD) deficiency is most prevalent (24). G6PD is an X-linked recessive disorder whose primary effect is the reduced level of the enzyume G6PD in red blood cells, causing increased destruction of the cells. It is interesting to note that G6PD deficiency among neonates with hyperbilirubinemia varies widely between the affected population groups. Studies conducted within the last 10 years show this disorder to account for low to intermediate prevalence amongst Turks (3%), Iranians (7.5%), and Egyptians (11%), to a very high prevalence in Saudi's (30%) (24).

Abdel-Fattah and colleagues state that the fluctuating estimates in different countries is explained by the fact that the G6PD deficiency is inherited as an X-linked recessive condition, incidence and transmission of such disease is greatly increased if the incidence of consanguineous marriage is also high in such communities (24). Indeed this presumption is reasonable, as G6PD deficiency among neonates with hyperbilirubinemia is prevalent in the medical records of communities where consanguineous marriage has occurred: Jerusalem, Israel (16%; 1989), as well as the isolated Greek Island of Rhodes (7%; 1966) and Sassarri (4%; 1980) on the Italian Island of Sardinia (25).

The pediatric community's recent experience with kernicterus is notable for an increased number of reported cases in the United States due to the decreased length of hospital stays for new mothers and babies (26). Plasma UCB levels rapidly rise after 24 h and reach a peak (> 200 μM) 3–5 days after birth, after which plasma UCB levels plateau and slowly decrease reaching normal adult homeostatic levels (5–20 μM) within

a month (27-29). With earlier discharge, mothers and infants may not benefit from intervention by health care professionals as UCB peaks occur when the mother and baby have returned home (29). Furthermore, hyperbilirubinemia often goes undetected by parents (especially for babies with darker skin tones and/or first time mothers) as visual recognition of jaundice is not a sensitive measure (30). Significant differences in UCB content exist across populations, and there is also a substantial variability in rates of plasma UCB increase (28). Thai neonates reach the maximum peak for plasma UCB levels within 72 h of life, while this peak occurs in neonates of European and primarily white ancestry neonates between 73 and 96 h of life, followed by Hispanic neonates where this occurs after 96 h of life (28). UCB toxicity ceases to be an issue in normal infants after the age of 1 month, as the process of hepatic uptake, storage, conjugation and biliary secretion of UCB have matured to near adult levels, and plasma UCB levels return to normal adult homeostatic levels (27).

UCB encephalopathy cannot be diagnosed by a simple analysis of total free and conjugated serum bilirubin (TSB) or the concentration of B_f. Rather, a combination of both of these values is required in addition to the albumin to UCB ratio, and variations in the albumin to UCB binding constant (K_{A-UCB}) (31, 32). Clinical studies suggest that the risk for kernicterus, characterized by severe irreversible neurotoxicity that can result in death, is related in part to the degree and duration of hyperbilirubinemia (33, 34). The purported neurotoxic threshold (71-800 nM) for B_f can vary by more than 10 times between different neonates (27, 35, 36). At high TSB levels (>300 μM) increased entry of UCB into the central nervous system via passage through the BBB, may cause neurotoxicity and UCB encephalopathy; this condition, however, has also been observed

at TSB levels as low as 150 µM (22, 27). Variations in the neurotoxic threshold for UCB encephalopathy are also attributed to the fact that the $K_{A\text{-}UCB}$ is not "constant" but varies considerably between newborns, is impaired in sick infants, and increases with increasing gestational age and postnatal age (31, 32, 37).

Although the molecular pathogenesis of UCB-induced neuronal cell injury has yet to be ascertained, a review of the literature documented the effect of high concentrations of UCB on cell membranes (plasma, mitochondria, and endoplasmic reticulum), cellular bioenergetics, and intracellular calcium homeostasis (26). When B_f exceeds its aqueous solubility, it reversibly binds to the outer leaflet of the membranes, near the polar phospholipid head groups (38, 39). This binding results in changes that damage the plasma membranes of astrocytes, leading to the leakage of enzymes, defective uptake of glutamate, and damage to mitochondrial membranes that cause impaired cellular energy metabolism and apoptosis (36, 40-42, 42-44). Our laboratory has demonstrated that in the murine hepatoma cell line (Hepa 1c1c7), UCB-mediated apoptosis is mediated both through the caspase-dependent mitochondrial pathway, whereby caspase 9 acts as the initiator caspase, and caspase-dependent cell surface death receptor-mediated apoptosis is activated by caspase 8, and that this process is associated with increased oxidative stress (45, 46). Very recently, our group has also shown that UCB causes ER stress and activation of caspase 12 in Hepa 1c1c7 cells, another signaling pathway for apoptosis (47).

1.1.3   Formation and Metabolism of Bilirubin

In the pre-hepatic stage of UCB metabolism, erythrocytes are phagocytosed by macrophages releasing hemoglobin within the macrophage which is broken down into

heme and globin. Globin is degraded into its constituent amino acids for recycling, whereas HO-1 or HO-2 catalyzes the breakdown of heme to produce biliverdin (Fig. 1.1A), a non-toxic compound which in turn is reduced to UCB by biliverdin reductase (Fig. 1.1B) (4). UCB predominately binds to serum albumin becoming albumin-bound UCB, which is transported by blood into the liver and further metabolized (Fig. 1.1C) (1). B_f is the form of UCB which is of pathological significance in neurotoxicity because it can move through the immature BBB, and enters the brain, interstitial fluid, and cerebrospinal fluid (Fig. 1.1D) (1). The multidrug resistance protein (MRP1) and multidrug resistance P-glycoprotein (MDR1) can transport B_f outside of the brain, however the delayed maturity of these transport proteins in neonates contributes to the elevated concentrations of UCB in the brain (27).

At the hepatic stage, albumin-bound UCB goes to the liver via systemic circulation in the blood. In the liver UCB disassociates from albumin, and is actively transported by either organic acid transporter 2 (OATP2) or bilitranslocase (BT) into hepatocytes (48). Whilst in the hepatocyte, UCB undergoes glucuronidation whereby UGT 1A1 transfers glucuronic acid from UDP-glucuronate to UCB forming conjugated bilirubin (CB) (Fig. 1.1E) (49-51). CB the non-toxic, water-soluble form of bilirubin exists predominately as bilirubin diglucuronide, but can be found in low concentrations as bilirubin monoglucuronide (52, 53). CB is finally actively transported into the bile by MRP2, the hepatocyte canicular isoform of MRP1 which is located on the bile-canalicular membrane, and enters the gut (54). In the post-hepatic stage, CB can be hydrolysed back to UCB by β-glucuronidase of either bacterial or human origin (Fig. 1.1F) (55, 56). UCB is reduced to urobilinogen by intestinal bacteria (Fig. 1.1G),
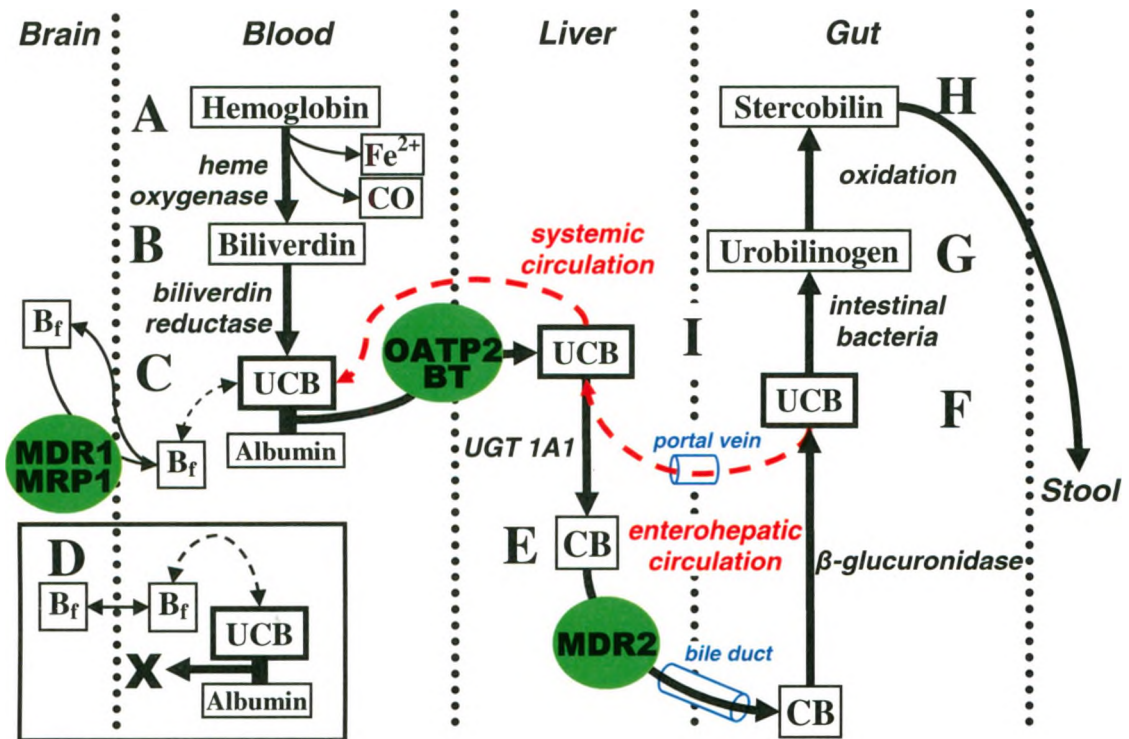
Figure 1.1: Metabolism and resorption of unconjugated bilirubin (UCB). Bilirubin is formed from hemoglobin. Heme oxygenase (HO) enzymatically cleaves the tetrapyrrole ring of heme to produce equimolar amounts of three biologically active products: biliverdin, ferrous iron, and carbon monoxide (CO) *(A)*. Biliverdin is reduced by biliverdin reductase into unconjugated bilirubin (UCB) *(B)*. UCB predominately binds to serum albumin becoming albumin-bound UCB *(C)*. Free UCB (B_f) the form of UCB which is not bound to albumin and is of pathological significance in neurotoxicity, can enter the brain, but can be actively transported back into the blood by the multidrug resistance protein (MRP1) and/or multidrug resistance P-glycoproteins (MDR1) *(D)*. Albumin-bound UCB is actively transported into the liver hepatocytes by either organic acid transporter 2 (OATP2) or bilitranslocase (BT) where it is conjugated with glucuronide by UDP-glucuronosyltransferase 1A1 (UGT 1A1) forming conjugated UCB (CB) (E). CB is actively transported into the bile by MRP2 and enters the gut where it is hydrolyzed into UCB by β-glucuronidase *(F)*. UCB is reduced into urobilinogen by intestinal bacteria *(G)*. Urobilinogen is oxidized in the gut to stercobilin and excreted in the stool out of the body *(H)*. Some UCB is resorbed back into the bloodstream (red dashed arrows) and returns to the liver via enterohepatic circulation, however it is inefficiently conjugated back into CB, resulting in UCB spill-over into the blood stream via the systemic circulation *(I)*.

Adapted from (1).

oxidized to sterocobilin (Fig. 1.1 h) and excreted in the stool out of the body (57, 58).

Resorption of UCB back into the body via enterohepatic circulation can occur passively in the gut from any part of the small or large intestine (59). Reabsorbtion of UCB via enterohepatic circulation is especially pronounced in newborns due to (1) the deficiency in the intestinal microflora capable of reducing UCB to urobilonogen; (2) high β-glucuronidase activity in human milk which hydrolyzes CB to UCB; and (3) bile salt malabsorption associated with intestinal immaturity (60-62). Albumin-bound UCB is returned to the liver via the portal vein, however it is inefficiently conjugated back into CB (~30% in adults and less so in newborns), and there is significant spill-over into the systemic circulation (59). The enhanced resorption of UCB in concert with the lack of urobilinogen production contributes to the elevated UCB levels found in newborns (59).

1.1.4 Antioxidant and Oxidant Properties of Bilirubin

From a teleological perspective, the biosynthesis of UCB as the end product of heme degradation does not make a great deal of sense. Biliverdin would seem to be an appropriate end product of the pathway, being readily excreted in the bile to enter the intestine and leave the body in the feces (11). Birds, reptiles, and amphibians do have biliverdin as their end product of heme degradation (63). Mammals on the other hand reduce the innocuous biliverdin to the more toxic UCB, a step that consumes the energy resource nicotinamide adenine dinucleotide phosphate (NADPH) (64). This evolutionary lacuna was solved in the late 1980's when UCB, the once thought to be toxic waste product of heme degradation, was found to play an important physiological role as an antioxidant in mammals at low, "physiological" concentrations (~0.01-10 μM in plasma) (65, 66).

Whereas glutathione (GSH), the principal cellular antioxidant in mammals is found in mM concentrations, UCB is found in nM concentrations and is a prominent antioxidant capable of protecting cells from 10,000-fold higher concentrations of the oxidant hydrogen peroxide due to the efficiency of bilirubin reductase in the oxidation-reduction cycle of bilirubin (17). Lipophilic reactive oxygen species (ROS) readily oxidize UCB into biliverdin, which is immediately reduced back to UCB by biliverdin reductase (Fig. 1.2) (67). In a recent study it was demonstrated that water-soluble GSH primarily protects water soluble proteins, whereas the lipophilic UCB protects lipids from oxidation (7). At the clinical level, a recent large cross-sectional study of middle-aged and elderly Japanese men and women reported that high concentrations of serum bilirubin were associated with decreased prevalence for the incidence of type 2 diabetes (68). Furthermore, a variety of clinical evidence has demonstrated that mild to moderately elevated levels of total bilirubin are associated with better outcome in almost 30 diseases with an oxidative stress component (11).

Approximately 300 mg of UCB (3.8 ± 0.6 mg/kg BW) are produced daily by normal adult humans (66). However, the TSB concentration (0.3–1.2 mg/100mL; 5–20 μM in adults) fluctuates due to a balance between its production from heme and its elimination as glucuronide metabolites into the bile (48). When the TSB falls out of this physiological balance, elevated levels of UCB become responsible for a range of pathological and physiological conditions. Although the precise molecular mechanism(s) of UCB toxicity remain(s) unknown, this laboratory has demonstrated that elevated UCB levels are characterized by an increased generation of ROS (45, 46). In Hepa 1c1c7 cells, UCB concentrations greater than 25 μM were shown to cause a significant increase in
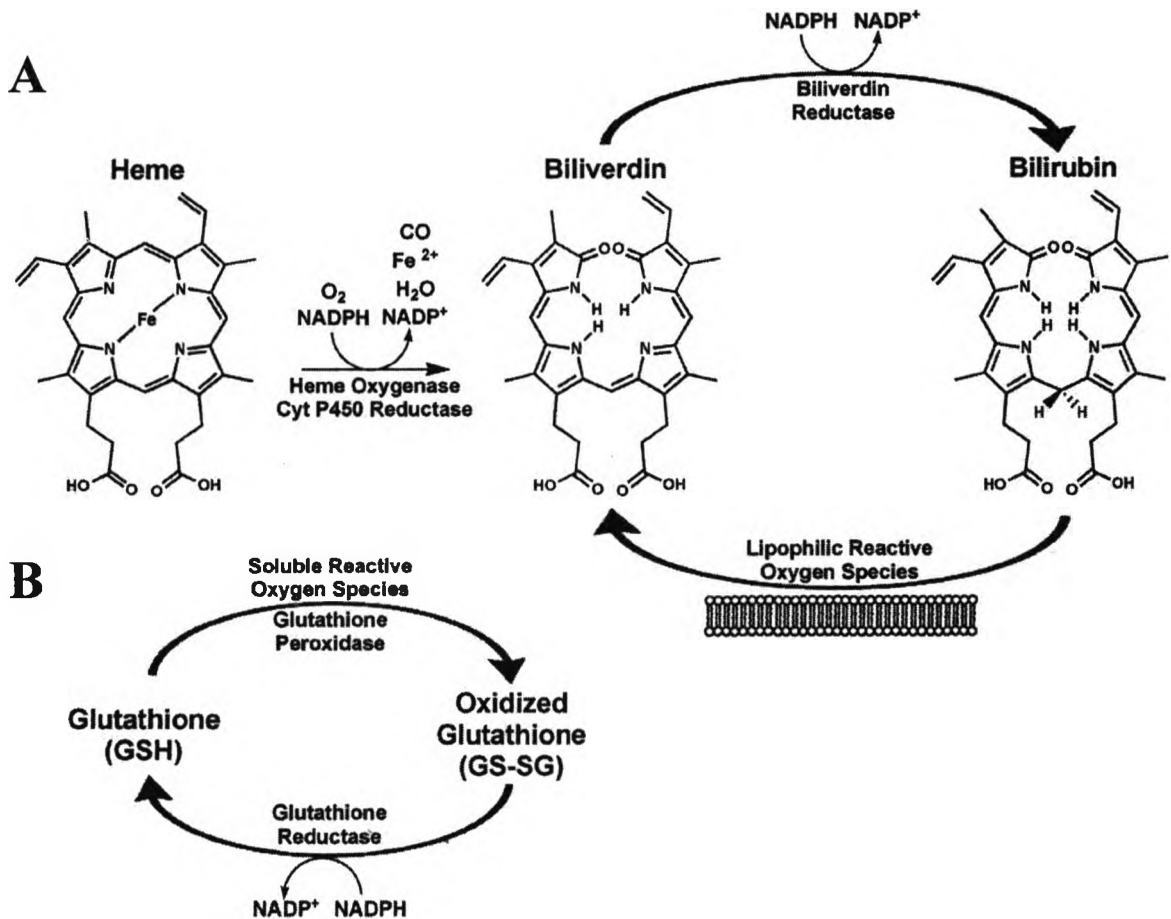
Figure 1.2: Oxidation-reduction cycles for UCB and GSH. Lipophilic reactive oxygen species (ROS) act directly on UCB, leading to its oxidation to biliverdin *(A)*. Biliverdin reductase catalyzes the reconversion of biliverdin to UCB, permitting UCB to detoxify a 10,000-fold excess of ROS oxidants. Soluble ROS oxidants are detoxified by GSH, a cycle that requires 2 enzymes, glutathione peroxidase which oxidizes GSH to form glutathione disulfide (GSSG), and glutathione reductase which reduces GSSH back to GSH *(B)*.

Adapted from (11).

ROS production, loss of mitochondrial membrane potential and cell death primarily by apoptosis (45, 46). Rising concentration of UCB play a role in contributing towards oxidative stress within a cell.

1.2   Oxidative Stress

When reactive oxygen species (ROS) or reactive nitrogen species (RNS) levels exceed the cellular antioxidant capacity, a deleterious condition known as oxidative or nitrosative stress occurs (69).   ROS is a collective term that describes the chemical species that are formed upon incomplete reduction of oxygen and includes the superoxide anion (O_2^-), hydrogen peroxide (H_2O_2), and the hydroxyl radical (HO^-) (70).   Oxygen can be converted into these radical intermediates exogenously by radiation, ultra violet light or chemicals, and ROS can also be produced endogenously by the electron transport system in mitochondria, or as a metabolic byproduct (71).   This toxicological stress is either due to excessive production of ROS or RNS, loss of antioxidant defenses or both (69).   Unchecked excessive ROS/RNS generation can lead to the destruction of cellular components, and ultimately cell death via apoptosis, or necrosis (72).

1.2.1   Pathological Significance of Oxidative Stress

ROS react at nearly diffusion-limited rates with many components of the cell, including lipids, nucleic acids, and proteins (72).   The result of this nonspecific free radical attack is a loss of cell integrity due to lipid peroxidation, genomic instability and mutations due to nucleic acid oxidation, and loss of enzyme function due to modification of amino acid side chains (73-75).   Brain tissue is especially susceptible to oxidative damage, due to its high oxygen consumption, relatively low antioxidant levels and low

regenerative capacity (76). A common feature of neurodegenerative diseases such as Alzheimer's disease (AD), Parkinson's disease (PD), and amyotrophic lateral sclerosis (ALS), is the extensive evidence of oxidative stress. Similarly, increased ROS leads to an acceleration in ageing and age-related diseases (77, 78).

1.2.2 Oxidative Modification of Lipids, Nucleic Acids, and Proteins

Lipid peroxidation is the result of attack by ROS on the double bond of unsaturated fatty acids, such as linoleic acid and arachidonic acid, to generate highly reactive lipid peroxy radicals that initiate a chain reaction of further attacks on other unsaturated fatty acids (76). This chain reaction leads to the formation of breakdown products including 4-hydroxy-2,3-nonenal which have been found at elevated levels in AD and PD brain tissue, as well as in the cerebral spinal fluid of ALS patients (79-82). ROS are not a direct cause of genetic mutations; however direct modification of nucleic acids by $HO^{\cdot}$ can generate more than 15 products, and the addition of H_2O_2 to mammalian cells often causes DNA strand breakage, and can stimulate cell proliferation at low levels but halt it at higher levels (76, 83, 84). ROS, however, can indirectly cause mutations in DNA by damaging DNA polymerases, and repair enzymes thereby decreasing the fidelity of replication and slowing the repair of lesions, and the breakdown products of lipid peroxidation can bind to DNA to generate potentially-mutagenic lesions (85-88). Protein modification induced by ROS or secondary by-products of ROS, can lead to oxidation of amino acid side chains, formation of cross-linked protein aggregates, and cleavage of polypeptide chains. The latter two modifications result in irreversible modifications with loss of protein function, however under conditions of moderate

oxidative stress, cysteine (cys) oxidation can lead to the reversible formation of protein mixed disulfide groups.

1.2.2.1 Oxidative Modification of Protein Cysteine Thiols

Proteins with a reactive cysteine (Cys) thiol or free ionized cysteine thiol (PS⁻) residue can undergo oxidation in the presence of low concentrations of H_2O_2 to form the highly reactive sulfenic acid (PSOH), which can then non-enzymatically form a protein mixed disulfide by reaction with another protein or the tripeptide, glutathione, or become oxidized to the more stable sulfinic (PSO_2H) or sulphonic (PSO_3H) acids. The reactivity of these Cys residues is dictated by their solvent exposed localization and ionization state; PS⁻ are far more nucleophilic and easily oxidized than PSH (89). When the pK_a of a PSH is less than or equal to intracellular pH (4.5-5.5), it will become deprotonated forming PS⁻, which is stabilized by neighboring positively charged residues (89, 90). PSOH and occasionally PSO_2H can be reversibly oxidized, and are known to operate in redox signaling (91). The formation of disulfides in substrate proteins is a process known as *S*-glutathionylation, a reversible reaction in which the thiol groups of two cysteine residues are oxidized to form a covalently linked disulfide (92). *S*-Glutathionylation refers to the post-translational modification of PSH/PS⁻ by the addition of the tripeptide GSH forming a protein GSH disulfide (PSSG) as well as the formation of any protein bound disulfide (PSSP) (91). PSSPs include intermolecular bound proteins (PSS), or intramolecular protein disulfides that can be homodimeric (P^1SSP^1), heterodimeric (P^1SSP^2), or oligomeric $(PSSP)_n$.

1.2.3 Physiological Defenses that Counteract Oxidative Stress

All organisms have defense mechanisms to combat the deleterious effects of oxidative damage. The majority of intracellular ROS production is derived from the mitochondria, and it is estimated that the mitochondria convert 2% of the oxygen molecules consumed into O_2^- (93). A sophisticated enzymatic and non-enzymatic antioxidant defense system including catalase, superoxide dismutase (SOD), and glutathione peroxidase (GSH-Px), detoxifies and regulates overall ROS levels to maintain physiological homeostasis. SOD speeds the conversion of O_2^- to H_2O_2, whereas catalase and GSH-Px convert H_2O_2 into water. Additionally, isoforms of peroxiredoxin (Prx), members of a new family of peroxide scavengers, catalyze the reduction of H_2O_2, organic hydroperoxides, as well as peroxynitrites (94). Furthermore a variety of non-enzymatic, low molecular mass molecules such as ascorbate, pyruvate, flavonoids, carotenoids, UCB, and most importantly GSH play a critical role in scavenging ROS (77).

GSH, the tripeptide γ-glutamyl-cysteinyl-glycine, is the major endogenous low molecular weight non-protein thiol and is well established as an antioxidant defense (95). Total glutathione includes both GSH and GSSG, and is found in concentrations between 1 - 11 mM, with an intracellular GSH:GSSG ratio in healthy cells exceeding 100 (96). The GSH:GSSG ratio is the primary determinant of intracellular redox state as cellular GSH levels are ~500 – 1000 fold higher than any of the other functional redox cycles (97). GSH deficiency or a decrease in the GSH:GSSG ratio manifests itself largely through an increased susceptibility to oxidative stress, and the resulting damage is manifested in pathologies including neurodegenerative diseases, cancer, and ageing (98). GSH-Px uses GSH as a reductant by releasing 2 electrons which reduce hydroperoxides

(ROOH) forming the corresponding alcohol (ROH) and GSSG. GSSG is subsequently reduced by glutathione reductase (GSH-Rx) back into GSH at the expense of NADPH, the co-factor for GSH-Rx. The NADPH:NADP$^+$ ratio is normally magnitudes (100:1) away from equilibrium to effectively facilitate the reduction of GSSG, and any decreases in this ratio have a detrimental effect on the GSH:GSSG ratio (97).

1.2.3.1 Adaptation – the Nrf2-Keap1 System

Endogenous or exogenous chemical toxins must be metabolized and biotransformed prior to excretion in a process mediated by two consecutive reactions. Phase I enzymes (cytochrome P450 mono-oxygenase systems and flavin-dependent monooxygenases) can oxidize hydrophobic compounds to metabolites, including reactive electrophiles. Both hydroxylation and reduction reactions are common, introducing functional groups that are able to react with water-soluble moieties, a reaction catalyzed by phase 2 enzymes, including glucuronosyltransferases (99). Xenobiotics often serve as ligands of the key transcription activators for Phase I enzyme genes, whereas the Phase II enzyme genes are induced by the metabolites of phase I enzymes, which are often highly electrophillic (100). Phase II enzymes (E.g. GST, UGT 1A1, sulfotransferases) catalyze conjugation of Phase I products with various hydrophilic moieties (Eg GSH and glucuronic acid) and allow for effective excretion of these products which are substrates for efflux transporters into bile and/or urine (99). Transcription and expression of several Phase 2 enzymes is redox sensitive and is mediated by the interactions of the redox sensitive Kelch-like ECH-associated protein 1 (Keap1) with nuclear factor 2 (Nrf2), in an arrangement known as the Nrf2-Keap system (Fig. 1.3) (99).
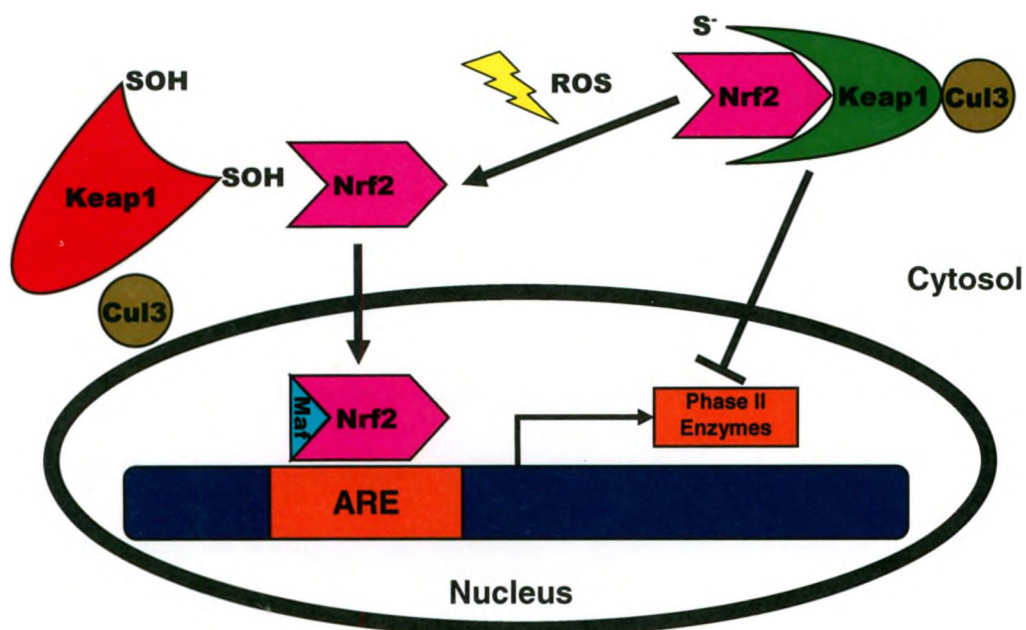
Figure 1.3: The Nrf2-Keap1 System. Under basal conditions Phase II enzymes are not transcribed in a Nrf2-Keap1-dependent manner as Nrf2 undergoes ubiquitination by Cul3, and is bound to the reduced form of Keap1 (green). When the cells redox status changes due to an oxidative insult or the production of Phase I electrophilic metabolites, active free cysteine thiol (S$^-$) in Keap1 becomes oxidized (SOH) forcing the oxidized Keap1 (red) to undergo a conformational change which releases Nrf2. Nrf2 translocates into the nucleus where it forms a heterodimer with a Maf protein and binds to the antioxidant response element (ARE) of Phase II genes inducing their expression.

The transcription factor Nrf2 binds to the antioxidant response element (ARE) of several Phase II genes inducing their expression (101-103). Nrf2 is also an important regulator of oxidative-stress inducible genes including *HO1* and *Prx1*, and transporter genes including *Mrp1* and the gene encoding the cysteine-glutamate-exchange transporter (104-106). Under basal conditions, Keap1 is bound to Nrf2 and mediates association with a Cullin 3 (Cul3)-dependent ubiquitin ligase complex (107-109). Keap1 anchors Nrf2 in the cytoplasm, and targets it for ubiquitinatoin and proteasomal degradation, thereby repressing its ability to induce Phase II genes, and preventing it from activating target genes (110, 111).

ROS or electrophilic products generated by Phase I enzymes, are responsible for inducing Phase II genes. Redox sensitive Keap1 is a PS⁻, as its intervening region is a functional domain that contains two highly reactive cysteine residues which are responsible for Keap1-dependent Nrf2 repression (111, 112). During an oxidative insult, these two Cys residues become oxidized provoking a conformational change in the Keap1 molecule, leading to the dissociation of Nrf2 from Keap1, and preventing the interaction of Cul3 with Keap1 (113). Once Keap1 is released, it translocates into the nucleus where it readily binds with one of the small Maf proteins, and induces the expression of Phase II genes (102). The Nrf2-Keap1 system is involved in the neuroprotection against oxidative insults in the nervous system and plays a critical function in maintaining the redox homeostasis of a cell (114). It has also been reported that Nrf2 deficiency leads to several common pathogenic conditions including susceptibility to chemical carcinogenesis, acute hepatotoxicity after medication, and acute respiratory distress following the ingestion of food preservatives (115-118).

1.3   *S*-Glutathionylation

Protein *S*-glutathionylation, the reversible binding of GSH to PS⁻ or PSH, is involved in protein redox regulation, storage of GSH, protection of PS⁻ from irreversible oxidation, and cellular signaling (119). *S*-glutathionylation is promoted by oxidative or nitrosative stress but also occurs in unstressed cells under basal conditions where it is usually referred to as constitutive *S*-glutathionylation (120-122). Constitutive *S*-glutathionylation is demonstrated in hemoglobin in red blood cells, γ-crystallin from human lens, and actin in human fibroblasts, and is believed to play a role in cellular signaling and redox regulation of protein functions (69, 122, 123).

Of importance all of these proteins have one or more ionized or reactive cysteine protein thiol groups (PS⁻) at physiological pH. Less than 1% of all proteins undergo *S*-glutathionylation because of the requirement for a reactive cysteine thiol group, despite this it plays a critical function in cell viability as a number of proteins involved in transcription, translation, and degradation (which are key proteins of cellular adaptation as they control protein expression levels), can be regulated by *S*-glutathionylation (69, 124). The modulation of protein function by redox regulation is in several ways analogous to phosphorylation, except that protein modifications no longer occurs on specific serine, threonine, or tyrosine residues, but instead on redox-sensitive Cys (PS⁻) residues (69). Furthermore, reversible oxidation by *S*-glutathionylation must (1) change the function of the modified protein, (2) occur in intact cells in response to a physiological stimulus and elicit a physiologic response, (3) occur at physiological conditions and GSH:GSSG ratios, and exhibit rapid and efficient biological mechanisms for (4) formation, and (5) reversal of PSSP/PSSG (125).

1.3.1   Molecular Mechanisms of *S*-Glutathionylation

PS⁻ is particularly sensitive to biological oxidative modifications and can undergo a diverse array of redox reactions, which are largely dependent on the species and concentrations of the oxidants responsible (Fig. 1.4).   In the presence of increasing ROS concentrations and an oxidative cellular environment, PS⁻/PSH can be reversibly oxidized into PSSP, PSSG, or PSOH.   PSOH, which is also formed from PS⁻ at physiological concentrations of hydrogen peroxide, is the least stable of the three intermediates and in the absence of GSH can undergo further oxidation to become an irreversibly oxidized protein such as PSO_2H and PSO_3H depending on the cellular redox state, GSH:GSSG ratio, and characteristics of the structure of the protein (126).   The formation of PSSP does not require any enzyme, the redox properties of Cys allow formation of intra and intermolecular disulfide bridges, which enable proper protein folding and formation of stable protein complexes (127).

S-glutathionylation does not occur with a cysteine thiol (PSH), because a redox reaction involving the loss of two electrons per sulphur atoms is needed (128) *S*-glutathionylation of PS⁻ into a PSSG can occur under conditions of increased oxidative stress.   This direct reaction involves a thiyl radical of GSH (GS⁻) and is facilitated by a special class of GSTs known as GSTπ (129).   Townsend and colleagues observed that null GSTπ knockout mice had no noticeable difference in PSSG formation compared to WT GSTπ mice (129).   However under increased conditions of oxidative stress, they observed a time and dose dependent increase in PSSG formation in WT GSTπ mice compared to the null GSTπ mice (129).   Their data suggests GSTs are involved in basal levels of oxidative stress, and catalyze the *S*-glutathionylation of PSOH into PSSG,

Figure 1.4: Oxidative modifications of cysteine. Upon oxidation, both PSH and PS⁻ are capable of forming a disulfide bond producing PSSP, however, steric hindrance prevents this reaction from becoming the predominant pathway. PSSP can be readily reduced back into PSH/PS⁻ by a broad range of redox-active enzymes *(A)*. Increasing oxidative conditions result in PSSP becoming further oxidized into specific reversible post-translational forms of a protein sulfenic acid (PSOH). Proteins with a cysteine thiol residue (PSH) undergo reversible oxidation into PSOH under strong oxidizing conditions *(B)*, whereas proteins with a reactive cysteine thiol residue (PS⁻) are readily reversibly oxidized into PSOH under basal conditions *(C)*. GST facilitates *S*-glutathionylation of PSOH into PSSG *(D)*. Glutaredoxin (Grx) is the main enzyme that allows PSSG to undergo deglutathionylation via reduction *(E)*. Under excessive oxidative conditions, GSTπ contributes significantly to *S*-glutathionylation, by catalyzing a thiyl radical of GSH (GS⁻) directly with PS⁻ to produce PSSG *(F)*. Excessive levels of oxidative stress result in the further oxidation of PSOH into irreversible post-translational sulfinic (PSO_2H) *(G)* or sulfonic (PSO_3H) acids *(H)*. Recent findings have demonstrated that sulfaredoxin (Srx) is involved in the reversible oxidation of 2-Cys-Peroxiredoxin in the PSO_2H form. Cysteine residues colored in turquoise indicate reversible oxidation of the protein thiol, purple indicates irreversible oxidation. The oxidation number of the sulfur atom in each of the chemical forms of cysteine is shown. Turquoise lines indicate a decrease in the oxidation state of the sulfur atom, purple lines indicate an increase. A lightning bolt signifies a significant increase in ROS levels above basal conditions.

Abbreviations: Grx, glutaredoxin; GS⁻, glutathione thiyl radical; GSH, glutathione; GSSG, glutathione disulfide; GST, glutathione S-transferase; PDI, protein disulfide isomerase; PS⁻, reactive (oxidized) protein thiol; PSH, proteine cysteine thiol; PSSG, protein glutathione mixed disulfide; PSSG⁻, protein glutathione disulfide radical; PSSP, protein disulfide; PSOH, protein sulfenic acid; PSO_2H, protein sulfinic acid; PSO_3H, protein sulphonic acid; Srx, sulfaredoxin; Trx, thioredoxin.
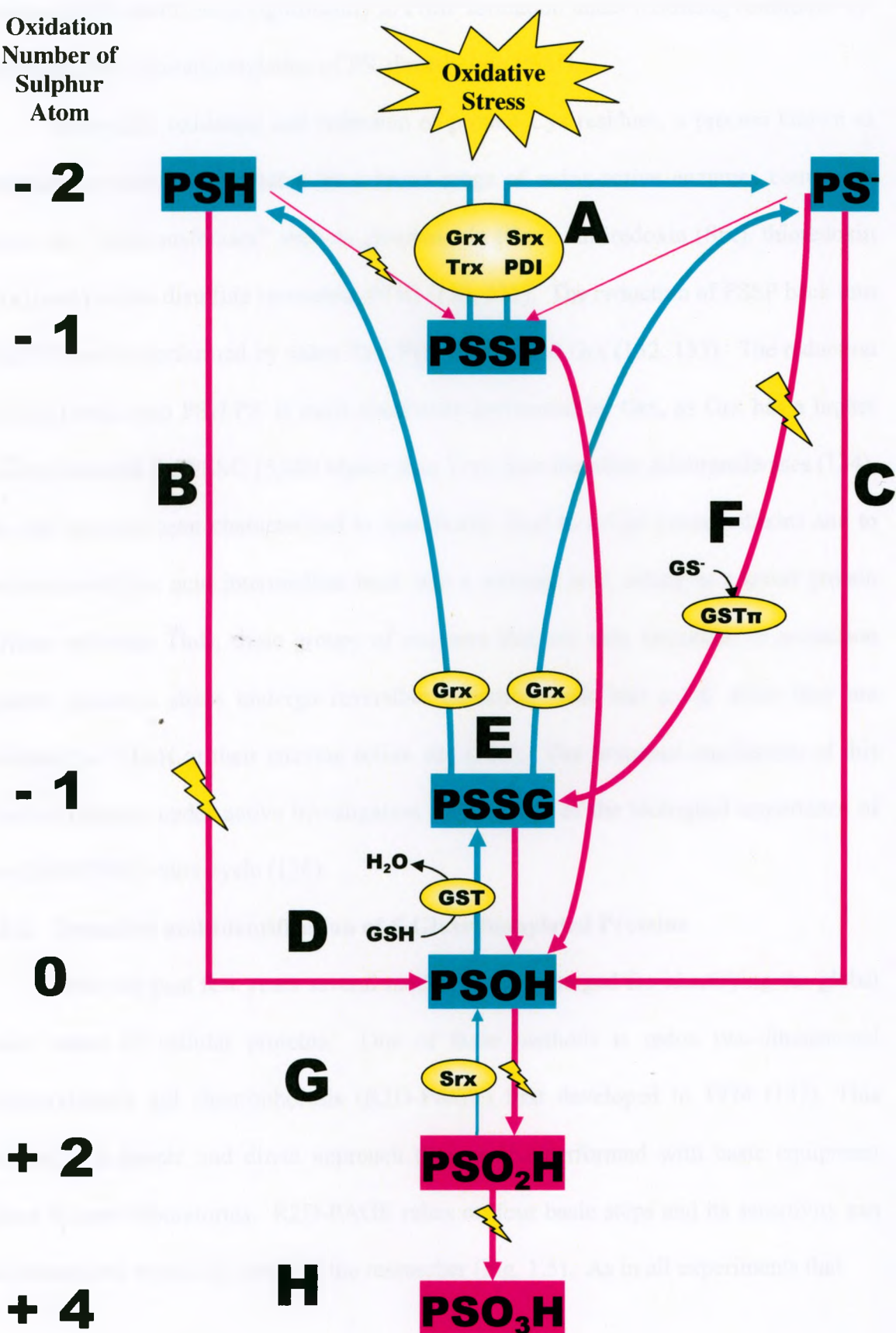
whereas GSTπ contributes significantly to PSSP formation under oxidizing conditions by catalyzing the S-glutathionylation of PS⁻ directly into PSSG.

Reversible oxidation and reduction of protein Cys residues, a process known as deglutathionylation, is mediated by a broad range of redox-active enzymes commonly known as "thioltransferases" such as glutaredoxin (Grx), sulfiredoxin (Srx), thioredoxin (Trx), and protein disulfide isomerase (PDI) (130, 131). The reduction of PSSP back into PSH/PS⁻ can be performed by either Trx, PDI, or Srx, and Grx (132, 133). The reduction of PSSG back into PSH/PS⁻ is most commonly performed by Grx, as Grx has a higher binding constant for PSSG (5,000 higher than Trx), than the other thioltransferases (134). Srx has recently been characterized to specifically bind to 2-Cys peroxiredoxins and to reduce its sulfinic acid intermediate back into a sulfenic acid, acting as a novel protein salvage pathway. Thus, these groups of enzymes that are very important in protection against oxidative stress undergo reversible reduction back into a PS⁻ when they are oxidized to PSO$_2$H at their enzyme active site (135). The proposed mechanism of this reaction remains under active investigation and because of the biological importance of the GSH/GSSG redox cycle (136).

1.3.2 Detection and Identification of S-Glutathionylated Proteins

Over the past few years several methods have emerged for identifying the global redox status of cellular proteins. One of these methods is redox two-dimensional polyacrylamide gel electrophoresis (R2D-PAGE) first developed in 1974 (137). This method is a simple and direct approach that can be performed with basic equipment found in most laboratories. R2D-PAGE relies on four basic steps and its sensitivity can be customized to suit the needs of the researcher (Fig. 1.5). As in all experiments that

Figure 1.5: Basic steps in labeling disulfide bonded proteins for analysis with redox two-dimensional polyacrylamide gel electrophoresis (R2D PAGE).
A putative redox-regulated protein with three cysteine residues exists under (left) control conditions in a fully reduced form. Under (right) oxidative conditions, two of the cysteine residues form an intramolecular disulfide bond (red circle) *(A)*. In the blocking step, all free cysteine residues are rapidly and irreversibly blocked using a thiol reactive reagent (such as iodoacetamide) *(B)*. In the reduction step, a reducing agent (such as dithiothreitol) is added to the proteins in solution or suspension. This will not alter the (left) reduced protein cysteine thiols, but will reduce the oxidized cysteine thiols in the (right) oxidized protein, resulting in the formation of two new reduced thiol groups (green circle) *(C)*. In the labeling step, a thiol-specific reagent can be added, which carries a detectable label such as a fluorescent group, an immunoreactive group, or a radioactive chemical. This reagent will covalently modify the newly accessible thiol groups. An approach such as this can be theoretically used to specifically label all thiol groups that arise from proteins that occur as either protein disulfides or protein-glutathione mixed disulfides in vivo *(D)*.
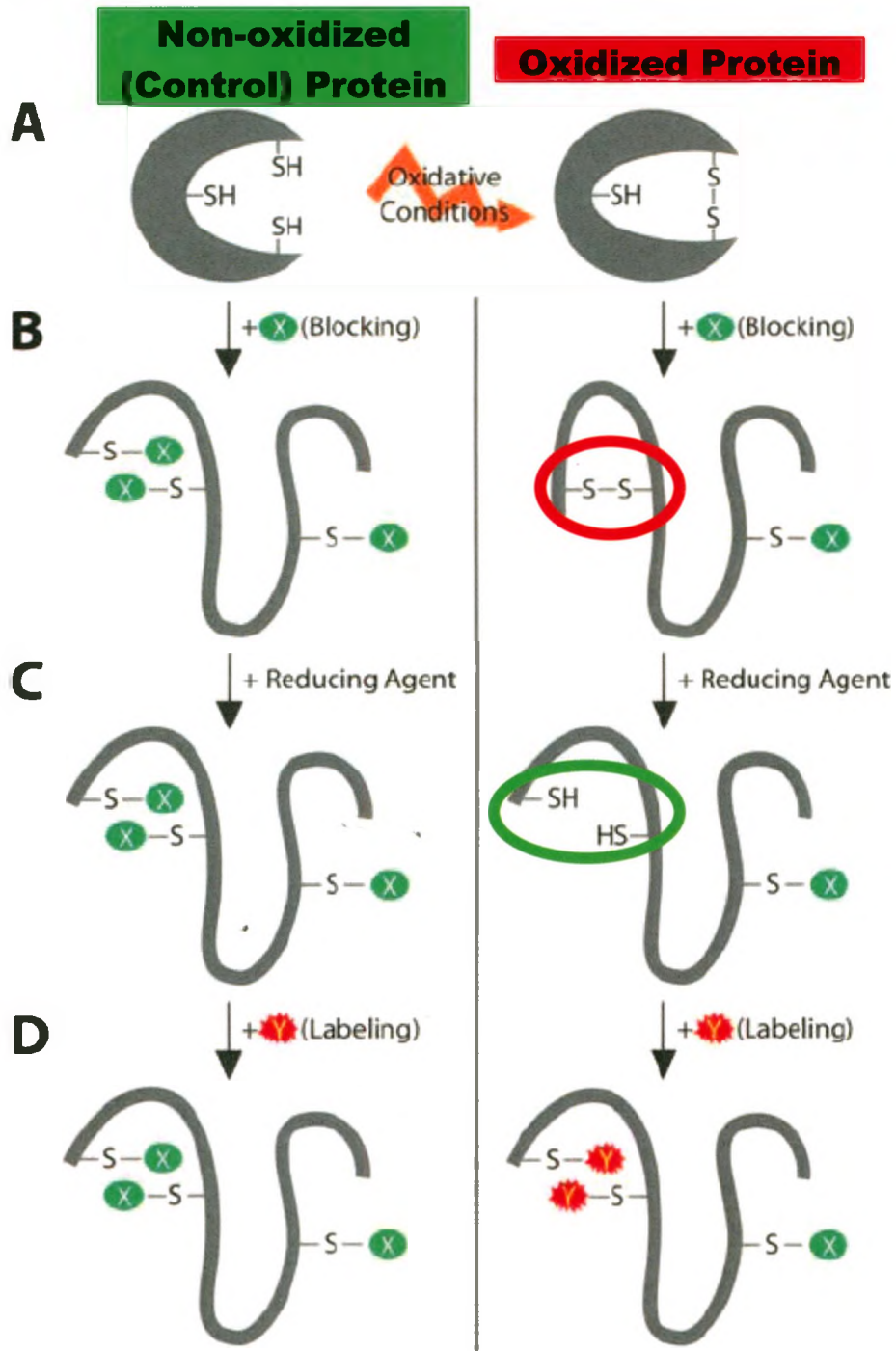
Adapted from (138).

investigate the *in vivo* thiol/disulfide state of proteins, the first step necessarily involves the rapid blocking of all free thiol groups to prevent unwanted thiol-disulfide reactions (138). To prevent nonspecific air oxidation of protein thiols or GSH during sample preparation and cell lysis, membrane permeable thiol-reactive reagents such as iodoacetamide (IA) which react covalently with –SH are added to the cell culture to block further reactions of thiol groups while the proteins are still within the cells. After the first step, proteins are electrophoresed in the first dimension in a slab gel under non-reducing conditions. In the second step, this slab with the resolved proteins is removed and the proteins are reduced, still within the gel matrix. To detect all reversible thiol modifications, general reductants such as dithiolthreitol (DTT) can be used. To detect specific post-translational modifications at protein cysteine thiols, specialized reductants like sodium arsenite to reduce sulfenic acids, or glutaredoxins to reduce S-glutathionylated cysteines must be used (139). The third step involves removing the chemical reductant(s) and treating the proteins with chemicals that prevent oxidation of the modified thiols. This is accomplished by re-treating the cells with IA to react with protein thiols formed during reduction to provide a general overview, or utilizing thiol selective chemicals that label the newly reduced thiols and are capable of probing for distinct thiol modifications (121, 140). Once this is done, the gel slab containing the resolved proteins from the first dimension separation is layered onto a second gel and electrophoresed at a 90° angle to the original direction. In the fourth step the proteins are visualized by conventional staining (e.g. silver or Coomassie blue), label specific reactive dyes, or by Western blot analysis (141).

After staining a gel that has been run in the second dimension, three groups of proteins can be distinguished (Fig. 1.6). The majority of cellular proteins do not form disulfide bonds, run identically in both the first and second dimension because resolution is based on monomeric molecular weight in both cases, and will fall on the 'diagonal' in this system. These proteins are not affected by the chemical reduction that has occurred, and so their migration behavior is identical in both dimensions. They will migrate approximately equal distances in both directions during electrophoresis lying exactly on the diagonal line and connecting opposite corners of the gel (142). The second group is proteins that form intramolecular disulfide bonds (PSS), which are found slightly above the diagonal line. In the first dimension these proteins migrate quicker than their respective mass as they form a more compact structure with their internal disulfide bonds still intact, while in the second dimension their structure becomes unfolded and they migrate at the speed of their respective monomeric mass (142). The third group includes proteins that form homodimeric or heterodimeric disulfide bonds (PSSP), which are found below the diagonal line. In the first dimension they migrate to a position corresponding to their combined mass while in the second dimension, they migrate according to their respective monomeric mass (138). To identify the individual proteins, the protein spots are excised from the gel, subjected to trypsin digestion and the tryptic digests analysed using mass spectrometry. Unless a GSH label is used, proteins bound to GSH (PSSG) can not be visualized by conventional staining as the mass of GSH is considered negligible compared to the significantly more massive protein that it is bound to, and thus PxS^- and PxSG will appear on the prominent diagonal line.
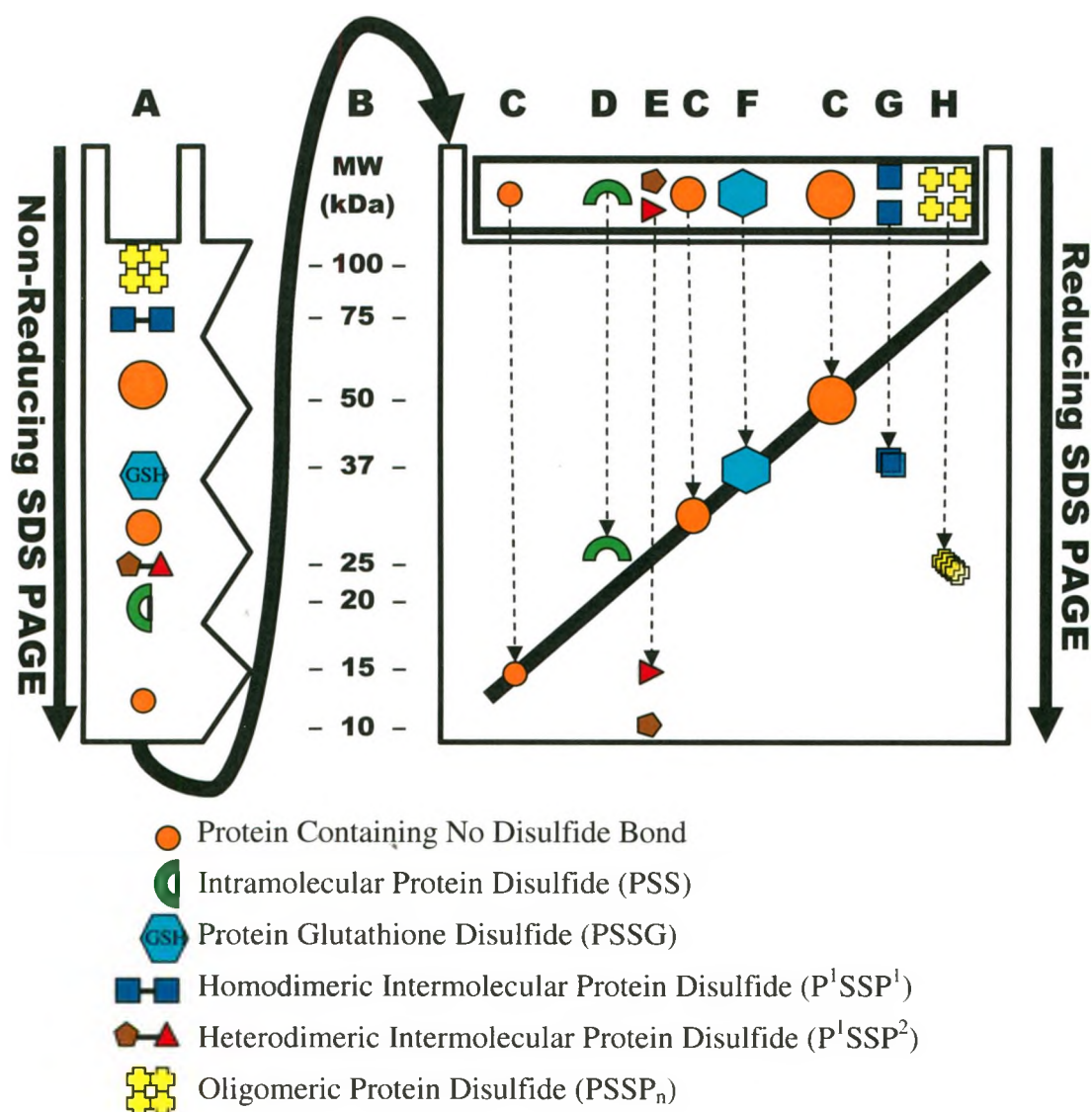
Figure 1.6: Separation of disulfide linked proteins through redox two-dimensional polyacrylamide gel electrophoresis. The protein sample in non-reducing buffer is separated in the first dimension by non-reducing SDS PAGE *(A)*. After running to completion, the gel lane is removed from the gel, incubated in reducing buffer, placed horizontally onto another gel and run in the second dimension. The reducing buffer reduces protein cysteine thiol disulfide bonds to protein cysteine thiols *(B)*. Upon staining and visualizing proteins a prominent diagonal line appears. Proteins located directly on the prominent diagonal line indicate either a protein that forms no disulfide bond *(C)*, or a protein glutathione mixed disulfide *(F)*. Proteins containing an intramolecular disulfide bond will appear above the diagonal *(D)*. Proteins that form intermolecular protein disulfide bonds are located beneath the line. The presence of two proteins above one another indicates a heterodimeric protein bonded disulfide *(E)*, while the presence of a single protein indicates either a homodimeric *(G)*, or oligomeric disulfide bonded protein *(H)*.

Other methods for protein identification include techniques that utilize radiolabeled GSH involving either radiographs or high pressure liquid chromatography (HPLC). The first method is based on the incorporation of radioactive glutathione [^{35}S]GSH into proteins as described in 1985 (143). Cells are preincubatd with cycloheximide to block protein synthesis, incubated with L-[^{35}S]Cys to radiolabel the GSH pool, and exposed to oxidative conditions. Proteins are routinely then separated by two dimensional isoelectric focusing (2D IEF), and S-glutathionylated proteins are located by autoradiograpy and identified by mass spectrometry (119). The second method is similar to the first but involves labeled GSH and the usage of a HPLC column specific for GSH that traps PSSG. These GS- or PS-containing proteins are then eluted from the column by higher ionic strength buffer or increasing methanol concentration and run on 2D IEF gels for separation and identification via mass spectrometry (119).

1.3.3 Impact of *S*-Glutathionylation on Protein Function

Under physiological conditions, S-glutathionylation results in protein-specific functional changes (activation or deactivation), which are important in the regulation or modulation of signal transduction that are critical for cell function (144). S-glutathionylation is involved in cell signaling as the kinase activity of key signaling proteins such as PTP1B and MEKK1 in addition to transcription factors (NF-κB) fundamental for cell growth, differentiation and apoptosis contain reactive cysteine thiol residues that are redox regulated (145, 146). For example, during oxidative stress the NF-κB subunit p50 forms an inter or intramolecular disulfide bond at Cys-62 that prevents it from inducing transcription during oxidative stress (147). This inter or intramolecular bond has been proposed to be the product of the formation of a GSH

reaction with the sulfenic acid intermediate of p50 however it is only responsible for 10% of the oxidatively modified protein (148). The remaining 90% is believed to undergo oxidative modification by S-glutathionylation at Cys-62, and this mechanism is believed to be regulated by GSH:GSSG ratios (147). Thus, S-glutathionylation represents a general mechanism by which many protein functions, including several kinases and phosphatases are regulated by preventing activation-loop phosphorylation or by changing protein-substrate interactions (144). Additionally various studies have enabled the identification of different metabolic enzymes susceptible to redox regulation by S-glutathionylation. GAPDH along with other glycolytic enzymes including pyruvate kinase, aldolase, phosphoglycerate kinase and triose phosphate isomerase can all undergo S-glutathionylation in primary rat hepatocytes and human HepGt hepatoma cells exposed to artificial oxidant conditions, for example with peroxides. These studies demonstrate that S-glutathionylation can coordinate cellular metabolism in response to oxidative stress by modulating glycolysis (149).

1.3.3.1 *S*-Glutathionylation of C-Jun and Thioredoxin F

C-Jun the protein product of the proto-oncogene c-*jun* forms a heterodimeric complex that interacts with the DNA regulatory element known as the activator protein-1 (150). Nitric oxide induced stress results in the formation of an intermolecular disulfide bridge between Cys residues in the leucine zipper site of c-Jun monomers and prompts S-glutathionylation whereby GSH binds to Cys-269 which is located on the DNA binding site of the protein (151). The covalent dimerization of c-Jun did not affect its DNA binding activity; however the formation of a mixed disulfide with GSH at the DNA binding site correlated well with the inhibition of transcription factor binding to DNA

(151). These findings demonstrate that *S*-glutathionylation and deglutathionylation are a potential mechanism by which nitrosative or oxidative stress may be transduced into a functional response at the level of transcription.

In addition to protecting sensitive reactive protein thiols from irreversible oxidation during oxidative stress, *S*-glutathionylation regulates redox homeostasis. In the green algae *Chlamydomonas reinhardtii*, the f-type thioredoxin (Trxf), which is involved in photosynthesis, undergoes *S*-glutathionylation during oxidative stress, impairing its reduction in the light resulting in the impaired light activation of target enzymes involved in photosynthesis and ultimately decreasing the generation of free radicals as a result of photosynthetic metabolism (152). *S*-Glutathionylation also plays a role in regulating calcium homeostasis and ion channel activity; for example patients with cystic fibrosis have a markedly inhibited transmembrane conductance regulator chloride channel due to *S*-glutathionylation and other modifications of reactive cysteine thiols (153). Finally, *S*-glutathionylation plays an essential role in regulating protein folding and stability. Experiments performed *in vitro*, demonstrate that *S*-glutathionylation is required for full peptidase enzyme activity and also that it controls thimet oligopeptidase (involved in oligopeptide metabolism both outside and within cells) self-oligomerisation, with profound functional consequences for intracellular peptide metabolism because the oligomerised enzyme has reduced enzymatic activity (154).

1.3.3.2 *S*-Glutathionylation of Actin and Transthretin

The rapid rearrangement of actin filaments allows cells to respond to extracellular signals and environmental changes such as the cellular redox status, by moving, changing shape, and translocating intracellular organelles (155). This is achieved by actin

polymerization, translocation, polarity and rate of assembly of a number of actin-binding proteins (156). Among the proteins involved in this organization are small heat shock proteins (HSP) that under basal conditions exist as multimeric non-phosphorylated complexes that are broken down following phosphorylation by stress-activated kinase pathways (156). During conditions of oxidative stress, these small HSP become *S*-glutathionylated or broken down, rendering actin incapable of regulating its structure and making it prone to denaturation. *S*-glutathionylation of actin is another method of protecting actin structure as it forms a mixed disulfide with GSH at Cys-374 (157). This oxidative modification of actin at reactive cysteine thiol is essential for cell spreading and cytoskeleton organization, and has a key role in disassembly of the actin myosin complex during cell adhesion (158). During conditions of oxidative stress, actin undergoes *S*-glutathionylation forming glutathionylated actin which changes its conformational structure thus causing it to have a decreased capacity to polymerize and prevents protein denaturation as the protease site between Met-47 and Gly-48 is less accessible to proteases within the surface loop of subdomain 2 (156). Thus, the supramolecular structure of actin is protected by two independent mechanisms; HSP binding to actin filaments and *S*-glutathionylation (156).

Transthyretin (TTR) is a 55 kDa homotetramer protein that causes the human amyloid diseases: senile systemic amyloidosis (SSA), familial amyloidotic polynuropathy (FAP), and familial amyloidotic cardiomyopathy(FAC) (159). Amyloidosis is a condition in which proteins undergo a conformational change in their tertiary structure thereby making them insoluble fibrous protein aggregates that accumulate in organs and are believed to play a role in various other neurodegenerative diseases such as AD and

PD (160). SSA is a cardiac disease characterized by TTR deposits in the heart that affects 25% of the population over the age of 80. Wild type (WT) TTR has a residue at Cys10 that is capable of forming a mixed disulfide with either GSH (TTR-GSH), or Cys (TTR-Cys), or which becomes oxidized and forms a protein sulphonic acid (TTR-SO_3H)(159). Studies have demonstrated that TTR-GSH and TTR-Cys are associated with amyloidogenesis rates that are much faster than WT TTR, whereas TTR-SO_3H has a slower rate of amyloidogenesis under mildly acidic conditions (pH 4.4 – 5.0) (159).

The other two amyloid diseases are genetic and are characterized by point mutations whereby Val is replaced by Met at position 30 (TTR V30M) in FAC, and by Ile at position 122 (TTR V122I) in FAP. In a recent study in transgenic mice, expressing human WT, TTR V30M, and C10S/V30M (double mutant that lacks the ability to form a disulfide at Cys-10 but still contains the same mutation at V30M), only the TTR V30M mice revealed amyloidosis (161). It is probable that TTR undergoes a conformational change in V30M and V122I isoforms that increases access to Cys-10 thereby increasing the probability of forming a mixed disulfide. These data demonstrate that familial TTR amyloidosis is related to the accumulation of Cys-10 mixed disulfides and helps to explain the incomplete clinical expression of familial amyloid disease (161).

1.3.3.3 Peroxides, Peroxidatic Cysteines, and the Peroxiredoxin Family

Peroxiredoxins (Prx) reduce peroxides by a catalytic mechanism whereby the redox-active Cys, which is the peroxidatic Cys (Cys_P-SH) in the active site of Prx becomes oxidized by a peroxide substrate forming Prx-SOH (reversible), or is further oxidized to Prx-SO_2H (reversible), or Prx-SO_3H (irreversible) (162, 163). Mammalian cells express six isoforms of Prx (Prx1-6), which are classified into three subgroups (2-

Cys, atypical 2-Cys, and 1-Cys) based on the number and position of Cys residues that participate in catalysis (164). All Prx subgroups involve the nucleophilic attack on the Cys_P-SH which forms Cys_P-SOH and creates Prx-SOH; however the recycling of Prx-SOH back to Prx-SH is what distinguishes the three enzyme classes (Fig. 1.7) (165).

The 2-Cys subgroup includes Prx1-4, which exist as homodimers and have conserved N and C terminal Cys residues that are separated by 121 amino acid residues (164). Upon oxidation of typical 2-Cys Prx, Cys_P-SH which is located on the N terminus forms Cys_P-SOH (Prx-SOH) (166). Prx-SOH undergoes a conformation change thereby bringing Cys_P-SOH closer to the resolving Cys (Cys_R-SH) located on the C terminal of the other 2-Cys subunit, so that Cys_P-SOH forms a disulfide bond with Cys_R-SH thus forming Prx-S-S-Prx, a homodimeric protein disulfide (70). The disulfide bond in Prx-S-S-Prx is subsequently removed as the Trx system (Trx, Trx-Rx, and NADH) reduces the homodimeric protein disulfide intermediate thereby creating Prx-SH homodimers (164). At this stage the Cys_P-SH is non-reactive due to shielding (70). The Prx-SH homodimers oligomerize to form penta-homodimers, this decamer however is unstable and breaks apart forming Prx-SH homodimers that have undergone a conformational change that increases the reactivity of the Cys_P-SH thus forming typical 2-Cys-Prx (167, 168).

Prx can undergo "hyperoxidation" whereby Cys_R-SH forms Cys_R-SO_2H (a reaction that can be reversed by Srx) or Cys_R-SO_3H (a reaction that is irreversible) (164). The presence of H_2O_2 alone is not sufficient to cause oxidation of Cys_R-SH to Cys_R-SO_2H. The presence of complete catalytic components (H_2O_2, Trx, Trx-Rx, and NADPH) is required, indicating that such hyperoxidation occurs only when Prx I is engaged in the catalytic cycle (166). Prx-SOH is a stable structure that will not oxidize

Figure 1.7: Mechanism for Recycling Peroxiredoxins (Prx). The common first step of peroxide reduction involves the nucleophilic attack by the peroxidatic cysteine (S_P^-) of a Prx and the formation of the cysteine sulfenic acid intermediate (S_POH) *(A)*. In typical 2-Cys Prx, oxidation forms S_POH, however under hyperoxidized (large excess of peroxide) conditions, irreversibly oxidized S_PO_3H can form directly from S_P^-. S_pOH is a highly reactive intermediate and readily reacts with any accessible thiol to form a disulfide or in the presence of strong oxidizing agents, rapidly undergoes further oxidation with oxidants such as H_2O_2 to form the sulphinic acid (S_pO_2H), and sulphonic acid (S_pO_3H). Formation of the disulfide bond requires S_POH to undergo a conformational change thereby bringing S_POH closer to the resolving cysteine (S_R) of the other subunit of the 2-Cys Prx thus forming a homodimeric protein disulfide. As the formation of the homodimeric protein disulfide requires a conformational change, it can only occur at low oxidation levels, otherwise S_POH will oxidize into S_PO_2H, and can form S_PO_3H in hyperoxidized conditions. (Due to the conformational change that is required to form the disulfide in peroxiredoxin, S_PO_2H and S_PO_3H are formed directly from SPOH and the process does not involve a disulfide intermediate. Thus SPOH is essential in the biologically reversible portion of the disulfide proteome.) Sulfiredoxin (Srx) reduces S_PO_2H of some Prx back into S_POH, but oxidation into S_PO_3H is irreversible. The homodimeric protein disulfide is reduced by Thioredoxin (Trx) thus removing the intermolecular disulfide and forming a Prx homodimer with a nonreactive peroxidatic cysteine (S_PH). This Prx homodimer oligomerizes to form homopentamers. However, this decamer product is unstable and breaks apart forming Prx homodimers with a S_p^- *(B)*. In atypical 2-Cys Prx which do not exist as a homodimer, the S_p^- condenses with the S_R on the same subunit to form an intramolecular disulfide bond. This intramolecular protein disulfide is reduced by Trx back into S_PH which subsequently oxidizes into S_p^- *(C)*. The specific mechanism for 1-Cys Prx which has no S_R has yet to be elucidated. It is theorized that one donor thiol forms a transient mixed disulfide bond with the enzyme, followed by its reduction by a second donor thiol, thus recycling the enzyme *(D)*. In the figure, solid black lines indicate the predominate recycling pathway. Red lines indicate the hyperoxidized product of Prx.

Abbreviations: nonreactive protein peroxidatic cysteine, S_pH; peroxiredoxin, Prx; peroxidatic cysteine, S_p^-; resolving cysteine, S_R; sulfiredoxin, Srx; sulfenic acid intermediate, S_POH; sulfinic acid intermediate, S_PO_2H; sulphonic acid intermediate, S_PO_3H; thioredoxin, Trx; unknown thiol, ?.

Adapted from (70, 165).

A

B Typical 2-Cys Prx

C Atypical 2-Cys Prx

D 1-Cys Prx
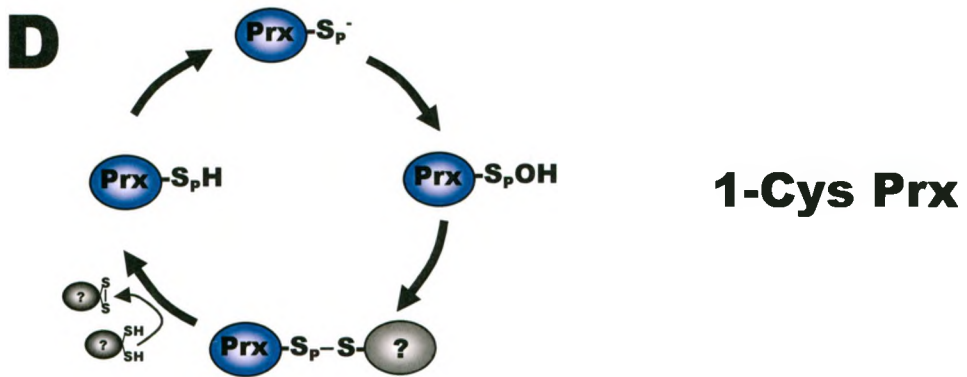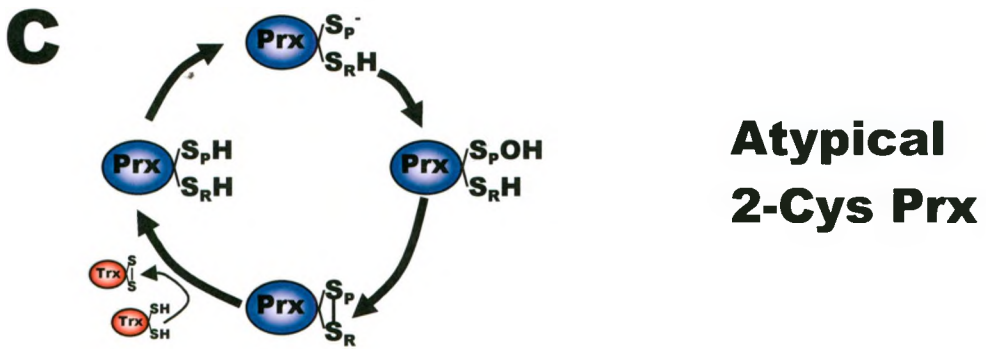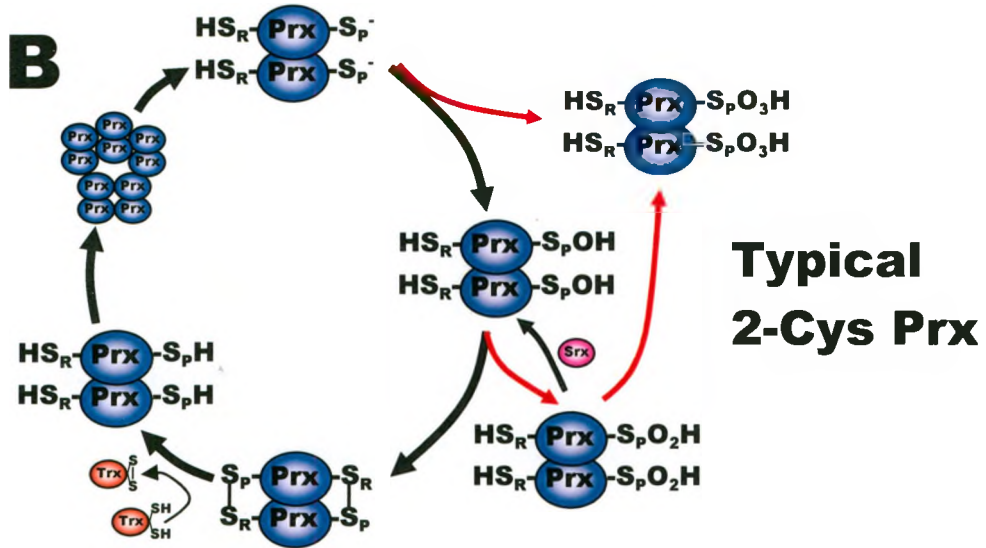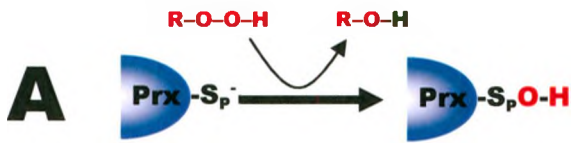
further due to the sulfenate oxygen being buried deep within the molecule (165). Hyperoxidation is believed to occur when Prx-SOH undergoes a conformational change (allowing Cys_P-SOH and Cys_R-SH to be brought close together so that they can create a disulfide bond) exposing the sulfenate oxygen in the presence of a strong oxidizing environment which hyperoxidizes Cys_R-SOH into Cys_R-SO_2H or Cys_R-SO_3H (165).

Recent studies performed on *Saccharmocyes cerevisiae* have demonstrated that the irreversible hyperoxidizded form of Prx3, Prx3-SO_3H is not an autoxidation product of Prx3-SO_2H (163). The Prx3-SO_3H multimer lost its peroxidase activity, however it gained 4-fold higher chaperone activity compared with Prx3-SH, the longest of all Prx3 molecular chaperones among the Prx3 redox forms in yeast cells (163). The study concludes that Prx3-SO_3H can be used as a molecular marker of cumulative oxidative cells as it has a half-life of more than two doubling times in yeast, is not an autoxidation product of Prx3-SO_2H, and is an irreversibly hyperbolized product that is not degraded by proteolytic systems as is the case with other irreversibly oxidized proteins in cells (163).

Typical 2-Cys Prxs are considered the first class of Prxs and include Prx1-4. Prx1 and Prx2 are both cytosolic proteins where the Cys_P-SH is Cys51 and the Cys_R-SH is Cys172 (166, 169, 170). Prx2 is one of the most abundant proteins in erythrocytes after hemoglobin, and is the major peroxiredoxin in Jurkat Cells (169). Prx3 is present in mitochondria with Cys_P-SH at Cys47 and Cys_R-SH at Cys170 (171, 172). Prx4, the largest of all Prx is a cytosolic protein with Cys_P-SH at CysXX and Cys_R-SH at CysXX

Atypical 2-Cys Prxs, the second class of Prxs, include Prx5 which is found in both the Mit and cytosol (165). Like typical 2-Cys Prx, atypical 2-Cys Prx require two Cys residues to perform their catalytic activity (164). In atypical 2-Cys Prx, Cys_P-SH is

conserved and is located at Cys47 while Cys_R-SH is unique and located at Cys151. Additionally, the distances between the Cys residues is substantially smaller than the 121 residues that separate the two conserved residues in typical 2-Cys Prx enzymes (173, 174). Atypical 2-Cys Prx is functionally monomeric with Cys_P-SH and Cys_R-SH located on the same polypeptide, with the condensation reaction resulting in the formation of Prx-SS, an intramolecular protein disulfide bond (173).

1-Cys Prxs, the third class of Prxs, include Prx6 which is found in the cytosol (165). Like the other two subclasses, 1-Cys Prx has a conserved N terminal Cys_P-SH found at Cys47, however it has no Cys_R-SH (175). After Cys_P-SOH is formed, no subsequent inter/intra molecular disulfide bond is formed (175). It is believed that one donor thiol probably forms a transient mixed disulfide bond with the enzyme, followed by its reduction by a second donor thiol, thus recycling the enzyme (165).

1.3.5 *S*-Glutathionylated Proteins in Human Diseases

GSH deficiency or a decrease in the GSH:GSSG ratio manifests itself largely through an increased susceptibility to oxidative stress, and the resulting damage is thought to be involved in diseases such as cancer, PD, and AD. Overproduction or underscavanging of ROS can irreversibly oxidize PS^- into PSO_2H and PSO_3H. This irreversible oxidation eliminates thiol-dependent signaling mediated by *S*-glutathionylation, the reason that salvation of 2-Cys peroxiredoxins by sulfiredoxin is such an important biological activity. *S*-glutathionylation (or lack of) is implicated in a variety of diseases, with many patients exhibiting impaired protein function, or impaired signaling that affects the activation or deactivation of multiple proteins (98). The key question when addressing the significance of *S*-glutathionylation in human diseases is

whether *S*-glutathionylation is a cause or a result of a particular disease process. It is important to demonstrate that *S*-glutathionylation is related to altered function and not simply a parallel event, and that a positive correlation exists between altered protein function and development of disease (119). Many studies suggest that oxidized proteins are the link between oxidative stress and disease, and *S*-glutathionylation is an indication of oxidative stress (119). The more proteins that are *S*-glutathionylated, the greater the oxidative stress. When GSH is depleted, more severe non-reversible oxidation to protein sulfinic and sulphonic acids occurs. Many contemporary studies demonstrate that reactive cysteine thiol residues of specific proteins are oxidized in different tissues or cells during the development of specific diseases (119). Further studies are likely to clearly demonstrate the correlation between *S*-glutationylation and the development of disease.

S-Glutathionylation of hemoglobin has been analyzed in some diseases as a marker of whole-body oxidative stress (119). Studies performed *in vitro* demonstrate that *S*-glutathionylation of hemoglobin (Hb) increases its oxygen affinity and may play an important role in maintaining hemoglobin structure and function (176, 177). Glutathionylated Hb (G-Hb) is produced in normal and sickle cells and has been found to inhibit the sickling of 70% of red blood cells at 21 mm Hg in individuals with sickle cell anemia (178). Sickling decreases the cells' flexibility due to a point mutation in the β-globin chain of hemoglobin that causes Glu to be replaced with the hydrophobic amino acid Val. This single amino acid change causes a structural change with deoxygenated Hb causing Hb proteins to form fibers between one another resulting in decreased solubility that results in an increase in heme-heme interactions and the polymerization of hemoglobin. This change is linked to various complications (178). GSH forms a

disulfide bond with Hb at Cys-β93 (178, 179). Deoxygenated G-Hb has a high oxygen affinity, reduced heme-heme interactions, and diminished polymerization due to (1) a structural change of the tertiary pocket of the β chain; (2) elimination of the salt bridge between His-β146 and Asp-β94; and (3) stabilization of the interaction between deoxygenated Hb at Asp-$\beta_2$99 and Tyr-$\alpha_1$42 (179).

In addition to individuals with sickle cell anemia, people with Friedreich's ataxia, an autosomal recessive neurodegenerative disease accompanied by significant decrease in intracellular GSH:GSSG ratio and a decrease in reduced GSH have a significant increase in S-glutathionylated hemoglobin (123, 180). Increased levels of S-glutathionylated hemoglobin have also been found in smokers, and patients suffering from type I and type II diabetes mellitus, conditions characterized by oxidative stress (181-183). A large percentage of the proteins that make up the human eye lens contain thiols susceptible to oxidation; hence GSH is present in very high concentrations in the lens (119). The GSH pool diminishes as the lens ages, and in aging human lenses, there is well documented evidence pertaining to the increase in S-glutathionylation of protein sulfhydryl groups (184, 185). HIV-infected cells suffer from oxidative stress, have a decreased GSH:GSSG ratio, and form PSSG. However, the ability of these cells to reduce PSSGs to PS$^-$ and GSH is severely diminished unless the GSH precursor N-acetylcysteine (NAC) is restored to the level of that in uninfected cells, to enhance GSH biosynthesis (186, 187). These findings are in agreement with previous data that demonstrate that NAC raises GSH levels in lymphocytes from AIDS patients (187).

Alzheimer's is a protein conformational disease or protein conformational disorder in that the Tau protein undergoes polymerization forming a paired-helical

filament instead of assembling into straight filaments, as a result of S-glutathionylation (188). As patients with AD have a low PSH:PSSG ratio, the reduced Tau monomer (PSH) is oxidized by PSSG thereby regenerating PSH and increasing PSH:PSSG ratio; this however produces Tau-SSG which forms paired-helical filaments resulting in the gain of a toxic activity (188, 189). It is believed that this paired-helical filament formation may be relevant to the mechanisms of Tau dysfunction and AD neuropathology (190, 191). Furthermore patients with AD have decreased PSH levels in their hippocampus, a vulnerable region of the brain. This suggests that insufficient induction of protective antioxidant gene response may contribute to the accumulation of oxidatively modified proteins in the AD brain (192). Additionally, specific proteins that are well known to have redox regulated reactive cysteine thiol residues (Cys149, 153, 244 and 281) in glyceraldehyde 3-phosphate dehydrogenase (GAPDH) (193) and Cys118 and 388 in α-enolase (194)) are also targets of S-glutathionylation in AD patients resulting in reduced activity of both these enzymes in the brain (195).

1.3.6 The Disulfide Proteome and Human Diseases

Many proteins undergo post-translational modification via well defined mechanisms such as acetylation, phosphorylation and glycosylation and thereby control a spectrum of biochemical processes. A growing body of evidence has demonstrated that the reversible reduction of disulfide bonds also alters the structure and activity of proteins (196). Mild oxidant exposure can result in irreversible oxidation of protein reactive cysteine thiols in the absence of GSH, resulting in the formation of PSO_2H/PSO_3H and/or leading to excessive disulfide bonding, protein misfolding, and aggregation, as in AD

(197). A number of studies have demonstrated that GAPDH plays an active role in various forms of apoptosis and may participate in neuronal death in patients with HD, PD, or AD (198-200). The pro-apoptopic role of GAPDH appears to depend upon its accumulation in the nucleus, and although the specific mechanism has yet to be determined it is believed that disulfide bonding contributes towards this toxicity, however future studies are required to validate this (141, 201).

Recent studies have demonstrated that the accumulation of disulfide-linked GAPDH results in an insoluble conformation within neurons, and this bonding is strongly associated with the pathophysiology of AD (141). The authors of that study suggest that aberrant disulfide bond formation of only a small fraction of an aggregate-prone protein can, via a nucleation process, hasten protein polymerization and aggregation (141). Disulfide bonding of only a fraction of GAPDH in AD brains may act as a seed leading to insolubility and further aggregation of GAPDH monomers via a disulfide-independent mechanism (141). Even more likely is the heterodimeric oligomerization of multiple proteins containing reactive cysteine protein thiol residues, and this could serve as a common mechanism for the initiation and progression of oxidative stress-mediated diseases.

CHAPTER 2: HYPOTHESIS AND OBJECTIVES

2.1   Hypothesis

UCB, the end product of heme catabolism is an important physiologic antioxidant at nM concentrations, but becomes a pro-oxidant at μM concentrations by increasing the release of reactive oxygen species (ROS) from mitochondria (46). Earlier work in our laboratory utilizing redox sensitive green fluorescent protein (roGFP2) which was transfected into Hepa 1c1c7 cells established that 50 μM UCB resulted in irreversible oxidation of the cytosol, whereas treatment with 70 nM UCB showed a pronounced reduction in the cytosol (Oakes and Bend, pending publication).   The higher concentration (50 μM) of UCB resulted in oxidation of the cytosol within 30 min, that was partially reversed at 2 h, followed by subsequent and significant oxidation at 3 h, deemed to be irreversible, as it persisted beyond the course of the experiment (6 h). Since there was no reversal of this oxidation of the cytosol during the course of the experiment it was assumed to be irreversible. The much lower concentration of UCB studied (70 nM) showed a pronounced reduction of the intracellular compartment within 30 min, which persisted for 6 h, indicating a prolonged antioxidant effect of this concentration on the cellular compartment.

The hypothesis underlying this research is that changes to the disulfide proteome due to irreversible and perhaps reversible protein oxidation are the cause of or a major contributor to UCB-mediated toxicity. We believe that toxic levels of UCB affect the redox status of the cell which in turn causes post-translational modification of proteins with reactive cysteine thiol residues (PS⁻; ionized at physiological pH) by intracellular

formation of protein mixed disulfides with glutathione (PSSG), termed *S*-glutathion-ylation, a reversible change, or of homodimeric (P^1SSP^1), heterodimeric (P^1SSP^2), or oligomeric protein disulfides ($(PSSP)_n$) in the absence of glutathione (GSH). The latter, along with the formation of protein sulfinic (PSO_2H) and sulphonic (PSO3H) acids are normally irreversible changes. Such reversible and irreversible changes in post-translational modification can affect cell signaling and survival. To re-emphasize, *S*-glutathionylation of proteins is reversible and dependent upon the redox status of the cell, which can vary from one subcellular compartment to another.

2.2 Specific Objectives

The primary objective of this thesis is related to the analysis of changes in the disulfide proteome in Hepa 1c1c7 cells due to reversible and irreversible protein oxidation as a result of concentration-dependent treatment of cells with UCB.

To achieve this, this project is designed with the following specific aims:

1. Demonstrate how redox one-dimensional polyacrylamide gel electrophoresis (R1D-PAGE) visualizes the post-translational modification of proteins with PS⁻ that are known to undergo reversible oxidation.

2. Determine whether redox two-dimensional polyacrylamide gel electrophoresis (R2D-PAGE) is a reliable and reproducible method for determining the post-translational modification of proteins with PS⁻.

3. Implement a method that would allow analysis of cellular proteins by R2D-PAGE accurately with many concomitant replicates without having to resort to custom made machinery.

4. Determine the changes that occur in the disulfide proteome of mitochondrial, microsomal, and cytoplasmic fractions in Hepa 1c1c7 cells as a result of treatment with pro-oxidant (50 μM) or anti-oxidant (70 nM) concentrations of UCB by utilizing R2D-PAGE.

5. Analyze and identify a few specific proteins that are redox regulated following treatment with UCB utilizing matrix assisted laser desorption/ionization (MALDI) mass spectrometric (MS) analysis of tryptic digests of proteins isolated from R2D-PAGE gels.

CHAPTER 3: MATERIALS AND METHODS

3.1 Chemicals and Reagents

All solutions and reagents were prepared using Milli Q water unless otherwise indicated. Specific composition and suppliers for all solutions and reagents can be found in Appendix I.

3.2 Cell Culture, Treatment, and Lysis

3.2.1 Cell Culture

Mouse hepatoma Hepa 1c1c7 cells (ATCC No. CRL-2026) were generously provided by Dr. O. Hankinson (University of California, Los Angeles, CA). These cells were grown in minimum essential medium (Invitrogen, Grand Island, NY) supplemented with 10% FBS (Gibco, Grand Island, NY) (final concentration of 40 μM), 20 μM L-glutamine (Gibco, Grand Island, NY), 50 μg/mL gentamycin sulfate (Gibco, Grand Island, NY), 100 IU/mL penicillin (Gibco), 10 μg/mL streptomycin (Gibco), and 25 ng/mL amphotorecin B (ICN Biomedicals, Aurora, OH). The medium was prepared in advance and stored at -20 °C prior to use.

3.2.2 Cell Treatment

Cells were routinely grown in 75 cm^2 tissue culture flasks at 37 °C in a 5% CO_2 humidified environment. For experiments, cells were seeded and cultured for 24 h before being treated with either 70 nM unconjugated bilirubin (UCB) or 50 μM UCB for 0.5 - 6 h. Vehicle control cells were treated under identical conditions with the corresponding

0.1 M NaOH in PBS vehicle. UCB stock solution (4.4 mM) was prepared in a subdued light environment by dissolving 2.3 mg UCB (Poryphyrin Products, Logan, UT) in 0.2 mL 0.1 N NaOH, followed by addition of 0.8 mL 10 mM phosphate-buffered saline solution, ph 7.4 (138 mM NaCl, 2.7 mM KCl, Sigma, St. Louis, MO). The UCB solution was prepared freshly each day, just prior to use.

After treatment with UCB for various times, cells were scraped from the flasks and centrifuged for 3 min at 500 x g. The media was normally discarded and pelleted cells were washed with 30 mL ice cold PBS. Cells were centrifuged once again for 3 min at 500 x g after which the supernatant layer was discarded.

3.2.3 Cell Lysis

For cells where the disulfide proteome was evaluated, ice cold PBS (10 mL) containing 40 mM IA was added to the cells that were maintained on ice for the entire process for 5 min. After 5 min, tubes were spun gently for 3 min at 500 x g, and the supernatant fraction was discarded. PBS containing 40 mM IA (500 µL) was added to the pellet, and the pellet was transferred to a 1.5 mL centrifuge tube. PBS with 40 mM IA (200 µL) was used to rinse down any residual cells from the side of the original tube, and then solution plus cells transferred to the 1.5 mL tube. The centrifuge tube containing the cells from the pellet was spun for 3 min at 500 x g, the supernatant discarded, and 500 µL lysis buffer (1 protease inhibitor cocktail tablet (Roche Diagnostics, Indianapolis, IN) was added to 7 mL RIPA buffer and the solution stored at -20 °C prior to use) containing 40 mM IA were added to the pellet to prevent post-lysis oxidation of protein cysteine residues. The cell pellet was carefully homogenized with a

hand held homogenizer, vortexed, and placed on ice for 10 min, and then snap frozen in liquid nitrogen until further analysis.

3.2.4   Subcellular Fractionation of Lysed Cells

Lysed cell pellets were either freshly prepared or carefully thawed (see above) on ice, and centrifuged for 10 min at 700 x g to obtain the nuclear pellet. The 600 x g supernatant fraction (nuclear supernatant) was transferred to another tube and centrifuged for 20 min at 10,000 x g to obtain the mitochondrial pellet. The 10,000 x g supernatant fraction (mitochondrial supernatant) was transferred to another tube and centrifuged for 1 h at 100,000 x g to obtain the microsomal fraction. The 100,000 x g supernatant fraction (cytosol) was retained. The mitochondrial and microsomal pellets were individually resuspended in 50 μL 0.1 M KP buffer. The resuspended mitochondrial pellet was sonicated on ice with a Sonic Dismembrator (Fisher Scientific, Hampton, NH) four times with a 5 s pulse and a 30 s pause between each pulse, to break the mitochondrial membranes.

The protein concentration of all subcellular fractions prepared was determined using the Lowery Assay with BSA as a protein standard. An equal volume of non-reducing 2X SDS sample buffer (80 mM tris (JT Baker, Phillipsburg, NJ), 140 mM SDS (JT Baker), 1.1 M glycerol (BDH, Toronto, ON), and 0.75 mM bromophenol blue (Bio-Rad, Hercules, Ca) was added to each sample fraction, and samples were stored at -20 °C until analyzed. SDS Sample buffer was free from any reducing agents, and samples were not boiled before loading into gels.

3.3   Redox Two-Dimensional Polyacrylamide Gel Electrophoresis (R2D-PAGE)

Protein fractions were resolved by R2D-PAGE using a Protean II vertical electrophoresis system (Biorad, Hercules, CA) in the first dimension, and Protean Plus Dodeca Cell (Biorad, Hercules, CA) in the second dimension.   R2D-PAGE was performed using a modified version of the method described by Cumming and his colleagues (202).

3.3.1   Casting R2D-PAGE Gels

Glass plates (20 x 22 cm) were scrubbed thoroughly with Extran MN 01 phosphate free rinsable detergent (VWR, Westchester, PA), placed overnight in an acid bath (0.2 M HCl), washed with distilled water, and scrubbed one last time with 100% methanol.   Residual methanol was air dried or removed with lint free Kimwipe tissues (Kimberly-Clark, Irving, TX).   Assembling and pouring the gel mixture for 1.0 mm thick polyacrylamide gels used for the first dimension involved a series of plastic spacers of different widths placed alongside one another as demonstrated in Fig. 3.1.   The 1.5 mm thick gel used in the second dimension were assembled in a typical manner.

The 12.5% gel mixture (composed of distilled water, 1.5 M tris, ph 8.8, 10% SDS, 30 % bis-acrylamide, 10% APS and TEMED) was poured to a length of 13 cm from the bottom of the plate for the 1.0 mm thick first dimension gel, and 18 cm from the bottom of the plate for the 1.5 mm thick second dimension.   Gels were overlaid with 0.1% SDS solution to evenly flatten the gels, and allowed to polymerize at room temperature for 1 h. After the resolving gel hardened, the SDS solution was poured off, and the gel was washed twice with distilled water.   The 4% stacking gel mixture (composed of distilled

Figure 3.1: Assembling Redox Two-Dimensional Polyacrylamide Gel Electrophoresis (R2D-PAGE) Gels. Assembling the 1.0 mm first dimension R2D-PAGE gel involved eight 1.0 mm thick (1.8 cm wide) spacers (grey) placed alongside six 0.5 mm thick (0.9 cm wide) spacers (light grey) onto a 20 x 22 cm outer glass plate *(A)*. 20 x 20 cm inner glass plate was placed on top of spacer formation and firmly secured against outer plate with gel sandwich clamps (black) *(B)*. Inside lying 1.0 mm thick spacers were raised 0.5 cm to allow an even length for all of the gel slabs when pouring gel mixture and secured against outer glass plate with paper clasps (red) *(C)*. Glass plates were raised to allow 0.5 mm thick spacers to fall outside of the gel sandwich leaving a 0.9 cm wide space (white) between the 1.0 mm thick spacers *(D)*. Gel sandwich was secured in gel casting gel and separating gel mixture (blue) was slowly poured above the 0.9 cm space that was furthest to the right until all the 0.9 cm spaces were filled to a length of 13 cm from the bottom of the glass plate. 100 µL of 0.1% SDS (pink) was poured above each 0.9 cm space to flatten the gel, and gel was left to harden *(E)*. After the separating gel mixture hardened into a gel 0.1% SDS was poured off and resolving gel mixture (light blue) was slowly poured above the separating gel. 3 mm wide individual teeth from a gel comb (gold) were inserted on top of the separating gel mixture and secured with paper clasps *(F)*. After the resolving gel mixture has hardened into a gel comb teeth and paper clasps were removed from the gel sandwich, and the gel sandwich was removed from the casting stand. The 1.0 mm thick first dimension R2D-PAGE gel is ready to run 6 samples in the first dimension. Image of 1.0 mm thick, first dimension R2D-PAGE gel *(G)*. Assembling the 1.5 mm second dimension R2D-PAGE gel involved pouring the separating gel mixture (blue) between two 1.5 mm spacers (dark grey), and inserting a second dimension gel comb with reference a well. Image of 1.5 mm thick, second dimension R2D-PAGE *(H)*.
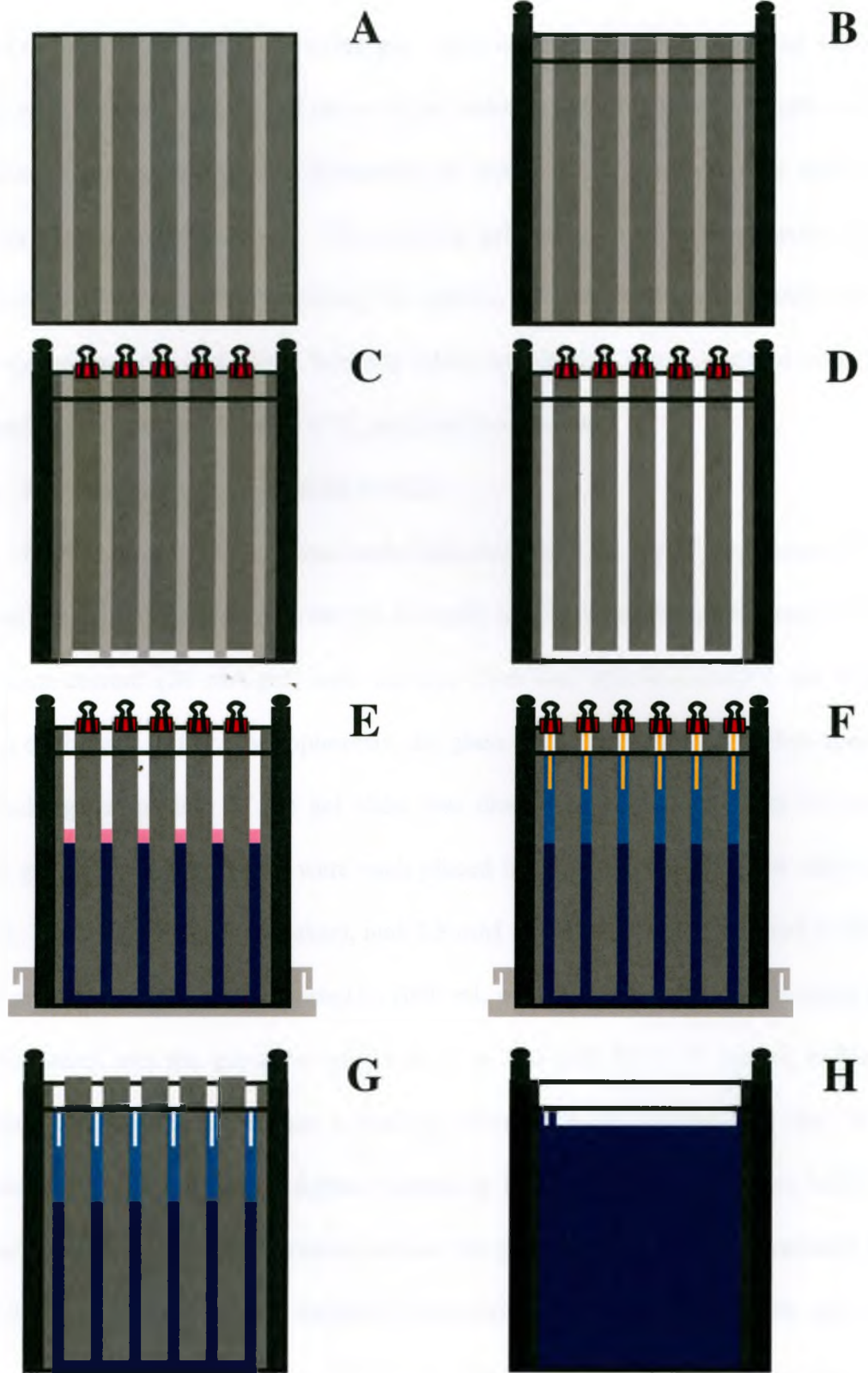
water, 0.5 M tris, ph 6.8, 10% SDS, 30% bis-acrylamide, 10% APS, and TEMED) was poured on top of the 12.5% resolving gel. Individual teeth (3 mm wide) of Teflon gel combs were inserted into the 0.9 cm wide gel slabs for the first dimension gels, and a 14 cm wide, 1.5 mm thick second dimension gel comb with 3 mm reference marker was used for the second dimension. The stacking gel was allowed to polymerize at room temperature for 1 h. After removing the combs, the gels were subsequently removed from casting stands, embedded between tissue towels that were saturated with water, wrapped in saran wrap, stored at 4 °C, and used the next day.

3.3.2 Running Proteins with R2D-PAGE

Protein sample (75 μg) was loaded into each well for the 1st dimension. The gel was run for 1 h at a constant current (16 mA/gel), and then run for approximately 3.5 h at a constant current (24 mA/gel) until the dye front was approximately 1 cm from the bottom of the gel. After electrophoresis, the glass plates were carefully taken apart, and the stacking gel portion of the gel slabs was discarded leaving an intact 13 cm long 12.5% gel slab. The gel slabs were each placed in 1X running buffer (24 mM tris (JT Baker), 192 mM glycine (JT Baker), and 3.5 mM SDS (JT Baker) dissolved in 800 mL water, and final volume was adjusted to 1000 mL with water) briefly. The running buffer was discarded, and the gel slabs were soaked in 100 mM DTT 2X sample buffer with reducing agents and placed on a rocking table at room temperature for 20 min. Immersing the gel slab in a solution containing 100 mM DTT 2X sample buffer with reducing agents ensures that proteins within the gel slab are completely reduced (203). After 20 min, the gel slab was washed 3-times briefly in 1X running buffer, and the gel slabs were soaked in 100 mM IA 2X SDS sample buffer and rocked at room temperature

for 10 min. Immersing the gel slab in 100 mM IA 2X sample buffer ensures that any free or oxidized thiols (PSH or PS⁻) are bound to IA and do not form subsequent disulfide bonds during the running of the gel in the second dimension. After 10 min, the gel slab was washed 3-times briefly in 1X running buffer and was ready to be run in the second dimension.

Prior to overlaying the gel slab over the 1.5 mm gel for the second dimension, the 1.5 mm gel was rinsed with water to ensure that no acrylamide residue used during casting was present in the gel. Running buffer (1 mL) was added across the lengths of the reference well in the 1.5 mm gel to ensure that the top of the gel was well lubricated so as to allow the 1.0 mm gel slab to easily slip onto the 1.5 mm gel. The gel slab was carefully lifted and laid on top of the second dimension gel ensuring that the side containing the loading dye was placed closest to the lane containing the reference marker. After ensuring that the gel strip was in complete contact with the second dimension gel, excess running buffer was carefully removed from with the gel. The molecular weight marker ladder (3 μL) prepared according to Manufacturer's instructions (low range silver stain SDS-Page Standard, Bio-Rad, Hercules, Ca) was loaded into the reference well. Freshly heated and dissolved 2% agarose overlay solution (1 mL) was laid on top of the wells, and the overlay solution was let to harden for 10 min.

For the second dimension, gels were run overnight at a constant current (10 mA/gel) until the dye front was approximately 1 cm from the bottom of the gel. After the gel had run to completion, the gel apparatus was dissembled and the gel was transferred to a Protean Dodeca Stainer (Bio-Rad) for silver staining.

3.4   Silver Staining of R2D-PAGE Gels

A mass spectrometric protein analysis compatible silver staining technique was adapted from Schevenko and colleagues (204). Gels were first placed in fixer solution (500 mL methanol (EMD Chemicals, Gibbstown, NJ) and 50 mL acetic acid (EMD Chemicals, Gibbstown, NJ) dissolved in 450 mL of water) for at least 30 min or stored at 4 °C for up to a week. Fixer solution was poured off and gels were washed in washer solution (500 mL methanol dissolved 500 mL of water) for 10 min, and then rinsed in water twice for 10 min to remove the remaining acetic acid. Gels were sensitized to silver by incubating them for 5 min in freshly prepared and chilled sensitizing solution (0.8 mM sodium thiosulphate (EMD Chemicals, Gibbstown, NJ)), and were then rinsed with 2 changes of distilled water for 5 min each. After rinsing, the gel was submerged in freshly prepared and chilled staining solution (11 mM silver nitrate (EMD Chemicals, Gibbstown, NJ)) for 30 min. After incubation, the staining solution was discarded, and the gel slab was rinsed 2X with water for 0.5 min and then developed with freshly prepared and chilled developer solution (283 mM sodium carbonate (EMD Chemicals, Gibbstown, NJ), 0.05% 37% formaldehyde by volume (VWR, Westchester, PA), and 2% sensitizer by volume solution dissolved in water). After the developer began to lose transparency, it was discarded and replaced with a fresh portion of developer. The desired intensity of staining was achieved within 10 min, after which development was terminated by discarding the developer, followed by washing the gel with stop solution (5% acetic acid by volume dissolved in water) for at least 5 min. Gels were subsequently scanned or stored in storage solution (1% acetic acid by volume dissolved in water) at 4 °C until scanned.

3.5 Scanning R2D-PAGE Gels

Gels were scanned with an Epson Perfection 4990 Photo (Epson, Suwa, Japan), which contains a built-in transparency unit with a moving light source. This scanner facilitates scanning in the transmission mode to ensure accurate image retention. Transmission mode eliminates any background color from the images as light is not reflected against a reflector; instead light passes through the gel and is directly measured by the detector on the opposite side of the gel.

3.6 Identification of Proteins by Mass Spectrometry

Protein spot picking and in-gel digestion was performed at the London Regional Proteomics Centre, University of Western Ontario. Mass spectrometry (MS) analyses were performed at the MALDI Mass Spectrometry Facility (Department of Biochemistry, UWO). Protein spots on the gel that appeared off the prominent diagonal line were excised from the gel with the Ettan Spot Picker (General Electric Healthcare, Piscataway, NJ), and transferred into a 96 well plate for digestion. In-gel digestion with trypsin, and lyophilization were carried out with a Mass Prep Automated Digestor (Waters, Milford, MA). Lyophilized peptide samples were dissolved in 5 µL 10% acetonitrile, and 0.1% trifluoroacetic acid. Samples were then mixed at a 1:1 ratio with the matrix solution (5 mg/mL α-cyano-4-hydroxycinnamic acid in 6 mM ammonium phosphate monobasic solution), and 0.75 µL sample was spotted on a sample target in duplicate to acquire a matrix-assisted laser desorption/ionization (MALDI) MS spectra.

The MALDI MS spectra were acquired with a 4700 Proteomics Analyzer (Applied Biosystems, Foster City, Ca), converted into data with 4000 Series Explorer

software (Applied Biosystems, Foster City, Ca), and processed into a peptide mass fingerprint with Data Explorer software (Applied Biosystems, Foster City, Ca). Protein identification using the peptide mass fingerprint from a MALDI MS spectra was obtained using a GPS engine connected to a Mascot server provided by the software manufacturer. Peptide mass fingerprints were compared to known peptide mass sequences obtained from the NCBI database. Samples with a peptide mass fingerprint that had a protein score above 99% were predicted to identify a particular protein.

CHAPTER 4: RESULTS

4.1 Visualizing Post-Translational Modification of Proteins Upon Exposure to Oxidants

Redox two-dimensional polyacrylamide gel electrophoresis (R2D-PAGE) is an extension of the resolution of oxidized protein disulfides by redox one-dimensional polyacrylamide gel electrophoresis (R1D-PAGE). In R1D-PAGE, identical protein samples are run together with or without β-mercaptoethanol in the loading buffer so that proteins with intact disulfide bonds and those with reduced protein disulfide bonds are compared. β-mercaptoethanol in the loading buffer reduces protein disulfide bonds. This allows resolution of proteins that undergo post-translational modification by redox-regulation at reactive protein cysteine thiols (i.e. proteins with PS⁻). The presence of multiple protein bands within a lane is indicative of disulfide bonding that occurs with that protein.

4.1.1 Post-Translational Disulfide Bonding in Bovine Serum Albumin

To demonstrate the utility of R1D-PAGE analysis, bovine serum albumin (BSA), a protein capable of forming 17 intramolecular (PSS) and intermolecular oligomeric protein disulfides $(PSSP)_n$ due to the participation of 34 of its 35 PSH in intramolecular disulfide bonding and its single reactive cysteine thiol in intermolecular disulfide bonding was used. Oxidized BSA (Fraction 5; 500 pg) was incubated in reducing or non-reducing loading buffer for 10 min and subsequently run on 12.5% PAGE. Upon silver staining, distinct protein bands were visualized consistent with the formation of protein disulfide

bonds (Fig. 4.1A). Oxidized BSA that was reduced by treatment with β-mercaptoethanol in reducing buffer appears alongside a molecular marker of 66 kDa, the measured mol wt value of BSA. In non-reducing loading buffer, the oxidation state of BSA did not change, thereby allowing the visualization of PSS and $(PSSP)_n$. Oxidized BSA that formed PSS (intramolecular disulfide bonding) occurred at 54 kDa because reduction of these bonds causes proteins to compact and to migrate further down the gel. On the other hand, oxidized BSA that formed intermolecular disulfide bonds occurred in multiple molecular forms depending upon the degree of oxidation. Thus, protein disulfide bonds that were either dimers of BSA at 108 kDa, trimers at 164 kDa, tetramers at 216 kDa, or oligomers of even higher mol wt were observed on the gel after silver staining.

4.1.2 GAPDH Forms Intra- and Intermolecular Disulfide Bonds Upon Oxidation

R1D-PAGE analysis readily demonstrates how rapidly disulfide bond formation can occur within a biological system. Glyceraldehyde 3-phosphate dehydrogenase (GAPDH) is readily susceptible to oxidation at its active site reactive cysteine thiol (Cys149) at neutral pH, resulting in the formation of intramolecular or intermolecular disulfide bonds with other cysteine residues (Cys153 and Cys181). GAPDH (1 μg from *Saccharomyces cerevisiae*) was oxidized with 5 mM H_2O_2 for 5 min, and peroxidation was subsequently stopped with the addition of bovine Catalase (200 Units) for 5 min (Fig. 4.1B). Oxidized GAPDH was subsequently loaded in reducing or non-reducing buffer and run on PAGE alongside GAPDH controls, that had not been treated with H_2O_2. Upon silver staining, the apparent mol wt of GAPDH and Catalase in the control samples that were placed in reducing buffer was calculated to be 37 kDa and 60 kDa, respectively which is similar to that of their actual values of 36 kDa and 62.5 kDa.

Figure 4.1A: Disulfide bonding in Bovine Serum Albumin (BSA). Oxidized BSA (500 pg, fraction 5) was placed in reducing buffer (R) or in non-reducing buffer (NR) and subsequently run on PAGE to demonstrate the effect of protein disulfide bonding when evaluated by R1D-PAGE. Treatment of oxidized BSA with reducing buffer containing β-mercaptoethanol results in the formation of reduced BSA (BSA-S-H) that runs with an apparent molecular weight of 66 kDa, the measured mol wt of BSA. In non-reducing loading buffer, the BSA protein remains oxidized. Upon oxidation of BSA, intramolecular disulfide bonding occurred forming a BSA protein disulfide (BSA-S-S) which migrated further than the reduced protein (intramolecular disulfide bonding compacts the protein) . The apparent mol wt of the intramolecular BSA disulfide was calculated to be 54 kDa. Oxidized BSA also formed multiple homodimeric protein disulfide $(P^1SSP^1)_n$ bonds, with dimers at 108 kDa (BSA-S-S-BSA), trimers at 164 kDa (BSA-S-S-BSA-S-S-BSA), tetramers at 216 kDa ((BSA-S-S-BSA)$_2$), as well as higher oligomeric forms ((BSA-S-S-BSA)$_n$).

Figure 4.1B: Intramolecular and intermolecular disulfide bond formation of glyceraldehyde 3-phosphate dehydrogenase (GAPDH) upon oxidation. GAPDH (1 µg, *Saccharomyces cerevisiae*) was oxidized with 5 mM H_2O_2 for 5 min, and peroxidation was subsequently stopped with the addition of bovine catalase (200 Units) for 5 min. Oxidized GAPDH was run on PAGE alongside GAPDH and catalase controls in reducing buffer (R) as well as in non-reducing buffer (NR). GAPDH and catalase controls placed in NR, migrated quicker than did their counterparts placed in R. Oxidized GAPDH in R runs identically with the GAPDH control in R, demonstrating that the disulfide bonds have been reduced. Oxidized GAPDH in NR has a distinctive protein band with an apparent weight of 33 kDa that migrated more rapidly than the dominant GAPDH monomer (GAPDH-S-H) with a measured weight of 36 kDa. The 33 kDa band is indicative GAPDH forming an intramolecuar disulfide bond (GAPDH-S-S) due to oxidation. Other protein bands in oxidized GAPDH appear to be GAPDH homodimers (GAPDH-S-S-GAPDH) with an apparent weight of 75 kDa, or higher oligomers ((GAPDH-S-S-GAPDH)$_n$) with apparent mol wts above 100 kDa. The distinctive protein bands with apparent weights of 83 and 87 kDa are postulated to be GAPDH-catalase dimers (GAPDH-S-S-Catalase).

Abbreviations: GAPDH, glyceraldehyde 3-phosphate dehydrogenase; NR, non-reducing buffer; R, reducing buffer.
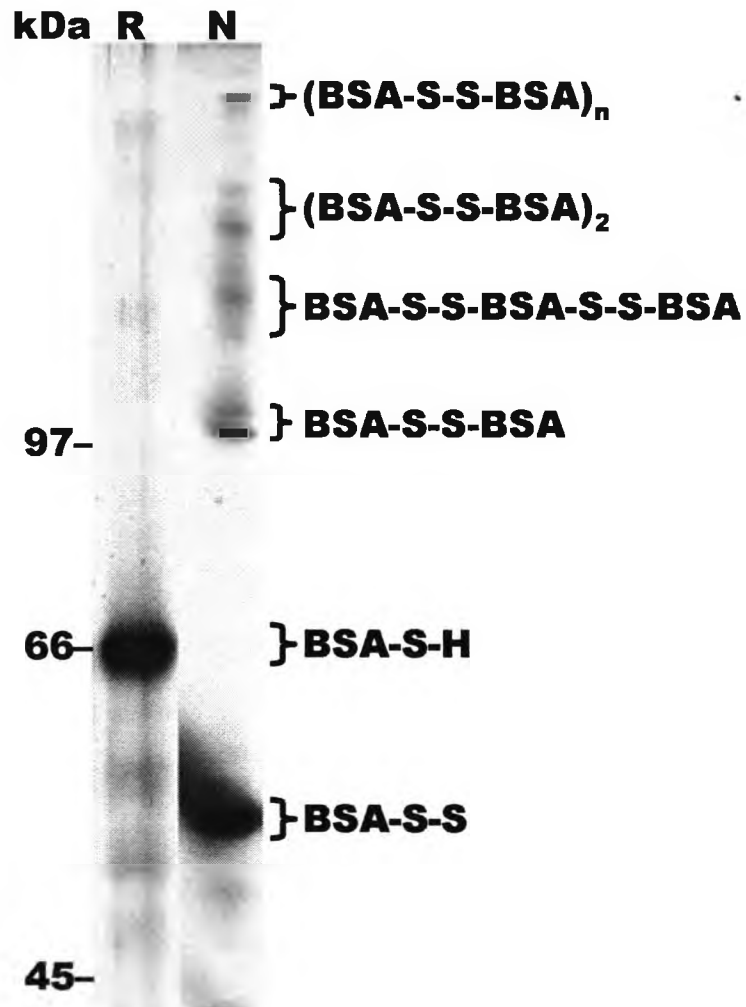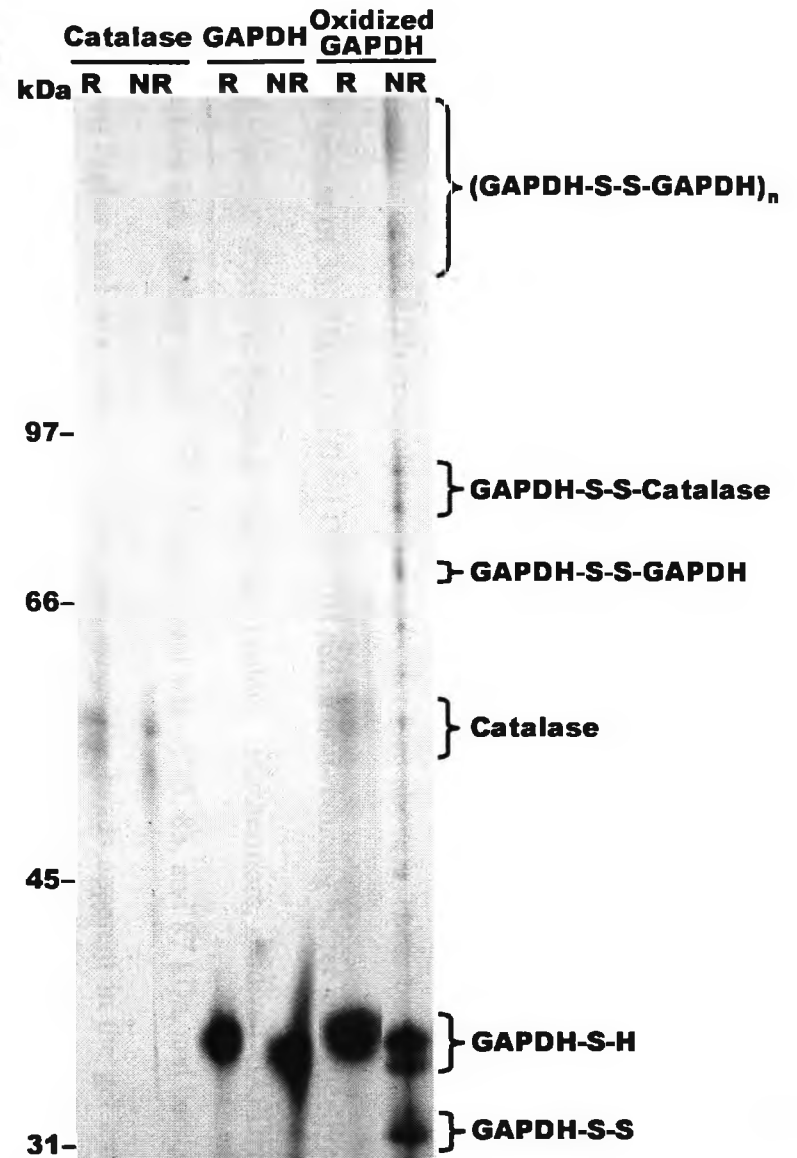
GAPDH and Catalase control samples that were placed in non-reducing buffer migrated quicker than did their counterparts placed in reducing buffer. Whether or not this is related to the reductant, sodium dithiothreitol that was used is unknown.

Oxidized GAPDH in non-reducing buffer contained distinct bands that were separated upon electrophoresis, some of which migrated faster than oxidized GAPDH in reducing buffer or GAPDH control in reducing buffer (see above). These bands with an apparent weight of 33 kDa in oxidized GAPDH run in non-reducing buffer are indicative of intramolecular disulfide bonding within the protein. Furthermore, oxidized GAPDH was resolved into distinct bands with apparent mol wts of 75, 83, and 87 kDa, and bands with even higher mol wts values. These slow migrating bands apparent in the gel are indicative of intermolecular disulfide bonding within the protein. The band with an apparent mol wt of 75 kDa is similar to the mol wt of dimeric GAPDH, whereas the bands with apparent mol wts of 83 and 87 kDa could correspond to a disulfide bond between GAPDH and Catalase. The bands with an apparent mol wt larger than 97 kDa are believed to correspond to higher oligomeric forms of GAPDH such as trimers, tetramers, or pentamers.

4.2 Live Cell Measurement of Intercellular Redox State with Mutated Green Fluorescent Protein (GFP) that Forms an Intracellular GFP Disulfide (Part of the Disulfide Proteome) Under Conditions of Mild (Reversible) Oxidative Stress

The novel mutated redox green fluorescent protein (roGFP2) plasmid can be transfected into cells. When this is done, the oxidation state of the expressed protein can be used to evaluate the overall redox status *in vivo* within the cytosol of a cell. This is a useful method for monitoring "reversible" and "irreversible" oxidative changes within the redox system of cells exposed to external oxidative stressors, such as *t*-butylhydroperoxide (TBHP) over a fixed period of time (205, 206). This technique is dependent upon a mutated GFP modified by the introduction of two Cys residues near the chromophore (S147C and Q204C) (Fig. 4.2A). Under oxidizing conditions, the two Cys residues form an intramolecular disulfide bond (PSSP) (Fig.4.2B) changing the conformational shape of roGFP2 by bending the chromophore. This structural change in the chromophore causes it to emit light (emission 530 nm) more readily when it is excited at 405 nm (oxidizied state of the protein) rather than 488 nm (the reduced state of the protein) (Fig. 4.2C). Therefore, the oxidative state of a cell can be measured *in vivo* continuously over time by live cell confocal microscopy as the formation of the GFP-GFP-disulfide under oxidizing conditions, results in markedly increased excitability at 405 nm and significantly decreased excitability at 488 nm.

Figure 4.2: Mutated redox green fluorescent protein (roGFP2) can visualize reduction-oxidation *in vivo*. By substitution of surface-exposed residues on the *Aequorea victoria* green fluorescent protein (GFP) with cysteines in near the chromophore to form disulfide bonds, reduction-oxidation-sensitive green fluorescent protein 2 (roGFP2) was created *(A)*. These engineered cysteines (Cys147 and Cys204) are reduction-oxidation-sensitive and form an intramolecular disulfide bond (PSS) when oxidized, or a thiol (PSH) when reduced *(B)*. roGFP2 have two fluorescence excitation wavelength maxima at 405 nm and 488 nm and display rapid and reversible ratiometric changes in fluorescence in response to changes in ambient redox potential. When oxidized, the conformational shape of roGFP2 changes due to the formation of PSS resulting in a highly strained and bent chromophore. This causes the chromophore to emit light (emission 530 nm) more readily than non-oxidized roGFP2 when it is excited at 405 nm, and less readily when it is excited at 488 nm. The ratios of fluorescence from excitation at 405 and 488 nm indicate the extent of oxidation and thus the redox potential for a cell *in vivo*. As an example, excitation spectra (emission 530 nm) from fully oxidized and reduced human epithelial cervical cancer cells (HeLa P388D1) transfected with roGFP2 is taken from (205) and shown *(C)*. Note the differences between the peaks in oxidized/reduced HeLa cells at 405 and 488 nm.

Images A and B taken from (205) and Image C taken from (206). Written permission from copyright holder reproduced in Appendix II and cited below according to their request.

"This research was originally published in the Journal of Biological Chemistry. Dooley C T et al. Imaging Dynamic Redox Changes in Mammalian Cells with Green Fluorescent Protein Indicators. *The Journal of Biological Chemistry*. 2004; 279:22284-22293. © the American Society for Biochemistry and Molecular Biology."

"This research was originally published in the Journal of Biological Chemistry. Hanson G T et al. Investigating Mitochondrial Redox Potential with Redox-sensitive Green Fluorescent Protein Indicators. *The Journal of Biological Chemistry*. 2004; 279:13044-13053. © the American Society for Biochemistry and Molecular Biology."

A

B

CysA147   CysA204

Oxidized

(ox)

Reduced

C

Excitation wavelength (nm)
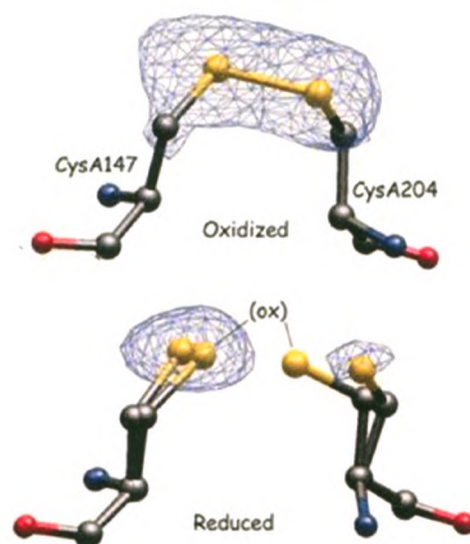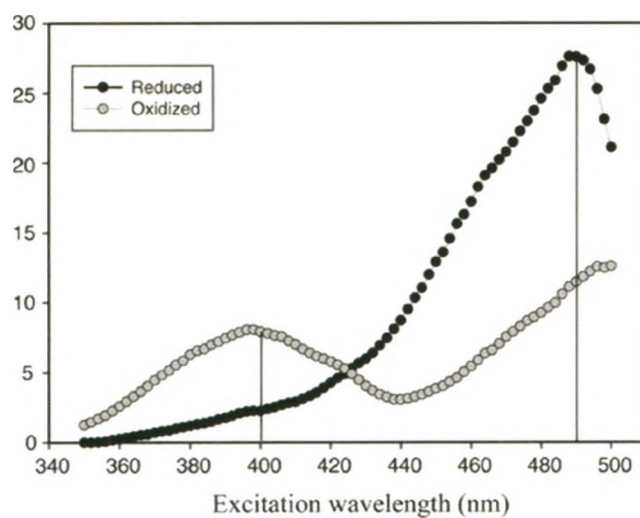
4.2.1 Reversible and Irreversible Oxidation of the Cytosolic Compartment of Hepa 1c1c7 cells as Determined by Mutated GFP (roGFP2) and Confocal Microscopy

Hepa 1c1c7 cells were transfected with a plasmid containing roGFP2 DNA and were, allowed to grow until roGFP protein was expressed and then treated with varying concentrations of the well-characterized cell permeant pro-oxidant TBHP for comparison to data with UCB. Following treatment with 5 µM TBHP, the roGFP2 within the cytosol of the cell became oxidized within 6 min because the the ratio of excitation fluorescence at 488 nm (green) vs 405 nm (red) was decreased (Fig. 4.3A). This change in fluorescence ratio for roGFP2 was subsequently reversed after 18 min, demonstrating that the redox status of these Hepa 1c1c7 cells had returned to normal (i.e. oxidized roGFP2 disulfide reduced roGFP2) after treatment with 5 µM TBHP. Cells containing roGFP2 protein treated with 100 µM TBHP also showed formation of roGFP2 disulfide within 6 min, but there was no reduction of roGFP disulfide to roGFP2 during the course of this experiment, illustrating irreversible oxidation of the cytosolic compartment. By comparison, treatment of roGFP2 expressing cells with 50 µM UCB resulted in formation of roGFP disulfide that was partially reversed by 2 h. However, this partial recovery of the redox status of the cells was followed by more oxidation at later time points (Fig. 4.3B). On the other hand, treatment with an anti-oxidant concentration of UCB (70 nM) resulted in a pronounced reduction of the intracellular environment by 3 h post-treatment (Fig. 4.3C).

Figure 4.3: Live Cell Measurement of Intercellular Redox State with Mutated Green Fluorescent Protein (roGFP2) that Forms an Intracellular GFP Disulfide Under Conditions of Oxidative Stress. Hepa 1c1c7 cells were transfected with a roGFP2 DNA-containing plasmid, incubated for 24 h to facilitate roGFP protein expression and visualized with a Zeiss LSM-510 META laser scanning microscope using dual excitation (405 or 488 nm) and an emission filter of 505 nm after treatment with the well-characterized cell permeant prooxidant, TBHP or UCB. Hepa 1c1c7 cells treated with 5 or 100 µM tBHP *(A)*. Each time frame image is an overlay of two images; Ex. 488, Em. 530 (set to green) is roGFP2 (reduced) and Ex. 405 nm, Em. 530 (set to red) is roGFP2 disulfide (oxidized). Note enhanced oxidation by 6 min that is reversed by 18 min in cells treated with 5 µM TBHP demonstrating irreversible oxidation of the indicator protein. roGFP was rapidly converted to roGFP2 disulfide in cells treated with 100 µM TBHP (by 6 min) and roGFP underwent further oxidation over time demonstrating irreversible oxidation of proteins containing reactive cysteine thiols within the cellular environment. Quantified fluorescence data from cells treated with either 50 µM *(B)* or 70 nM *(C)* UCB. Initially, treatment of cells with 50 µM UCB resulted in reversible oxidation that was partially reversed by 2 h, followed by subsequent and significant oxidation at later time points. Treatment of cells with an anti-oxidant concentration of UCB (70 nM) resulted in reduction of the intracellular environment by 3 h post-treatment. Data expressed as mean ± standard deviation, n = 4; *, P < 0.05 according to an ANOVA with a Dunnett's post test for Hepa 1c1c7 versus controls.
Abbreviations: roGFP2, mutated redox green fluorescent protein; TBHP, tert-butyl hydroperoxide; UCB, unconjugated bilirubin.

Data by Garth Oakes.
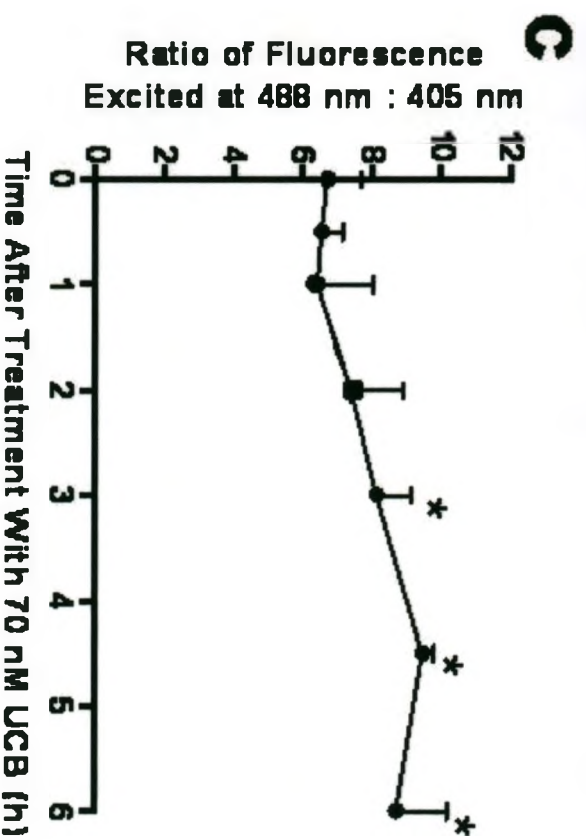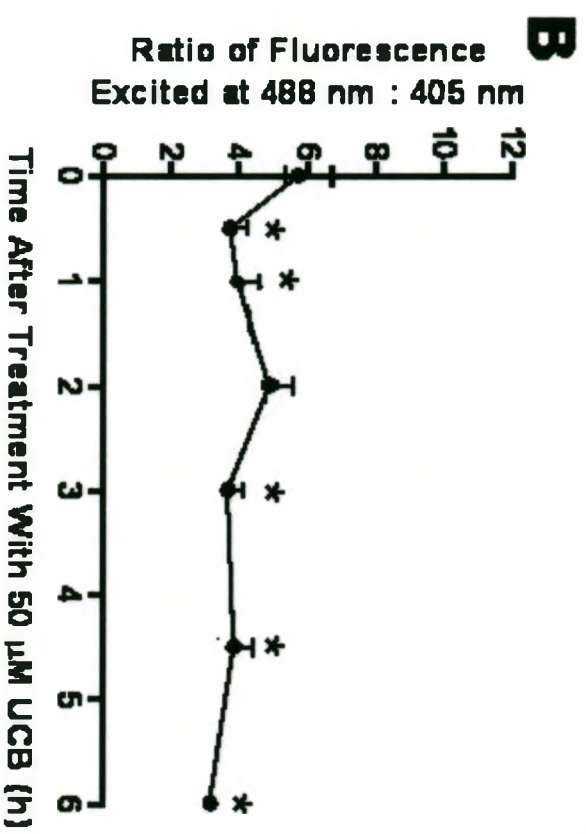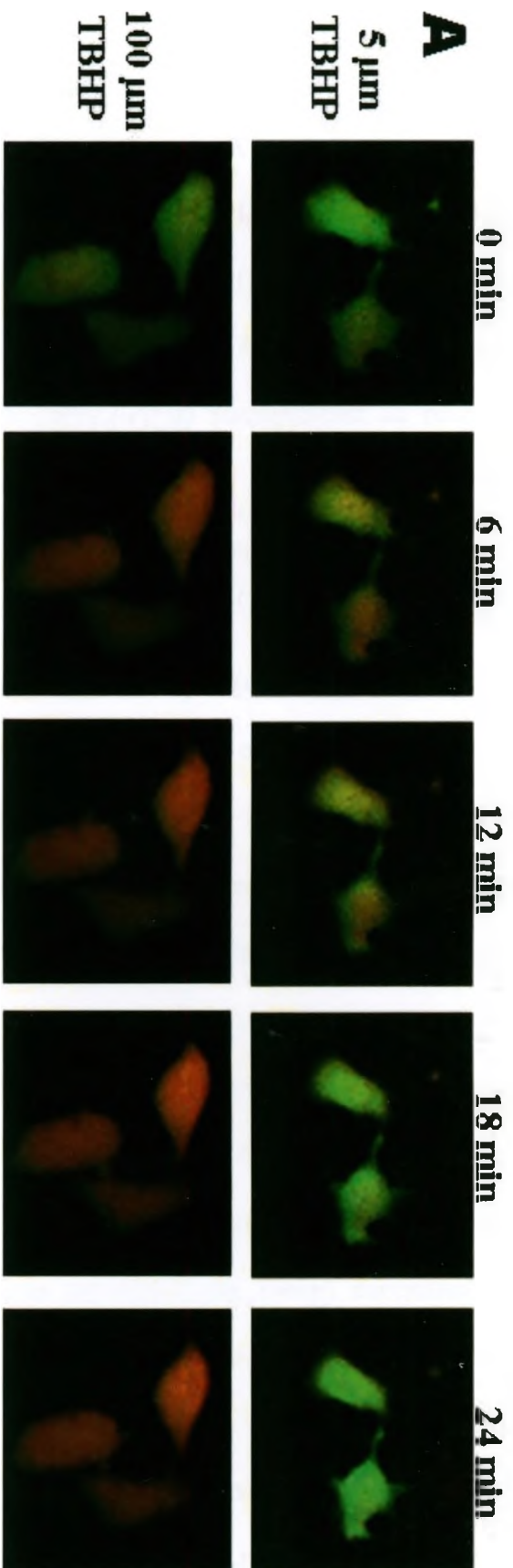
4.2.2 Validation of Protein Analysis by R2D-PAGE in Cytosol Prepared from Hepa 1c1c7 Cells of Oxidized vs Reduced roGFP2 Status as Determined by Confocal Microscopy

Experiments with Hepa 1c1c7 cells expressing roGFP established relevant concentrations (dose) and times for either TBHP or UCB to cause reversible or irreversible oxidation of this redox indicator in the cytosolic compartment. This critical information provided us with the ability to select appropriate time periods to harvest cells for R2D-PAGE analysis that would be expected to yield the greatest number of PSSP within the cell. For TBHP treated Hepa 1c1c7 cells, we determined that reversible protein disulfide oxidation is best characterized by a treatment of 5 μM for 5 min, whereas for irreversible oxidation a treatment of 100 μM for 30 min was found to be more appropriate (Fig. 4.3A). For UCB, we determined that 70 nM results in a significant reduction in the intracellular oxidative environment (i.e. less GFP disulfide than in untreated cells), whereas treatment with 50 μM UCB resulted in irreversible oxidation of the cells.

Protein extracts from cytosolic and crude membrane (mitochondrial or microsomal fractions) fractions (100 μg) from Hepa 1c1c7 cells were sequentially resolved by non-reducing (R2D-PAGE) and then reducing SDS PAGE in the second dimension followed by silver staining (Fig 4.4). As a negative control, the reducing agent DTT (100 mM) was added to proteins before they were developed in both dimensions to reveal a prominent diagonal line with no spots in either of the off-diagonal zones. This result validates the capability of R2D-PAGE analysis to visualize intermolecular protein-protein disulfide and intramolecular protein disulfide bonding
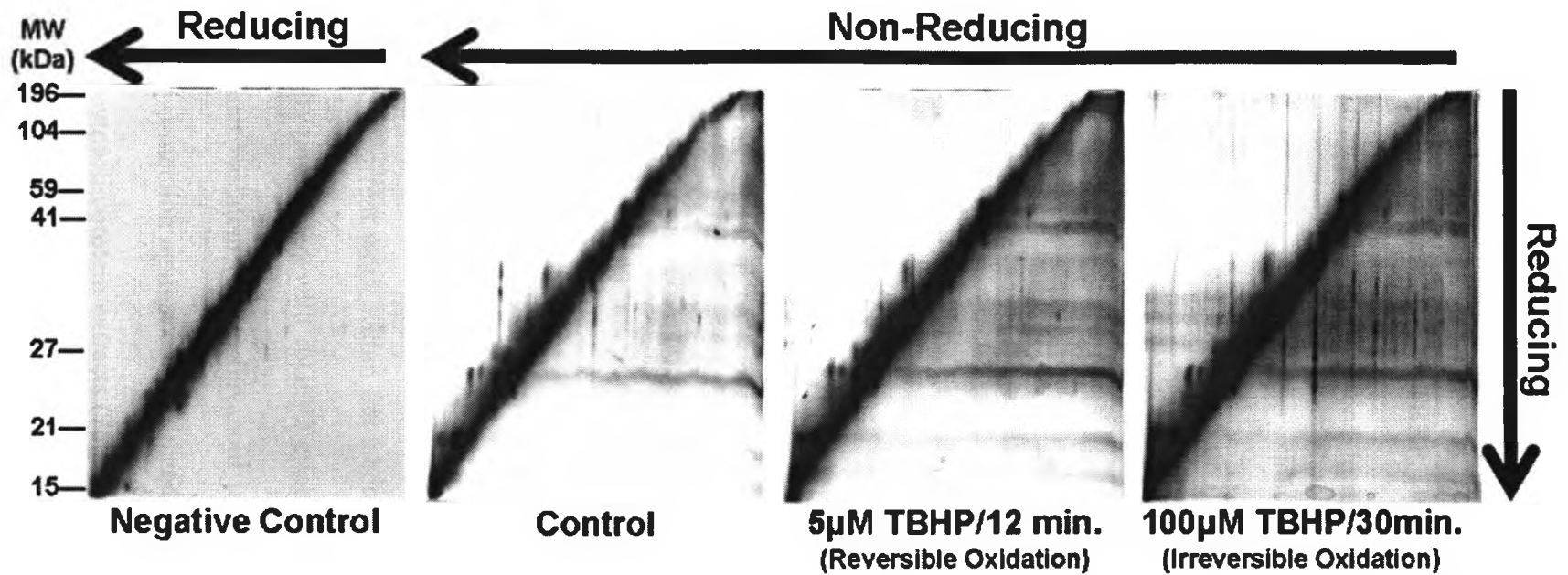
Figure 4.4: Separation of Protein Disulfides (the Disulfide Proteome) in Hepa 1c1c7 Cells Treated with Oxidative Stressors by R2D-PAGE. Cytosolic or crude membrane fractions (100 μg) prepared by differential centrifugation of homogenates prepared from Hepa 1c1c7 cells were sequentially resolved by non-reducing (SDS PAGE) or and reducing (R2D-PAGE) followed by silver staining. As a negative control, the reducing agent DTT (100 mM) was added to proteins prior to electrophoresis in both dimensions to reveal a prominent diagonal line with no spots in either of the off-diagonal zones. Cells were either untreated (control), treated with 5 μM TBHP for 12 min, or treated with 100 μM TBHP for 30 min prior to homogenate preparation. Cells that were treated with 5 μM TBHP for 12 min (reversibly oxidized roGFP2), had a greater number of proteins that formed disulfides when compared to the control, and cells treated with 100 μM TBHP for 30 min (irreversibly oxidized roGFP2), had considerably more proteins oxidized at PS⁻ than the reversibly oxidized cells. Images are representative of 3 separate cell preparations.

Abbreviations: DTT, dithiothreitol; TBHP, tert-butyl hydroperoxide

within cells. R2D-PAGE was subsequently used to analyze proteins prepared from untreated (control) cells, cells treated with 5 μM TBHP for 5 min (reversible oxidation), or cells treated with 100 μM TBHP for 30 min (irreversibly oxidation). The data revealed that protein disulfide bond formation readily occurs within the cytoplasm of control Hepa 1c1c7 cells as well as oxidant-stressed cells. A number of proteins oxidized at PS⁻ appear to be novel to either 5 or 100 μM TBHP treatments. Reversibly oxidized cells had a greater number of proteins that formed disulfides when compared to control cells, and cells that were irreversibly oxidized had considerably more proteins oxidized at PS⁻ than the reversibly oxidized cells. This data was obtained by counting the unique protein spots in each of the PAGE gels prepared from cytosolic fractions of control, 5 μM TBHP or 100 μM TBHP treated cells. This data demonstrates that protein disulfide bonding (i.e. the disulfide proteome) can be used as an indication of the redox status within a cell, and can be conveinetly visualized utilizing R2D-PAGE at biologically relevant concentrations of oxidative stressors.

4.3 Extension of R2D-PAGE Analysis to Evaluation of Redox Status in HEK 293 Cells Subjected to Oxidative Stress

Concurrent work within the laboratory utilizing human embryonic kidney (HEK 293) cells transfected with roGFP2 established that cells pretreated with 10 μM of the antioxidant baicalein (BE, a flavanoid isolated from *Scutellaria baicalensis*), provided minimal protection against cells oxidized with 50 μM TBHP. To further validate R2D-PAGE, cytosolic protein extracts (75 μg) were resolved by R2D-PAGE (Fig. 4.5). Cells were pre-treated with 10 μM BE for 10 min, treated with 50 μM TBHP for 30 min,

71

Figure 4.5: Representative R2D-PAGE gel of all disulfide bonded proteins from cytosol prepared from homogenates of Human HEK 293 cells. Cytosol was prepared from homogenates of HEK 293 cells (75 µg protein) and resolved in triplicate by R2D-PAGE. Protein spots are numbered accordingly, and proteins spots that were capable of being identified by mass spectrometry protein mass fingerprinting (MS PMF) are shown in Table 4.2. Cells were either untreated (control), pre-treated with 10 µM BE for 10 min (BE), treated with 50 µM TBHP for 30 min (TBHP), or pretreated with BE for 10 min and then treated with 50 µM TBHP for 30 min (BE/TBHP). Exposing cells to 50 µM TBHP resulted in the complete oxidation of protein spots 1-3. BE did not have any affect in preventing the oxidation of any of the protein spots. Images are representative of 3 separate cell preparations.
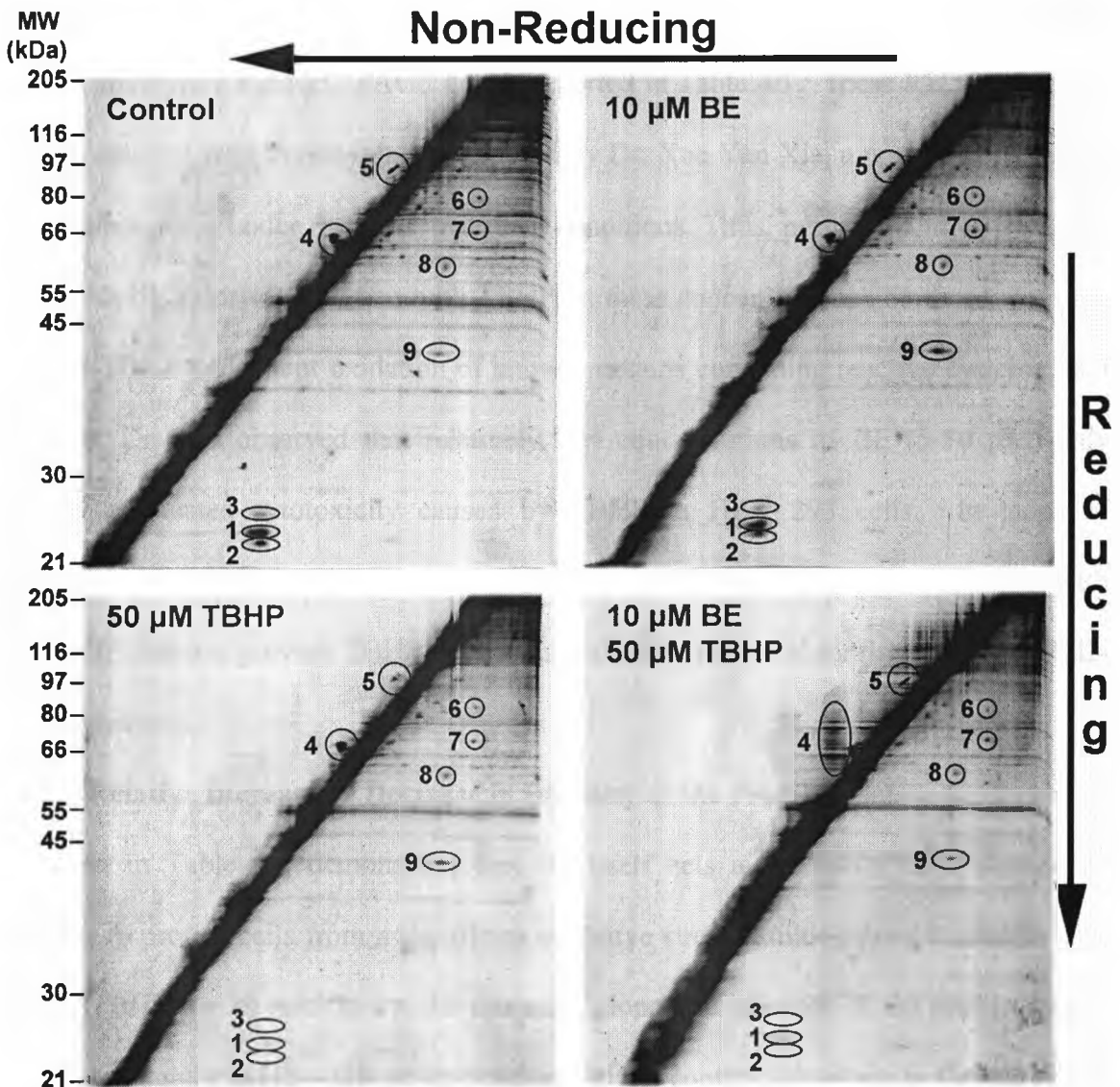
pre-treated with 10 µM BE for 10 min and then treated with 50 µM TBHP for 30 min, or untreated and compared with vehicle treated control.

The effect of BE and TBHP treatments on the disulfide proteome of HEK 293 cells was examined by determining the relative change in expression of nine protein spots found in extracts of cells with TBHP ± BE relative to the solvent-treated control (Fig. 4.6). The apparent mol wt of these nine protein spots was identified from eight protein markers with an R^2 value of 0.98, and the relative difference in expression between the protein spots from the R2D-PAGE gels is reported in Table 4.1. These R2D-PAGE data were consistent with toxicity data (generated by Dr. Xue Yan Xia, a post-doctoral fellow in the laboratory) under the same treatment conditions. Thus, pre-treatment of HEK 293 cells with BE prior to oxidation with TBHP, at these concentrations and times, does not prevent TBHP dependent oxidation of known proteins containing reactive cysteine thiol residues. Dr. Xia observed that relatively low concentrations of BE (5-10 µM) only slightly attenuates cytotoxicity caused by TBHP in HEK 293 cells. In terms of maintaining intracellular GSH content and the redox status in cells, pre-treatment with 10µM BE did not prevent TBHP dependent oxidative stress as confirmed by the R2D-PAGE analysis.

4.3.1 Relative Increase or Decrease in Intensity of the Protein Spots

The data in Table 4.1 demonstrate that BE itself acts as an antioxidant, despite its inability to protect cells from a significant oxidative stress resulting from treatment with 50 µM TBHP for 30 min. In the BE treatment alone, the intensity of the protein spot is decreased slightly in H5 – H8, when compared to the control. However in the BE/TBHP treatment, proteins H1 – H3 dissapeared entirely, demonstrating that the oxidative insult

Figure 4.6: Relative increase and decrease in intensity of protein spots in Human HEK 293 cells subsequent to treatment with the oxidative stressor, TBHP ± Baicalein (BE). Magnification of protein spots in the 2D-gels reveals redox related changes in the intensity of the protein spots between Human HEK 293 cells that were either untreated (control), pre-treated with 10 µM BE for 10 min (BE), treated with 50 µM TBHP for 30 min (TBHP), or pretreated with BE for 10 min and then treated with 50 µM TBHP for 30 min (BE/TBHP). The relative increase or decrease of the protein spot intensity is shown in Table 4.3.
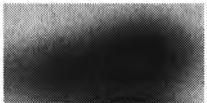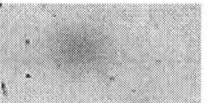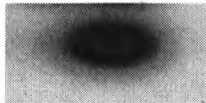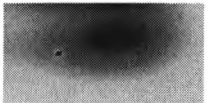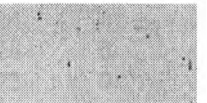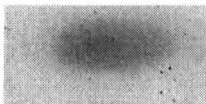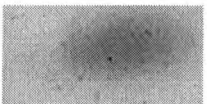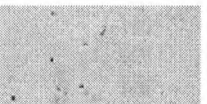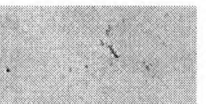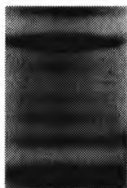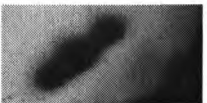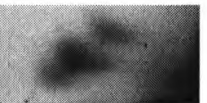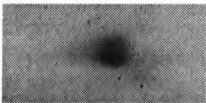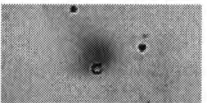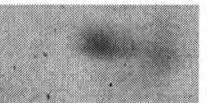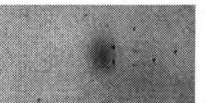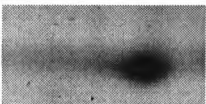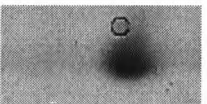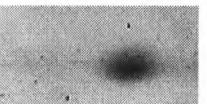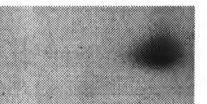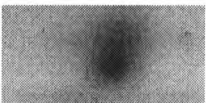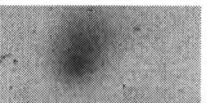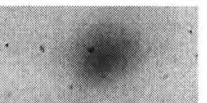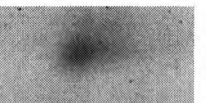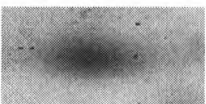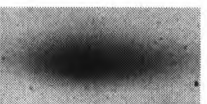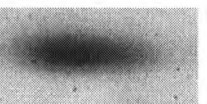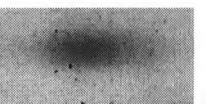
Table 4.1: Relative Increase or Decrease in Intensity of Protein Spots in Redox 2D Gels of *t*-Butylhydroperoxide (TBHP) Treated Compared to Untreated (Control) Lysate Samples from Human HEK 293 or Mouse Hepa 1c1c7 Cells. The relative increase or decrease in protein spot intensity was determined from visual observation of spots within the gel as compared to untreated (control) cells, shown in images produced in Fig. 4.6 (for HEK 293 cells) and Fig. 4.11, 4.12, and 4.13 (Hepa 1c1c7 cytosol, mitochondrial and microsomal fractions, respectively). HEK 293 cells were pre-treated with 10 µM BE for 10 min (BE), with 50 µM TBHP for 30 min (TBHP), or pre-treated with BE for 10 min and then treated with 50 µM TBHP for 30 min (BE/TBHP). Hepa 1c1c7 cells were treated with 50 µM UCB for 6h (50 µM 6 h), 50 µM UCB for 18h (50 µM 18 h), 70 nM UCB for 6h (70 nM 6 h) or 70 nM UCB for 18 h (70 nM 18 h).

Mouse (Hepa 1c1c7)						Human (HEK 293)				
Spot no.	Mass (kDa)	50 µM 6h	50 µM 18h	70 nM 6 h	70 nM 18 h	Spot no.	Mass (kDa)	BE	TBHP	BE/TBHP
Cytosol										
M1	25	0	– – –	0	0	H1	25	0	– – –	– – –
M2	23	0	–	+ + +	+ + +	H2	24	–	A	A
M3	69	0	– – –	–	– – –	H3	26	0	A	A
M4	81	0	0	0	+	H4	73	0	0	P
M5	88	0	–	–	– – –	H5	94	–	– – –	0
M6	91	+	+ + +	0	–	H6	84	– – –	– – –	– – –
M7	79	0	0	0	0	H7	74	–	– – –	–
M8	44	–	A	+	–	H8	64	–	0	–
M9	44	– – –	0 ·	+ + +	– – –	H9	47	+ + +	+	0
M10	53	+	A	–	–					
Mitochondrial Fraction										
M11	56	A	A	+	+					
M12	73	–	– – –	–	0					
M13	85	– – –	A	– – –	0					
M14	85	0	0	0	0					
M15	45	–	A	0	0					
Microsomal Fraction										
M16	73	–	–	0	+					
M17	86	–	+ + +	0	0					
M18	46	A	+ + +	+	+ + +					
M19	30	0	+ + +	0	+ + +					
M20	31	0	+ + +	0	+ + +					
M21	26	0	+ + +	0	+ + +					

Relative increase or decrease compared to controls

No Change: 0
Minor Increase/Decrease: + / –
Substantial Increase / Decrease: + + + / – – –
Complete Presence / Absence: P / A

from TBHP was so severe that BE was unable to prevent or attenuate this response.

4.3.2 Protein Identification by Mass Spectrometry Peptide Mass Fingerprinting (MS PMF)

To understand the redox 2D protein profile of HEK 293 cells and the effect of treatment with BE ± TBHP on these cells, 9 protein spots were analyzed by mass spectrometric peptide mass fingerprinting (MS PMF) of tryptic digests to identify the protein(s) within the protein spot. These protein spots were picked, digested with trypsin, and spotted on a sample target plate which was analyzed by a mass spectrometer (4700 Proteomics Analyzer, Applied Biosystems, Foster City, Ca) to obtain matrix-assisted laser desorption/ionization (MALDI) MS spectra. To obtain the MALDI MS spectra, a target plate is pulsed with laser energy causing proteins or protein fragments to ionize, and fly from the target plate down a vacuum tube to the detector plate. The time-of-flight is affected by the mass of the particle and the charge it bears (m/z ratio). The detector plate records the intensity of the signal at a given value, and a spectrum is generated. The different peaks in the spectrum correspond to different m/z protein species.

A computer program (4700 Proteomics Analyzer, Applied Biosystems, Foster City, Ca) acquired the MALDI MS spectra from the mass spectrometer, another computer program converted this information into usable data (4000 Series Explorer, Applied Biosystems, Foster City, Ca), and a final computer program (Data Explorer software, Applied Biosystems, Foster City, Ca), plotted the given signal intensity against the given m/z values generating a spectra. The sum of all the peaks in the spectra represents the peptide mass fingerprint (PMF) for the analyzed protein spot. The PMF generated for each trypsin digested protein spot was compared to known peptide mass sequences

available on the NCBI database using a search engine (MASCOT, Matrix Science, Boston, MA), and the protein score confidence (PSC) indicated as a percentage for each protein PMF was reported. The PSC is a statistical calculation that compares how closely the acquired PMF compares to known protein peptide sequences; it is a measure of the certainty for which the PMF identifies a specific protein. MS PMF analysis of the nine protein spots in HEK 293 cells yielded high PSC percentages for protein spots H1, H2, and H3. The other six protein spots did not yield any PSC data. This demonstrates that R2D-PAGE appears to be limited to proteins that are expressed in large amounts, i.e. "high copy number" proteins.

MS PMF analyses for BE/TBHP treated cells identified up to 6 protein and protein isoforms in spots H1, H2, and H3 (Table 4.2). Utilizing protein spot H2 as an example of how proteins were identified using MS PMF, a MALDI MS Spectra (Fig. 4.7) was generated when the protein spot was run on a mass spectrometer, subsequent to proteolytic digestion by trypsin. The PMF of H2 was determined by incorporating all the peaks in the spectra, after setting a precursor tolerance of 40 ppm to reduce the signal-to-noise ratio, and removing all the values that corresponded to tryptic autolysis. The resulting PMF was compared against NCBI Accession number GI 32189392 (Table 4.3A) (available online at http://www.ncbi.nlm.nih.gov/sviewer/viewer.fcgi?32189392:NCBI:24053012). The subsequent PSC score of 100% for H2, indicated that the unknown protein spot is peroxiredoxin 2 isoform A.

Table 4.2: Protein Identification by MS Peptide Mass Fingerprinting for HEK 293 and HEPA 1c1c7 Cells

Disulfide bonded proteins from Human HEK 293 cells (H) or Mouse Hepa 1c1c7 cells (M) were separated by redox 2D gel electrophoresis and the proteins in single spots were subjected to digestion with trypsin. Proteins were identified by mass spectrometry peptide mass fingerprinting.

Spot no.	Protein	Molecular Mass (kDa)	Protein Score Confidence (%)	No. of Spectral Matches	NCBI Accession no.
Human (HEK 293)					
H1	Peroxiredoxin 1 [Homo sapiens]	19	90.1	5	gi|55959887
H1	Peroxiredoxin 1, isoform CRA_b [Homo sapiens]	21	86.1	5	gi|119627382
H2	Peroxiredoxin 2 isoform a [Homo sapiens]	22	100	10	gi|32189392
H2	Chain A, Thioredoxin Peroxidase B From Red Blood Cells	22	100	10	gi|9955007
H2	TSA [Homo sapiens]	18	100	9	gi|1617118
H2	Thiol-specific antioxidant protein [Homo sapiens]	22	100	9	gi|438069
H3	Peroxiredoxin 3, isoform CRA_c [Homo sapiens]	11	76.9	5	gi|119569783
Mouse (Hepa 1c1c7)					
M1	Peroxiredoxin 1 [Mus musculus]	22	100	12	gi|6754976
M1	Peroxiredoxin 1 [Mus musculus]	20	100	10	gi|123230137
M1	Peroxiredoxin 1 [Mus musculus]	19	99.9	8	gi|123230136
M2	Type II peroxiredoxin 1 [Mus musculus]	22	91.9	6	gi|3603241
M2	Peroxiredoxin 2 (Thioredoxin peroxidase 1)	22	90.3	6	gi|2499469
M2	Peroxidase	22	86.3	6	gi|885932
M3	Serum albumin precursor	71	98.4	10	gi|5915682
M3	Albumin 1 [Mus musculus]	71	93.3	7	gi|33859506
M4	Transferrin [Mus musculus]	79	99.9	12	gi|17046471
M5	Protein kinase C substrate 80K-H [Mus musculus]	60	100	13	gi|6679465
M5	Prkcsh protein [Mus musculus]	60	100	13	gi|14602601

Figure 4.7: Matrix-assisted laser desorption/ionization (MALDI) Mass Spectrum (MS) of the tryptic digestion peptides of protein spots H2 and M1 when applied individually to a MALDI target plate. Protein spots on a target plate were pulsated with a laser and the time-of-flight and charge of the tryptic digest peptides (m/z ratio) was plotted against the intensity it showed. Each peak in the spectrum corresponds to a unique m/z protein species. Peaks with reported values indicate peptide sequences that were compared against known peptide mass sequences available on the NCBI database. Peaks with an asterisk indicate tryptic autolysis products which were excluded from identification of the proteins in H2 or M1. Spectra from Human protein spot H2 *(A)*, and Mouse, protein spot M1 *(B)* are displayed.
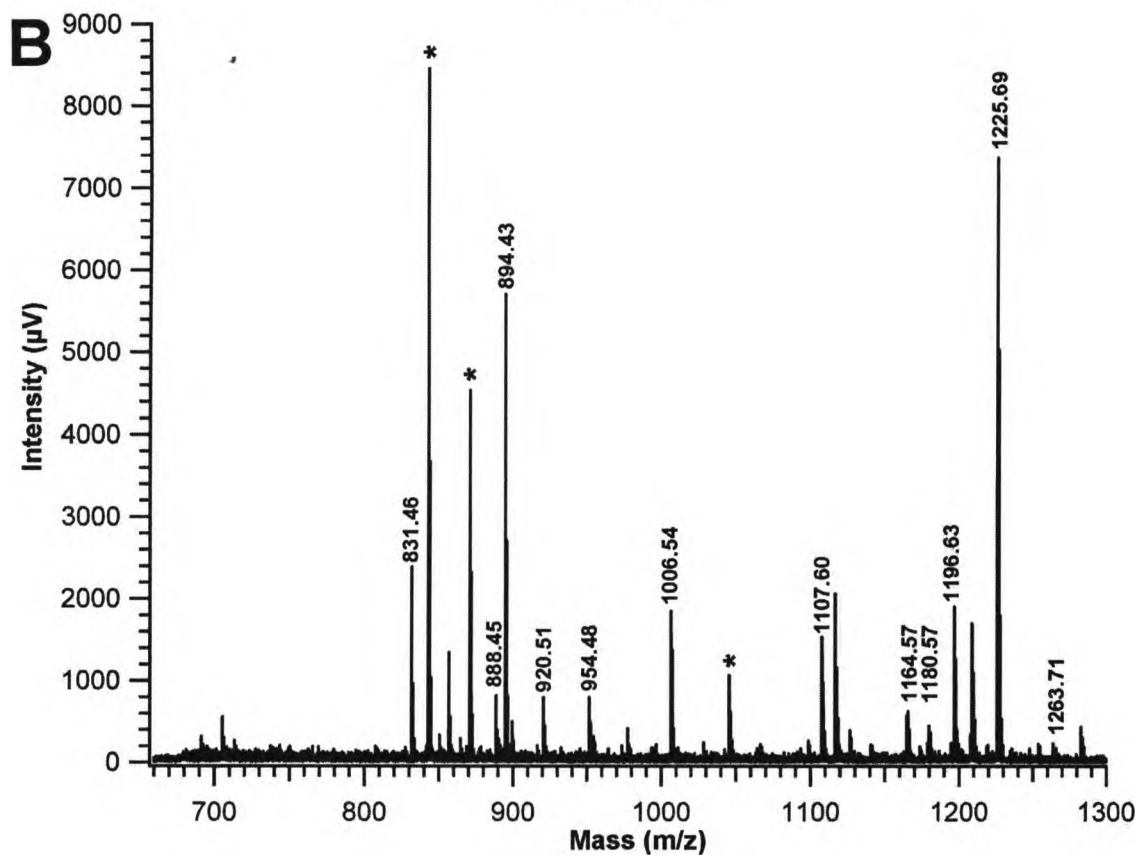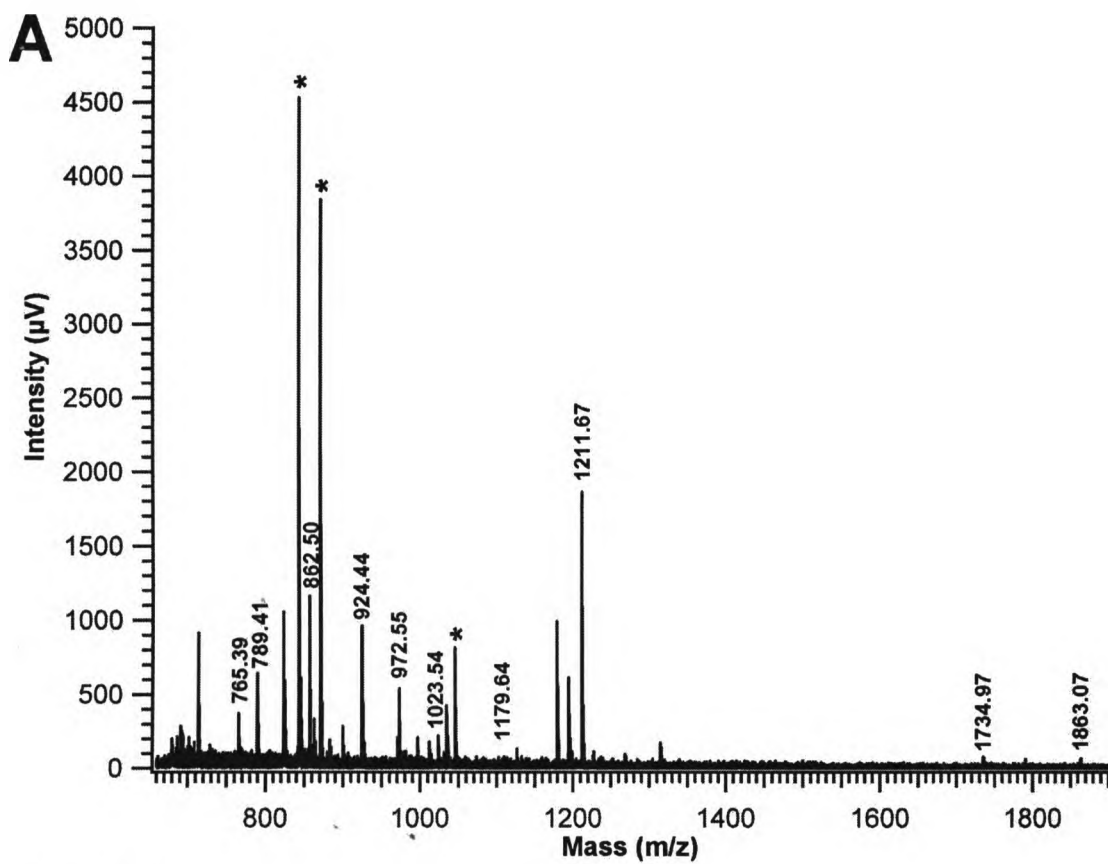
Table 4.3: Mass Spectrometric Peptide Mass Fingerprinting (MS PMF) Sequence Data for Human (HEK 293) Protein Spot H2, and Mouse (Hepa 1c1c7) Protein Spot M1. Data from MASCOT ®, a search engine which compared the peptide mass fingerprints of tryptic digests of protein spot H2 *(A)* or M1 *(B)* individually against an NCBI database of known protein peptide masses that were used to determine the identity of the disulfide bonded proteins separated by redox 2D-gels.

A – Human (HEK 293) Protein Spot H2

Gel Idx/ Pos	Rank	Instr./Gel Origin	Protein Name	Accession No.	Protein Score	Protein Score C. I. %	Protein MW	Protein PI	Pep. Species Count
102/E3	1	4700ms /Abudi_073108	peroxiredoxin 2 isoform a [Homo sapiens]	gi|32189392	130	100	22049.30	5.66	10

Peptide Information

Calc. Mass	Observ Mass	± da	± ppm	Start Seq.	End Seq.	Sequence	Modification
765.39	765.39	-0.0024	-3	62	67	AEDFRK	
789.41	789.41	-0.0012	-2	151	157	SVDEALR	
862.50	862.49	-0.0108	-13	128	135	GLFIIDGK	
924.44	924.44	-0.0003	0	120	127	TDEGIAYR	
972.55	972.55	-0.0049	-5	8	16	IGKPAPDFK	
1023.54	1023.54	0.00	1	111	119	LSEDYGVLK	
1179.64	1179.63	-0.0085	-7	110	119	RLSEDYGVLK	
1211.67	1211.67	-0.0039	-3	140	150	QITVNDLPVGR	
1734.97	1734.95	-0.0268	-15	93	109	EGGLGPLNIPLLADVTR	
1863.07	1863.02	-0.0523	-28	92	109	KEGGLGPLNIPLLADVTR	

B – Mouse (Hepa 1c1c7) Protein Spot M1

Gel Idx/ Pos	Rank	Instr./Gel Origin	Protein Name	Accession No.	Protein Score	Protein Score C. I. %	Protein MW	Protein PI	Rep. Species Count
120/E16	1	4700ms /Abudi_073108	peroxiredoxin 1 [Mus musculus]	gi|6754976	136	100	22390.4	8.26	11

Peptide Information

Calc. Mass	Observ Mass	± da	± ppm	Start Seq.	End Seq.	Sequence	Modification
831.46	831.46	0.003	4	152	158	SVDEIIR	
888.45	888.47	0.0259	29	191	197	SKEYFSK	
894.43	894.43	-0.0005	-1	121	128	ADEGISFR	
920.51	920.51	0.0007	1	129	136	GLFIIDDK	
954.48	954.47	-0.0046	-5	28	35	DISLSEYK	
1006.54	1006.53	-0.0022	-2	8	16	IGYPAPNFK	
1107.60	1107.60	-0.0026	-2	111	120	TIAQDYGVLK	
1164.57	1164.58	0.0126	11	17	27	ATAVMPDGQFK	
1180.57	1180.62	0.0489	41	17	27	ATAVMPDGQFK	Oxidation (M)[5]
1196.63	1196.63	-0.0028	-2	159	168	LVQAFQFTDK	
1225.69	1225.68	-0.0058	-5	141	151	QITINDLPVGR	
1263.71	1263.67	-0.0391	-31	110	120	RTIAQDYGVLK	

4.4 Global DNA Experiments Demonstrating Apoptosis from Mitochondria and Microsomes

Dr. Garth Oakes (then a PhD candidate in our laboratory), analyzed changes in gene regulation mediated by UCB to determine novel pathways that contribute to UCB-mediated toxicity (47). The studies employed microarray analysis (procedure described in (47)) to determine changes in gene regulation mediated by UCB at both 50 μM and 70 nM concentrations in Hepa 1c1c7 cells, at 1 and 6 h post-treatment. Those two time points were chosen for Hepa 1c1c7 cells as 1 h is the time at which reversible oxidation of the cytotosol by live cell imaging was detected following treatment with 50 μM UCB, and 6 h is the time at which

cells were observed to undergo enhanced intracellular oxidation and become committed to apoptosis following treatment with 50 μM UCB (47). Hepa 1c1c7 cells were found to undergo intracellular reduction at both time points following treatment with 70 nM UCB (47).

Earlier studies from our lab established that UCB is able to mediate apoptosis by the mitochondrial-mediated apoptotic pathway through activation of caspases 12, 9, and 3 (45, 46). The follow-up DNA microarray analysis study reveals that UCB is also able to mediate apoptosis through the up-regulation of many genes involved in ER stress (*ATF3, BiP, CHOP, Dnajb1*, and *HERP*) (47). This new finding demonstrates that UCB is able to activate the hepatic ER stress response pathway and that this stress either initiates or contributes to apoptotic cell death. Utilizing data from the DNA microarray analysis which was performed in triplicate, the current study involving R2D-PAGE

examined which redox-regulated genes were affected by UCB exposure. Data from this microarray study identified 13 genes that were up- or down regulated by at least two fold subsequent to treatment of Hepa 1c1c7 cells with 50 μM UCB were considered (Table 4.4A). A list of oxidant-related genes and the subcellular location of the proteins coded by these various genes was compiled from the literature (207-210).

4.4.1 DNA Microarray Analysis Demonstrates Changes in the Expression of Oxidant-Related Genes Subsequent to Treatment by Pro-oxidant (50 μM) Concentrations of UCB

The 13 oxidant-related genes compiled from the literature are categorized by function or pathway: GSH metabolism (*GSTA3, GSTA4, GSTK1, GSTM2, GSTM5, GSTP1, IDPm,* and *MGST2*), catalase/super oxide dismutase (*CAT*), other oxidant scavengers (*Prdx4*), and UCB-related (*Hmox1,* and *Uxs1*) (210). Despite the up- or down-regulation of these genes at a minimum threshold of at least two fold subsequent to treatment with the pro-oxidant (50 μM) concentration of UCB at either 1 or 6 h post treatment, no change was observed in Hepa 1c1c7 cells treated with the antioxidant (70 nM) concentration of UCB at either 1 or 6 h. At 6 h post-treatment, all the oxidant-related genes were down-regulated, with the exception of *heme oxygenase 1 (Hmox 1)* which was up-regulated.

In regards to the UCB-related genes, *Hmox1* and *UDP-glucuronosyltransferase (Uxs1)* were the only UCB-related genes that showed a change in transcript levels. *Hmox1* is the only gene in Table 4.4 whose expression was increased subsequent to treatment with 50 μM UCB, as well as the only gene that underwent a reversal in its regulation (1.5-fold down-regulation at 1 h, and 7.2-fold up-regulation at 6 h). In this

Table 4.4A: DNA Microarray Analysis of Changes in Expression of Oxidant-Related Genes Mediated by Treatment with Prooxidant (50 µM) or Antioxidant (70 nM) Concentrations of UCB, Compared to Vehicle-Treated Controls.

| Location | Gene Name | Gene Symbol | Fold Change | | | |
| | | | 50 µM UCB | | 70 nM UCB | |
			1 h	6 h	1 h	6 h
ER	Heme oxygenase (decycling) 1	*Hmox1*	↓ 1.5	↑ 7.2	NC	NC
ER	Peroxiredoxin 4	*Prdx4*	↓ 1.7	↓ 4.2	NC	NC
Cell Membrane	UDP-glucuronosyltransferase	*Uxs1*	↓ 1.5	↓ 4.0	NC	NC
Mit / Per	Glutathione S-transferase κ1	*GSTK1*	NC	↓ 3.5	NC	NC
Mit	Mit NADP$^+$ Isocitrate dehydrogenase 1	*IDPm*	NC	↓ 3.2	NC	NC
Mit / Cytosol	Glutathione S-transferase µ1	*GSTM1*	NC	↓ 3.2	NC	NC
ER	Microsomal Glutathione S-transferase 2	MGST2	NC	↓ 2.9	NC	NC
Mit / Per	Catalase	*CAT*	NC	↓ 2.8	NC	NC
Mit / Cytosol	Glutathione S-transferase α4	GSTA4	NC	↓ 2.7	NC	NC
Cytosol	Glutathione S-transferase α3	GSTA3	NC	↓ 2.6	NC	NC
Nuc / Cytosol	Glutathione S-transferase π1	GSTP1	NC	↓ 2.4	NC	NC
Cytosol	Glutathione S-transferase µ2	GSTM2	NC	↓ 2.4	NC	NC
Cytosol	Glutathione S-transferase µ5	GSTM5	NC	↓ 2.2	NC	NC

Abbreviations: Cytosol, Cyt; Endoplasmic Reticulum, ER; Mitochondria, Mit; No Change, NC; Nucleus, Nuc; Peroxisome, Per. Increase (↑) or decrease (↓) in gene expression as observed by analysis on a Affymetrix Mouse Genome 430 2.0 DNA microarray. Hepa 1c1c7 cells were exposed to 50 µM or 70 nM UCB for either 1 or 6 h. Change in gene expression compared to vehicle-treated controls. Data are expressed as mean of three individual cell preparations. Genes are categorized according to the Gene Ontology™ (GO) biological processes annotations attributed to each gene (Gene Ontology Consortium http://www.geneontology.org/). A list of oxidant-related genes and the location of proteins coded by the various genes was compiled from the literature (207-210).

Adapted from (47).

Table 4.4B: Real-time Reverse-transcription PCR (qRT-PCR) Analysis of Oxidant-Related Genes Treated with Prooxidant (50 µM) or Antioxidant (70 nM) Concentrations of UCB, and Positive Controls for Oxidative (50 µM TBHP / 3h) and ER Stress (1.2 nM Tunicamycin /24h) Compared to Vehicle-Treated Controls.

| | Fold Change Compared to Untreated (Control) Cells | | | | | |
| | 1.2 nM Tunicamycin | 50 µM TBHP | 50 µM UCB | | 70 nM UCB | |
Gene	24 h	3 h	1 h	6 h	1 h	6 h
Catalase	↓ 0.3	↑ 0.5 *	↓ 0.9 *	↓ 1.4 *	↑ 0.5	↓ 0.6 *
IDPm	↓ 0.2 **	↑ 0.1 *	↓ 0.3 *	↓ 0.7 *	↑ 0.2	↓ 0.2 *

Abbreviations: tert-butyl hydroperoxide, TBHP. Increase (↑) or decrease (↓) in gene transcription levels as observed by real-time reverse-transcription PCR (qRT-PCR) of oxidant-related genes. Hepa 1c1c7 cells were exposed to 70 nM or 50 µM UCB for either 1 or 6 h; treated with a 50 µM TBHP for 3 h (a positive control for oxidative stress); or 1.2 nM tunicamycin for 24 h (a positive control for ER stress). Change in gene expression compared to data from vehicle-treated controls. RNA was isolated using the Trizol reagent and gene changes were validated using qRT-PCR. Data are expressed as mean of three individual cell preparations. *p<0.05 according to analysis by a two-way ANOVA. **p<0.05 according to analysis by a one-way ANOVA.

Adapted from (47).

regard, *Hmox1* was the first gene in rank order for the amount of up-regulation at 6 h following 50 μM UCB treatment (47), and the highest induced oxidant-related gene, nearly doubling that for *Peroxiredoxin 4* (*Prdx4*), the redox regulated gene with the second highest induction. *Uxs1* was down-regulated 1.5-fold at 1 h, and 4.0-fold at 6 h. Microarray analysis did not detect a change in mRNA transcript formation of any major transporters involved in the influx or efflux of UCB from hepatocytes (46, 47). Thus, no change was observed for genes coding for multidrug resistance-associated proteins 1, 2, and 3 (*Mrp1*, *Mrp2*, and *Mrp3*), multidrug resistance protein 1 (*Mdr1*), or any of the organic anion transporter polypeptide proteins (*Oatps*).

The genes of proteins involved in GSH metabolism (*GSTA3*, *GSTA4*, *GSTK1*, *GSTM2*, *GSTM5*, *GSTP1* and *MGST2*) were only down-regulated at 6 h post treatment with 50 μM UCB and to similar degrees (-2.6-, -2.7-, -3.5-, -3.2-, -2.4-, -2.2- and -2.9-fold) respectfully. The well known redox-regulated gene, *mitochondrial isocitrate dehydrogeanse* 1 (*NADP$^+$*) (*IDPm*) was down-regulated -3.2-fold. The important antioxidant genes, *Prdx 4* (-1.7-fold at 1 h; -4.2-fold at 6 h), and *catalase* (*CAT*) (-2.8-fold at 6 h post treatment) were also down-regulated by exposure to UCB in Hepa 1c1c7 cells.

4.4.2   Real-time Reverse-transcription PCR (qRT-PCR) of Oxidant Related Genes

qRT-PCR (procedure described in (47)) was used to validate changes in transcription of oxidant-related genes identified by microarray analysis. The decrease in mRNA formation for *CAT* and *IDPm* at 50 μM UCB at 6 h post treatment was verified in this manner. Treatment with 70 nM UCB for 6 h down-regulated the transcription levels of *CAT* and *IDPm*, with fold values similar to treatment with 50 μM UCB at 1 h.

Treatment with 50 µM TBHP for 3 h (a positive control for oxidative stress) did not result in a significant down-regulation of either *CAT or IDPm*, gene, whereas treatment with 1.2 nM tunicamycin for 24 h (a positive control for ER stress), resulted in a down-regulation of *IDPm* but not *CAT*.

4.5 Protein disulfide changes in Hepa 1c1c7 cells after treatment with pro-oxidant (50 µM) and antioxidant (70 nM) concentrations of UCB.

To better understand the subcellular localization of oxidized (P-S-S-P) proteins subsequent to treatment with pro-oxidant (50 µM) and antioxidant (70 nm) concentrations of UCB, Hepa 1c1c7 cell homogenate was separated into cytosolic (100,000 x g / 60 min supernatant; Fig. 4.8), mitochondrial (20,000 x g / 10 min pellet; Fig. 4.9), and microsomal (100,000 x g / 60 min pellet; Fig. 4.10) fractions by differential centrifugation. Then, R2D-PAGE separation of proteins was performed with each of the individual subcellular fractions to evaluate differences. In all, 21 protein spots were found to be situated either above or below the prominent diagonal line of the gels. The apparent mol wt of these 21 protein spots was identified from 8 protein markers run on each gel with an R^2 value of 0.98 for each of the protein spots from the cytosol, mitochondrial, or microsomal fractions (Table 4.1).

MS PMF was attempted on all proteins spots, however only 5 proteins in the cytosol were expressed in large enough amounts (i.e. "high copy number" proteins) to be identified by our procedure (Table 4.2). The relative increase or decrease in the intensity of the silver stained protein spots for each fraction treated with 50 µM UCB (6 or 18 h) or

Figure 4.8: Representative R2D-PAGE gel of all disulfide bonded proteins from cytosol prepared from homogenates from Mouse Hepa 1c1c7 cells. Cytosol was prepared from homogenates of Mouse Hepa 1c1c7 cell (75 μg protein) and resolved in triplicate by R2D-PAGE. Protein spots are numbered accordingly, and proteins spots that were capable of being identified by mass spectrometry protein mass fingerprinting (MS PMF) are shown in Table 4.2. Cells were treated with either prooxidant (50 μM) or antioxidant (70 nM) concentrations of UCB for 6 or 18 h, and sample without UCB was treated with vehicle-treated control. Images are representative of 3 separate cell preparations.
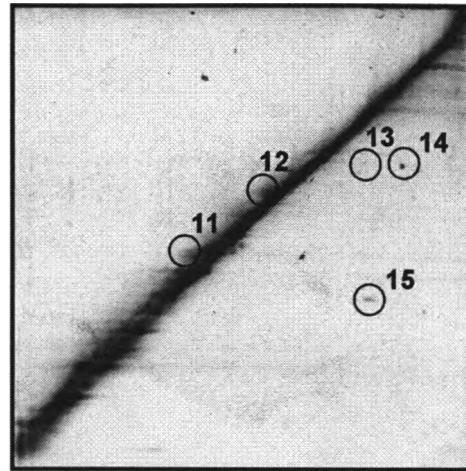
Non-Reducing

Control   50 μM UCB

Cytosol   70 nM UCB

6 h   18 h

Reducing

88
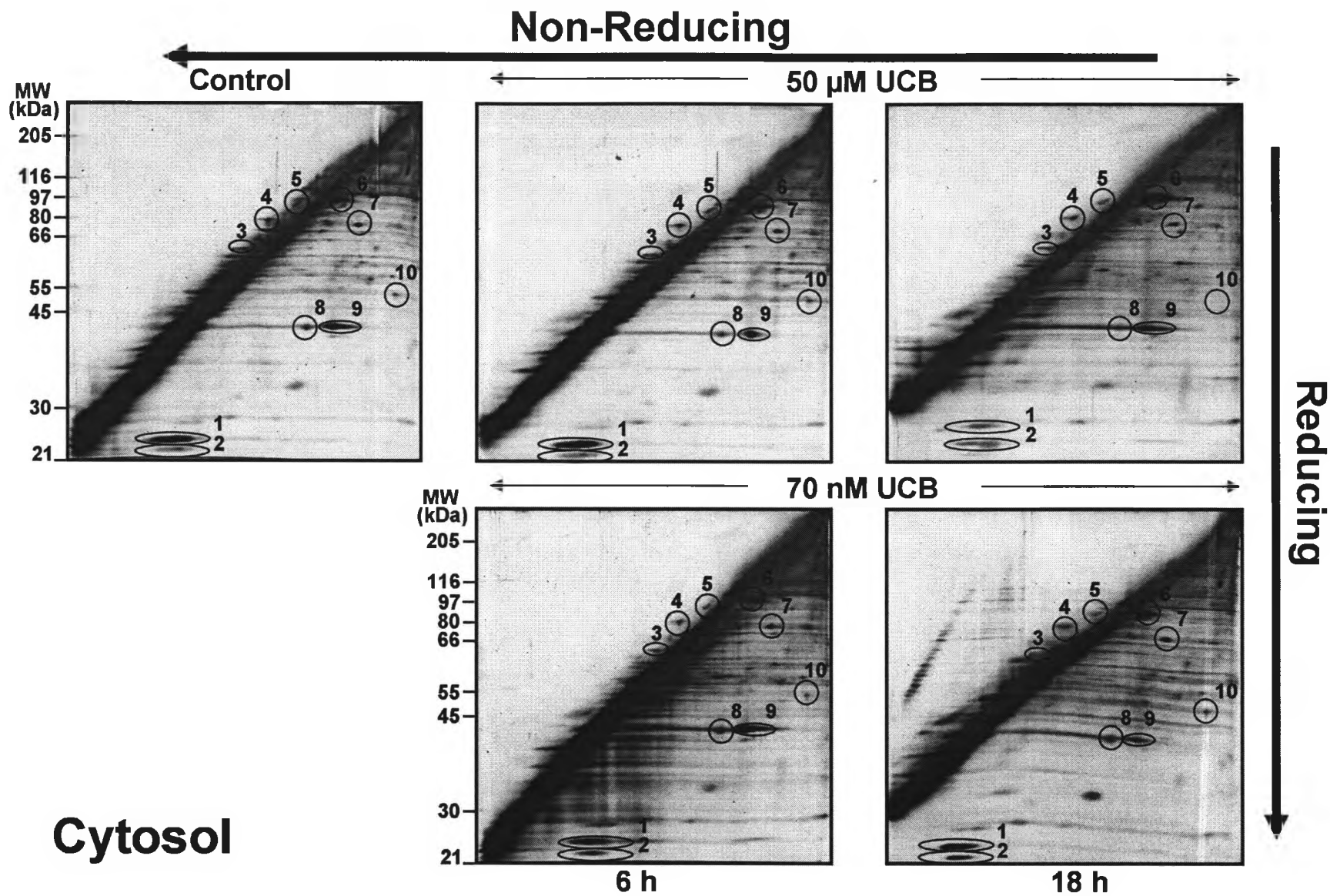
Figure 4.9: Representative R2D-PAGE gel of all disulfide bonded proteins from mitochondrial fraction (20,000 x *g* / 10 min) prepared from homogenates from Mouse Hepa 1c1c7 cells. Mitochondrial fraction (20,000 x *g* / 10 min) was prepared from homogenates of Mouse Hepa 1c1c7 cell (75 µg protein) and resolved in triplicate by R2D-PAGE. Protein spots are numbered accordingly. Cells were treated with either prooxidant (50 µM) or antioxidant (70 nM) concentrations of UCB for 6 or 18 h, and sample without UCB was treated with vehicle-treated control. Images are representative of 3 separate cell preparations.

Non-Reducing

Control

50 µM UCB

Reducing

70 nM UCB
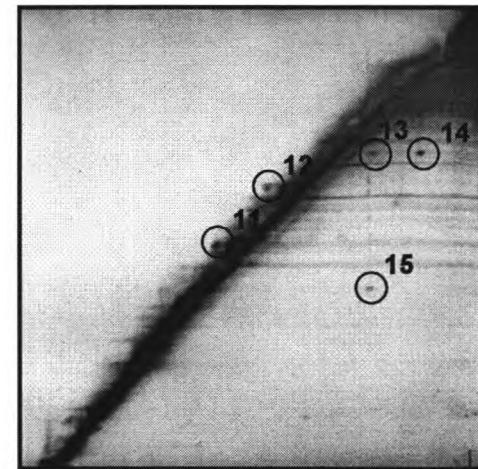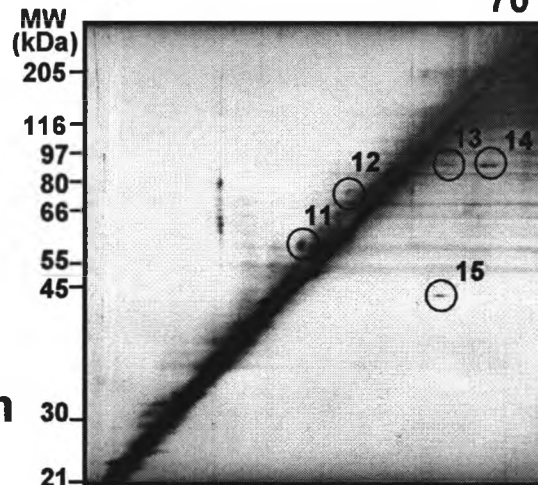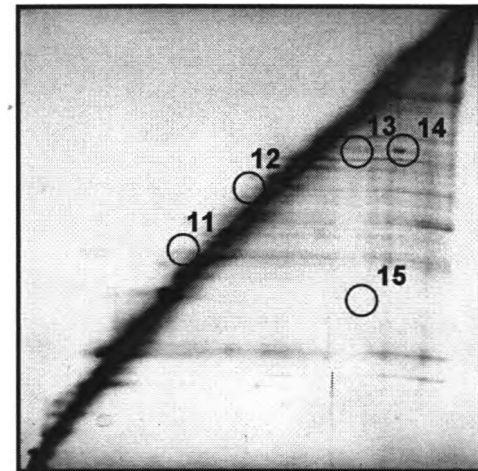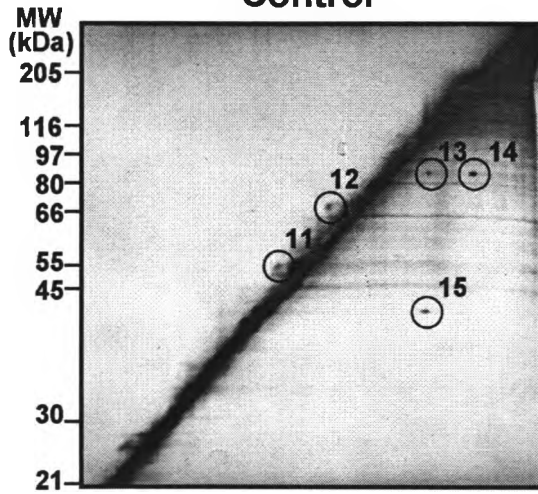
Mitochondrial Fraction
(20,000 x *g*) / 10 min)

6 h

18 h

Figure 4.10: Representative R2D-PAGE gel of all disulfide bonded proteins from microsomal fraction (100,000 x *g* / 60 min) prepared from homogenates from Mouse Hepa 1c1c7 cells. Microsomal fraction (100,000 x *g* / 60 min) was prepared from homogenates of Mouse Hepa 1c1c7 cell (75 μg protein) and resolved in triplicate by R2D-PAGE. Protein spots are numbered accordingly. Cells were treated with either prooxidant (50 μM) or antioxidant (70 nM) concentrations of UCB for 6 or 18 h, and sample without UCB was treated with vehicle-treated control. Images are representative of 3 separate cell preparations.

Non-Reducing

Control

50 µM UCB

70 nM UCB

Reducing

MW (kDa)
205 –
116 –
97 –
80 –
66 –
55 –
45 –
30 –
21 –

16
17
18
19 20
21

12

19 20
21

Microsomal Fraction (100,000 x *g*) / 60 min)

6 h

18 h

92
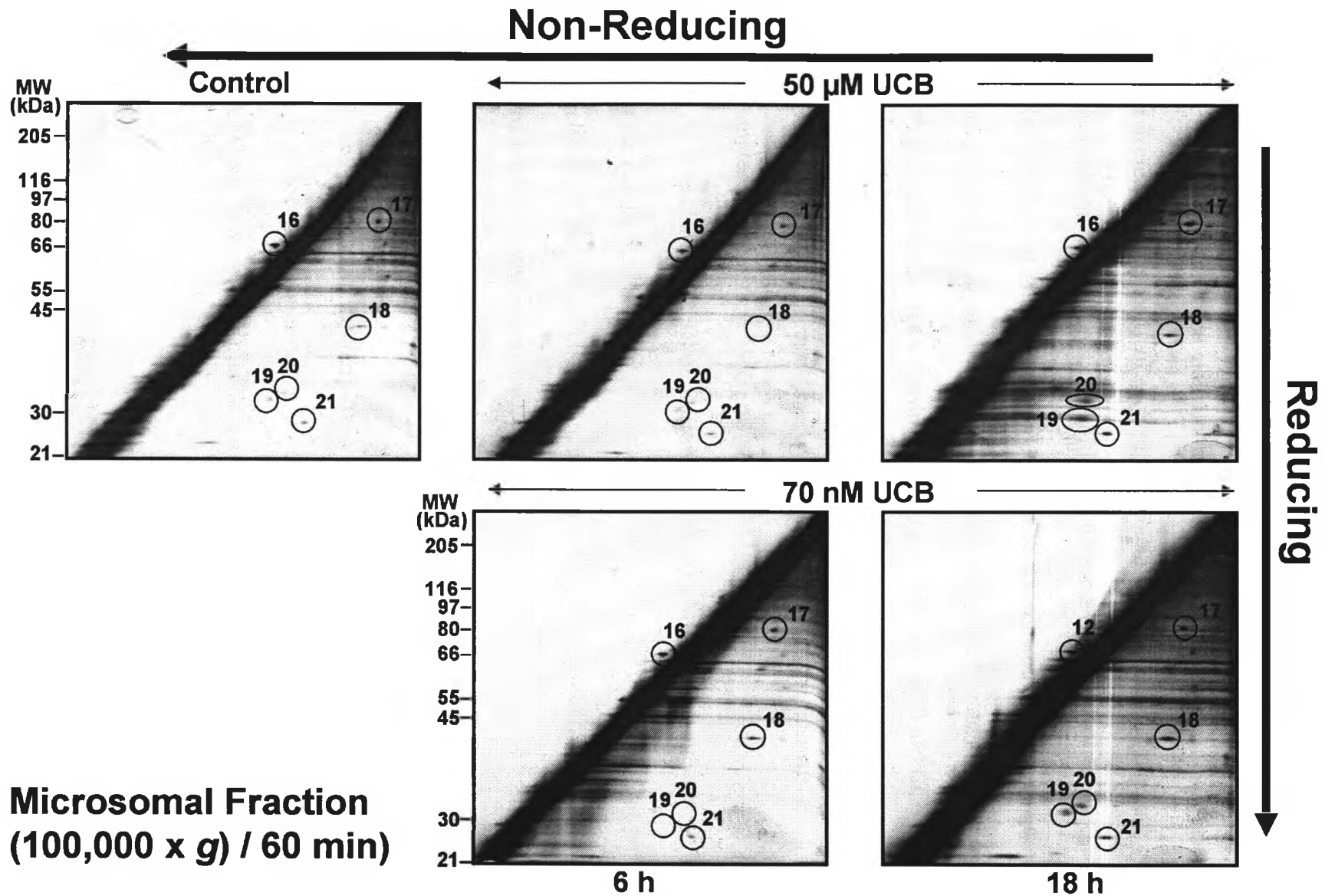
70 nM UCB (6 or 18 h) was individually compared against the protein spots from untreated (vehicle treated control) samples from cytosol (Fig. 4.11), mitochondrial fraction (Fig. 4.12) or microsomal fraction (Fig. 4.13). This change in the relative increase or decrease for intensity of each of the protein spots for each of the samples is reported from gels run under identical conditions at the same time (Table 4.1).

In the cytosol, exposure of cells to UCB for 18 h resulted in a substantial change (increase, decrease, or absence) in the intensity of several different proteins for either the 50 μM or 70 nM treatments. Not surprising, the changes between the 50 μM UCB and the 70 nM UCB treatments for 18 h were distinct, reflecting different changes with different proteins. On the other hand, minimal or no changes occurred in the intensity of protein spots for samples treated with either 50 μM or 70 nM UCB for 6 h.

In the mitochondrial fraction, treatment with 50 μM UCB for either 6 or 18 h resulted in the complete absence or a substantial decrease in the intensity of all protein spots detected; minimal or no change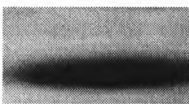s in the intensity of the protein spots (with the exception of M13) occurred in samples treated with 70 nM UCB for 6 or 18 h.

In the microsomal fraction, exposure of cells to UCB for 18 h resulted in a substantial increase in the intensity of identical proteins spots for both 50 μM and 70 nM treatments (i.e. the changes in the protein spots for the 50 /18 h and 70 nM / 18 h exposures were the same); minimal or no changes occurred in the intensity of protein spots (with the exception of M18) for cells treated with 50 μM or 70 nM UCB for 6 h.

Figure 4.11: Relative increase and decrease in intensity of protein spots from cytosol of Mouse Hepa 1c1c7 cells subsequent to treatment with pro-oxidant (50 μM) or antioxidant (70 nM) concentrations of UCB oxidative stressor. Magnification of protein spots from R2D-PAGE cytosol reveals redox related changes in the intensity of the protein spots between Hepa 1c1c7 cells that were either untreated (vehicle treated control), or treated with 50 μM UCB (a prooxidant concentration) for 6 or 18 h, or treated with 70 nM UCB (an antioxidant concentration) for 6 or 18 h. The relative increase or decrease of the protein spot intensity is shown in Table 4.1. Images are representative of 3 separate cell preparations.
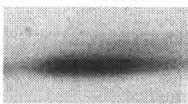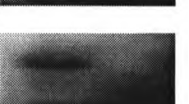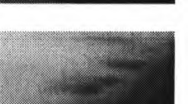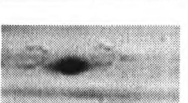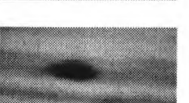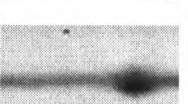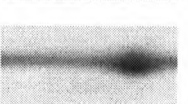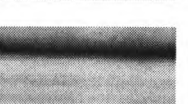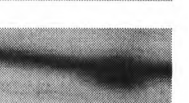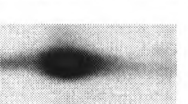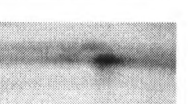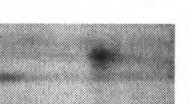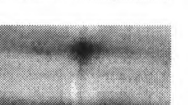
Mouse (Hepa 1c1c7) – Cytosol

Spot no.	Control	50 μM UCB		70 nM UCB	
		6h	18h	6h	18h
M-1					
M-2					
M-3					
M-4					
M-5					
M-6					
M-7					
M-8					
M-9					
M-10					

Figure 4.12: Relative increase and decrease in intensity of protein spots in mitochondrial fraction (20,000 x *g* / 20 min) of Mouse Hepa 1c1c7 cells subsequent to treatment with pro-oxidant (50 μM) or antioxidant (70 nM) concentrations of UCB oxidative stressor. Magnification of protein spots from R2D-PAGE mitochondrial fraction (20,000 x *g* / 20 min) reveals redox related changes in the intensity of the protein spots between Hepa 1c1c7 cells that were either untreated (vehicle treated control), or treated with 50 μM UCB (a prooxidant concentration) for 6 or 18 h, or treated with 70 nM UCB (an antioxidant concentration) for 6 or 18 h. The relative increase or decrease of the protein spot intensity is shown in Table 4.1. Images are representative of 3 separate cell preparations.
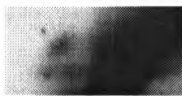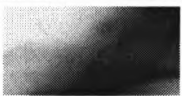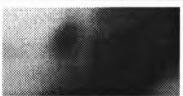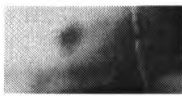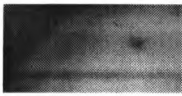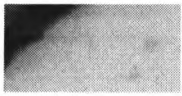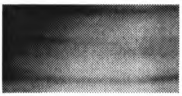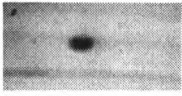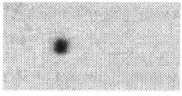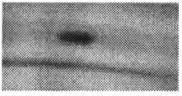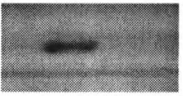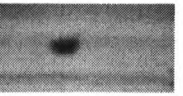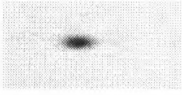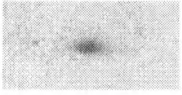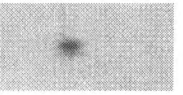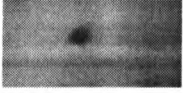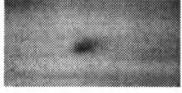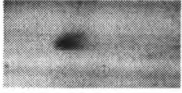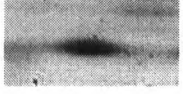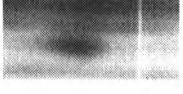
Mouse (Hepa 1c1c7) – Mitochondrial Fraction (20,000 x *g* / 10 min)

Spot no.	Control	50 μM UCB		70 nM UCB	
		6h	18h	6h	18h
M-11					
M-12					
M-13					
M-14					
M-15					

Figure 4.13: Relative increase and decrease in intensity of protein spots from microsomal fraction (100,000 x *g* / 60 min) in Hepa 1c1c7 cells subsequent to treatment with pro-oxidant (50 μM) or antioxidant (70 nM) concentrations of UCB oxidative stressor. Magnification of protein spots from R2D-PAGE microsomal fraction (100 x g / 60 min) reveals redox related changes in the intensity of the protein spots between Hepa 1c1c7 cells that were either untreated (vehicle treated control), or treated with 50 μM UCB (a prooxidant concentration) for 6 or 18 h, or treated with 70 nM UCB (an antioxidant concentration) for 6 or 18 h. The relative increase or decrease of the protein spot intensity is shown in Table 4.1. Images are representative of 3 separate cell preparations.

Mouse (Hepa 1c1c7) – Microsomal fraction (100,000 x *g* / 60 min)

Spot no.	Control	50 μM UCB		70 nM UCB	
		6h	18h	6h	18h
M-16					
M-17					
M-18					
M-19					
M-20					
M-21					

CHAPTER 5: DISCUSSION AND CONCLUSIONS

5.1   Discussion

As outlined in section 2.2, the primary objective of this thesis is the analysis of the changes in the disulfide proteome in Hepa 1c1c7 cells due to protein oxidation as a result of concentration-dependent treatment with pro-oxidant (50 μM) or antioxidant (70 nM) concentrations of UCB. The hypothesis, that some redox-regulated proteins important in toxication-detoxication pathways could be identified by mass spectrometry from separation by redox two-dimensional polyacrylamide gel electrophoresis (R2D-PAGE) was tested and proven to be successful.

5.2   Employing Polyacrylamide Gel Electrophoresis (PAGE) to Demonstrate Redox Regulation of Proteins

In the original design of this study, it was thought that employing polyacrylamide gel electrophoresis (PAGE) redox gels would demonstrate redox regulation in the cell by separating different forms of redox regulated proteins. Many redox regulated proteins contain the amino acid Cys, one of the most rarely used amino acids in proteins of all organisms (138). The unique chemical properties of Cys in redox regulation are due to the high reactivity of the free thiol group (PSH) which exists as an ionized or reactive protein Cys thiol (PS⁻) in redox regulated proteins (124). The thiol group allows proteins with Cys to form reversible thiol modifications with GSH or other proteins under oxidizing/reducing conditions. Cys residues play a crucial role in the structure and

function of proteins (69). This is due to their ability to stabilize protein structures by forming disulfide bonds, serving as active sites for protein function, or as the redox center in proteins (211, 212). PSH form intramolecular bonds with themselves (PSS), intermolecular bonds with other proteins (PSSP), and when reactive Cys thiol is oxidized form reversible protein sulfenic acids (PSOH), or irreversible protein sulfinic and sulphonic (PSO_2H / PSO_3H) acids (Fig. 1.4).

As PSH are highly susceptible to oxidation/reduction, employing strong oxidants/reductants during PAGE allows the unique separation of the disulfide forms of these proteins. Iodoacetamide is first used when lysing cells to block free PSH groups which might otherwise participate in post-lysis oxidation (e.g. air oxidation during sample preparation) or other disulfide interchange reactions that might occur between proteins in the buffer (137, 138). Cell fractions containing iodoacetamide-treated proteins are then placed in a non-reducing loading buffer that is free of any reducing agents. In regular PAGE reducing agents such as β-mercaptoethanol, or the more powerful reductant dithiothreitol are typically placed in PAGE protein loading buffers to eliminate the effects of protein disulfide bonding, allowing all proteins to be visualized as monomers. When these reducing agents are not utilized, the oxidized form of the PSH remains intact allowing the visualization of PSS, PSSG, PSSP and PSOH. PSO_2H, and PSO_3H are not reduced by either β-mercaptoethanol or dithiothreitol.

Though redox gels are capable of separating all redox regulated proteins, the limitation of this technique is that thiol selective dyes must be utilized to label specific disulfide interactions like PSSG, PSSP (with very low mol wt proteins), PSOH, PSO_2H, and PSO_3H to globally monitor the thiol-disulfide state of proteins *in vivo* (138). This

the absence and presence of β-mercaptoethanol accurately displays disulfide bonding and demonstrated that the lyophilized BSA we used as a positive control, even though stored at 4 °C is completely oxidized to disulphides.

In R1D-PAGE, GAPDH (Fig. 4.1B) from *Saccharomyces cerevisiae* stored at -20 °C was primarily in the reduced form because a single band at an apparent mol wt of 36 kDa was found in PAGE run both the reducing and non-reducing buffers. GAPDH, however is amenable to oxidation as multiple bands appeared in the gel run in non-reducing buffer after GAPDH was treated with 5 mM H_2O_2 for 5 min. The oxidized GAPDH showed a single band, at an apparent mol wt of 36 kDa, when placed in reducing buffer. On the other hand, oxidized samples placed in non-reducing buffer, had bands with an apparent mol wt of 33, 36, 75, 83, and 87 kDa. Our results show, that despite the formation of GAPDH intramolecular bonds (GAPDH-S-S; 36 kDa), GAPDH homodimers (GAPDH-S-S-GAPDH; 75 kDa), and GAPDH heterodimeric disulfides (GAPDH-S-S-Catalase; 83 and 87 kDa), the majority of the GAPDH protein remained in the reduced form (36 kDa) despite oxidative treatment with 5 mM H_2O_2.

Oxidation of GAPDH by H_2O_2 is dose and time dependent. Had a higher concentration of H_2O_2 or longer time periods been used, more oxidation would have occurred indicated by the formation of intermolecular disulfide bonding in GAPDH at 75 kDa and larger mol wt values (due to formation of GAPDH oligomers), at the expense of reduced GAPDH (36 kDa) (141). Our data with these proteins used as positive controls provides a snapshot of the GAPDH disulfide proteome *in vitro*, and demonstrates that oxidizing GAPDH with 5 mM H_2O_2 for 5 min does cause protein disulfide formation

consistent with redox regulation but that much of the protein remains reduced at this concentration of H_2O_2 for 5 min.

The experiments performed on pure BSA and GAPDH demonstrate that redox gels can reflect the oxidation state of a cell *in vitro* by providing a snap-shot of the disulfide proteome of cultured cells. Though R1D-PAGE gels can be performed quickly their application is limited because proteins are separated in a single dimension. This limitation restricts the use of R1D-PAGE gels for evaluating disulfide bonding on either pure or enriched protein fractions or (2) on specific proteins when appropriate antibodies are used for immunoblotting (e.g. western blots or immunoprecipitation).

5.2.2 Redox Two-Dimensional Polyacrylamide Gel Electrophoresis (R2D-PAGE), is a Reliable and Reproducible Method for Evaluating the Post-translational Modification of Proteins Containing a Reactive Cysteine Thiol Residue (PS⁻)

Whereas R1D-PAGE is a useful and quick method to identify specific proteins, redox two-dimensional PAGE (R2D-PAGE) (also known as diagonal PAGE) is the only redox gel procedure that is capable of identifying a cell's entire disulfide proteome. First developed in 1974 by Sommer and Traut for analyzing proteins with intermolecular disulfide bonds in *Escherichia coli* (137), this technique that in involves sequential non-reducing (first dimension) / reducing (second dimension) electrophoresis has been adapted and used to monitor protein mixed disulfide bond formation in a cell, to identify proteins, and to evaluate change in the disulfide proteome during physiological processes in bacteria (213), cyanobacteria (214), plants (196, 215), rodent nerve cell cultures (202), and cardiac myocytes (216). Though Cumming most recently developed a cutting tool that increases the accuracy in excising the gel strip (217), no notable change in this

butylhydroquinone, cause oxidation of Nrf2 in vitro and in vivo and so affect Nrf2 target genes. Furthermore, KO Hepa1c1c7 cells (for Nrf2) transfected with a Nrf2 plasmid were able to induce phase II enzymes upon exposure to arsenic which causes oxidative stress whereas KO cells transfected with mutant Nrf2 at positions Cys119, Cys235, and Cys506 were unable to form Nrf2 heterodimers with a Maf protein, the mutated Nrf2 heterodimers were unable to bind to the ARE of phase II genes or increase their rate of transcription. The findings of He and Ma (222) shed new light on the Nrf2-Keap1 system and demonstrated that Nrf2 cysteine residues critically regulate oxidant/electrophile sensing, receptor activation, and transcription activation.

These two studies provide two potential reasons for our observation that 50 μM UCB treatment down regulates oxidant-related genes in Hepa 1c1c7 cells to levels lower than normal. This pro-oxidant UCB concentration either (1) reversibly oxidizes Keap1 resulting in its inability to protect Nrf2 from proteasomal degradation in the nucleus (221), or (2) reversibly oxidizes Nrf2 thereby preventing it form binding to the ARE of any phase II enzymes (222).

5.4.2 UCB initially targets the ER

As UCB is known to effect the ER, it was not surprising that *Hmox1* (which codes for heme oxygenase 1 (HO-1), and *Prdx4* (which codes for peroxiredoxin 4 (Prx 4) to be down-regualted within 1 h, as both of these proteins are located in the ER (46, 223). *Prdx4* is the only peroxiredoxin gene we found to be downregulated after exposure to 50 μM UCB within 1 h as (1) *Prdx4* has already been reported to be affected by perturbations in intracellular calcium levels (224), (2) calcium levels are regulated by the ER (225), (3) peroxiredoxin 4 is the only peroxiredoxin located in the ER (223), and (4)

5.5.1 Proteomic Signature of the Disulfide Proteome in HEK 293 cells

Our R2D-PAGE data demonstrate that 10 μM BE does have some antioxidant properties because as it changes the intensity of some proteins from homeostatic (control) conditions (Table 4.1). Despite this, the proteomic signature of the disulfide proteome of BE and BE/TBHP treated cells is essentially the same (Fig. 4.5), showing that BE cannot protect cells against irreversible oxidation by 50 μM TBHP. More important for my work, the changes recorded in the disulfide proteome did reflect changes in the toxicity of these cells evaluated by LDH release, lipid peroxidation and depletion of intracellular GSH. This study also demonstrates that how the comparison of disulfide proteome of cells can be used to determine the efficacy of antioxidants, such as BE. Moreover, it is possible to compare the antioxidant effects of such treatments at the subcellular compartmental level as was done later in this thesis.

The reducing potential of BE on the intracellular redox environment is apparent in the 10 μM treatment as shown in Fig. 4.6 and Table 4.1. BE decreases the intensity of original protein disulfide dimmers (H2 – H8) that are found to occur under normal homeostatic conditions (Table 4.1). BE reduces these PPS proteins into either PS⁻ or PSH, which decreases the intensity of the original protein disulfide dimmer as these reduced proteins become located on (instead of above or below) the prominent diagonal line.

Although previous reports have demonstrated an increase in PSSP formation as a result of exposure to ROS by R2D-PAGE analysis (141, 202, 237), we did not find that this occurred in our 50 μM TBHP for 30 min treatments. Ours were short term exposure studies and this probably explains the differences between these experiments and those

with higher concentrations of oxidants (like the pro-oxidants 50 μM TBHP or 50 μM UCB), for longer time periods, conditions which we know cause irreversible oxidation leading to apoptosis. Instead, the reported studies referred to above analyzed cells that were persistently exposed to low levels of ROS due to either environmental contamination (237), or disease (141), or high concentrations of ROS but for very short time periods (e.g. 10 mM H_2O_2 for 5 min) (202). As ROS reacts at near diffusion rates (72), Cumming et al. (141) have demonstrated that increased ROS concentrations do not necessarily correlate with increased disulfide bonding. Using oxidants of different strengths, they have shown how despite the presence of less PSSP for a certain enzyme in samples treated with a stronger oxidant as compared to the weaker one, the activity of the enzyme was almost completely inactivated with the stronger oxidant, presumably because of irreversible oxidation of the enzyme into either PSO_2H, or PSO_3H, forms of the enzyme not normally reduced back to PSH. (Certain of the peroxiredoxins are novel in this regard, as discussed above).

5.5.1.1 Identifying Disulfide Bonded Proteins Irreversibly Oxidized by TBHP

We were only partially successful in identifying the disulfide protein spots by MS analysis, as proteins that were not expressed in large amounts did not yield a high protein score confidence percentage, meaning their unequivocal identification is impossible. In these cases, use of specific antibodies and western blot analysis could distinguish between a number of possible proteins. For any protein spots found repeatedly on R2D-PAGE analysis, molecular weights of the disulfide and the monomeric forms of individual proteins can be estimated with confidence. Fortunately, we were able to identify the three protein spots that form the most distinctive aspect of the proteomic

signature of HEK 293 cells oxidized by TBHP, and found that peroxiredoxins 1-3 (Prx 1-3)were oxidized (Table 4.2). Prx 1-3 are present in both control and 10 μM BE treatments, indicative that low concentrations of H_2O_2 are present. This is because the disulfide-linked dimeric intermediary (P-SS-P) is present in each case, part of the 2-Cys peroxiredoxin catalytic recycling mechanism that occur with Prx 1-4 (Fig. 1.7) (164-166). The presence of Prx 1-3 in the disulfide-linked dimeric form in the control cells, is supported by studies which have established that peroxiredoxins are constitutively expressed under normal homeostatic conditions, as they reduce endogenous low levels of H_2O_2 (238).

Treating cells with TBHP caused Prx 1–3 to hyperoxidize, presumably into their sulfinic acid forms that fall on the diagonal line during R2D-PAGE analysis. This occurred under our experimental conditions because catalase, which scavenges H_2O_2 efficiently at high concentrations, is unable to inactivate organic peroxides like TBHP (238). The resultant effect of this is that the Prx catalytic cycle which is only effective at eliminating low concentrations of H_2O_2, remained active as if it were the only mechanism for eliminating organic H_2O_2. After Prx-sulfenic acids were formed as a result of reducing H_2O_2 (a by-product of TBHP treatment), the strong oxidizing environment resulted in the formation of sulfinic Prx rather than the disulfide-linked dimeric intermediary that occurs at the lower H_2O_2 concentrations important in cellular signalling under homeostatic conditions (238). Hyperoxidation of Prx into sulfinic Prx can occur under normal basal conditions, and is reversed by Srx (238). This, however, occurs slowly as the Prx antioxidant system is only effective at eliminating low concentration of peroxides (238). The ability of BE to decrease the effect of endogenous levels of H_2O_2 is

demonstrated by the lower amounts of the PSSP form of Prx 2 present in the 10 μM BE treated cells compared to the untreated (control) cells.

We do not believe that 50 μM TBHP resulted in hyperoxidation and the immediate formation of sulfonic Prx directly from the reduced state (PS⁻), as this has been found to occur only in *Saccharomyces cerevisiae* (163). Although it is possible for the sulfinic Prx to hyperoxidize into sulfonic Prx over time, this may not have occurred here as the cells were only oxidized with TBHP for 30 min. Recent studies have demonstrated that hyperoxidation of sulfinic Prx into sulfonic Prx occurs over longer time periods of oxidation in cells (h) rather than shorter times (min) (238).

Even though we were unable to confirm the identify of spot H9 by MS analysis, it could be GAPDH based on: (1) the similarity of its apparent molecular mass, which we have calculated from the R2D-PAGE analysis to be the theoretical mass of the GAPDH monomer (Table 4.1); (2) its relative position based on previous studies identifying GAPDH in R2D-PAGE (141, 202, 216); and (3) the relative increase and decrease in disulfide bond formation (PSSP) upon pro-oxidant or anti-oxidant treatments (141, 202, 238). Under normal conditions, GAPDH is predominately found in its monomeric form (PS⁻), however, endogenouse H_2O_2 levels oxidize GAPDH into either its S-glutathionylated form, the reversible oxidative form of the disulfide, PSSP or PSOH, or into the irreversible oxidative form creating either PSO_2H (141) or PSO_3H (238). Upon hyperoxidation, a high molecular weight (HMW) disulfide aggregate is formed (> 100 kDa) directly action of RSO, PS⁻ and the PSSP (141).

In the control sample, H9 is present in small amounts as a PSSP, as expected for endogenous PSSP formation from monomeric GAPDH. In the BE treatment, a plausible

explanation for the significant increase in PSSP formation is that BE behaves similarly to low concentrations of the reductant, β-mercaptoethanol which previous studies have shown to increase PSSP formation of GAPDH in control cells (141). This presumably occurs here because the antioxidant effect of 10 μM BE reduces the amount of ROS available to oxidize GAPDH PSOH to GAPDH PSSP.

Consistent with this reasoning, there is more H9 PSSP present in the TBHP-treated cells compared to the control, vehicle-treated cells. Of interest, there was less H9 PSSP in TBHP-treated than in BE-TBHP-treated cells. We believe the reason for this is that BE decreases the amount of ROS that is available to oxidize the H9 monomeric PS$^-$ directly to its PSO_2H or PSO_3H form from its PSOH, a reaction that is favoured in high concentrations of ROS such as H_2O_2. Decreased ROS would mean enhanced formation of the disulfide product. We prefer this explanation to the other possibility, that H9 is oxidized to its HMW aggregate form because these cells were only treated with TBHP for 30 min. However, we showed earlier in the thesis that pure GAPDH is readily oxidized to HMW aggregate forms (Fig. 4.1B) (141, 202) and it is possible that some or all of the decrease in TBHP-treated cells referred to above is related to more oxidation of the H9 disulfide to HMW H9 aggregates. Either enhanced oxidation of H9 PSSP to HMW aggregates, or enhanced oxidation of PSOH to PSO_2H or PSO_3H would decrease the amount of PSSP present after R2D-PAGE analysis. Neither the H9 HMW aggregates nor the PSO_2H, or PSO_3H forms of H9 would be visible below the prominent diagonal line in our experiments. We believe these changes occurred because of the sudden change in the intracellular environment of these cells (reduction then oxidation) that were pre-treated with BE prioe to TBHP.

HMW GAPDH can be resolved by R2D-PAGE, but we do not believe we found any of these H9 HMW aggregates in our cell preparations contained any HMW GAPDH because 1) we utilized an SDS-based lysis buffer which is incapable of solubilising these aggregates (141), and 2) we discarded the nuclear fraction during our centrifugation procedure. Consequently, we believe that any HMW H9/GAPDH aggregates present would be missed by our analysis procedures because these aggregates were not of interest to us.

5.6　Signature of the Disulfide Proteome in Hepa1c1c7 cells

Separating proteins in different subcellular compartments by centrifugation prior to R2D-PAGE analysis allowed us to compare oxidized proteins (PSSP) by subcellular localization subsequent to treatment with pro-oxidant (50 μM) or antioxidant (70 nM) concentrations of UCB. Of the 21 protein spots that we identified in the different subcellular fractions, we were only able to identify five protein spots (all in the cytosol), by MS analysis (Table 4.2). As in our previous analysis in HEK 293 cells, only proteins expressed in large amounts could be identified. We were, however able to identify the apparent molecular mass of the monomeric form of all the protein spots from each of the subcellular fractions (Table 4.1). Despite not utilizing a sucrose based centrifugation method (239), we are confident that our mitochondrial and microsomal fractions are sufficiently enriched in mitochondrial and microsomal proteins to meet the goals of this thesis.

5.6.1 Proteomic Signature of the Cytosol

An analysis of the cytosolic proteomic signature of PSSP demonstrates that treating cells for 18 h with either 50 μM or 70 nM UCB resulted in a significant and different change in the intensity of protein spots, whereas treating cells for 6 h resulted in little (70 nM UCB) or virtually no change (50 μM UCB) compared to controls. We did find this somewhat surprising as our roGFP2 data demonstrated that this protein is already oxidized (50 μM UCB; Fig. 4.3B) or reduced (70 nM UCB; Fig 4.3C) by 3 h. In light of data from our R2D-PAGE experiments and previous work by other lab members (46), we believe that PSSP formation in the cytosol due to UCB is ultimately regulated by GSH:GSSG ratios, rather than the intracellular redox environment or the rate of ROS production.

Upon oxidation with 50 μM UCB, ROS production occurs at a rapid rate with the greatest increase occurring within 0.5 h, whereby after 2 h, ROS production decreases rapidly and becomes negligible after 3 h (46). Although the rapid formation of ROS slowly decreases the intracellular GSH content over time, this depletion becomes statistically significant at 3 h post-treatment (46). This demonstrates that at least up to 3 h, (1) sufficient NADPH is present in the system, allowing GSH-Rx to reduce GSSG back into GSH and (2) the redox environment is not sufficiently oxidized to inactivate GSH-Rx. As oxidation/reduction of the disulfide proteome depends on the cellular redox state (which affects oxidoreductases like Grx, Srx, and Trx), GSH:GSSG ratio, and characteristic of the protein structure, we believe we can now explain the differences in time in the proteomic signature of the cytosol by first describing the mechanism of formation of the disulfide at 0.5, 2, and 3 h in roGFP coded by the roGFP2 plasmid (126).

Furthermore, although the NADPH pools in the cytosol and the mitochondria are independent, our DNA microarray analysis shows that down regulation of *IDPm* does not occur by 1 h, but occurs by 6 h, demonstrating that $NADP^+$ is recycled into NADPH and reduction of GSSG back into GSH is affected some time between 1-6 h, at least in the mitochondria (240).

Previous reports have demonstrated that alterations in the disulfide bonding of roGFP2 are precipitated by changes in either the GSH:GSSG ratio, or reduced/oxidized Trx ratio (205). Upon oxidation with 50 µM UCB, ROS is rapidly released into the system effecting the intracellular redox environment of treated Hepa 1c1c7 cells. Within 0.5 h, PSH in the roGFP2 is oxidized into PSS, and thioltransferases like Trx are oxidized, which prevents them from reducing PSS/PSSP back into PS^-/PSH through a coupled reaction that consumes NADPH (124, 241). By 1 h, the rate of ROS production decreases, and Trx is reduced back to its normal reduced state allowing it to reduce roGFP2 back into PSH, with irreversible oxidation having been found to occur by 2 h. At 3 h, continued ROS production (albeit at a significantly lesser rate) continues to oxidize roGFP2 into PSS, however at this point in time, Trx no longer reduces roGFP2 PSS into PSH, and therefore roGFP2 continues to be present in its PSS form. Trx no longer reduces PSS because either (1) low GSH:GSSG ratios could inactivate it, or (2) lack of NADPH in the cell prevent the enzymatic conversion of Trx back to its reduced form.

Oxidation of cells with 50 µM UCB resulted in the formation of PSP, however our R2D-PAGE gels show there is little difference in the disulfide proteome of cells oxidized with 50 µM UCB for 6 h when compared to the control, whereas there is a significant difference in cells treated with 50 µM UCB for 18 h. We believe that the lack

of change in the intensity of the protein spots in the 50 μM for 6 h treatment is indicative of the fact that 50 μM UCB does not decrease the GSH:GSSG ratio of a cell to a significant enough degree to effect protein disulfide bonding. Indeed, any PSH that formed PSSP would be reduced back to PSH by either (1) Trx or another thiol transferase like PDI or Grx (132, 133) or (2) forms PSSG and then is reduced back into GSH and PSH by Grx (130, 131).

The pro-oxidant effects of 50 μM UCB on the disulfide proteome become readily apparent after 18 h treatment as there is a substantial decrease in the intensity of M1 and M3, and the complete disappearance of M8 and M10. These latter PSSP dimers are found in the control as well as all the other treatments. Their absence in the 50 μM for 18 h treatment is indicative of irreversible oxidation of these PSSP into either PSO_2H, or PSO_3H, changes which cause the protein to appear on the diagonal line. Although formation of PSSG would also cause these proteins to appear on the diagonal line, we do not believe there is enough GSH in these cells after prolonged oxidation to allow S-glutathionylation to proceed. Furthermore, as the intensity of M6 is found to only increase in the 50 μM UCB for 18 h treatment (vs the 6 h treatment), we believe this is consistent with the inability of the cell to reduce PSSP back into PSH, indicative of depleted GSH and NADPH by this point in time.

Our R2D-PAGE analysis demonstrates that 70 nM UCB is an effective antioxidant by 6 h post-treatment. We found the intensity of protein M2 to be increased (vs controls) by treatment with 70 nM UCB for 6 or 18 h. In this context, the substantial decrease in M5 might also be used as an indicator for antioxidants.

5.6.1.1 Identifying Disulfide Bonded Proteins (PSSP) Oxidized or Reduced by UCB

We were able to identify protein spots M1-M5 by mass spectrometry to be peroxiredoxin 1 (Prx 1), peroxiredoxin 2 (Prx 2), albumin, transferrin, and protein kinase C (PKC) (Table 4.2). Prx 1 and 2 are present in the control (untreated) cells indicating that the peroxiredoxin catalytic cycle is active and is reducing low, endogenous concentrations of H_2O_2 (238). The significant decrease in the intensity of Prx 1 in the 50 µM UCB for 18 h treated cells is indicative of hyperoxidation of Prx 1 into sulfinic Prx 1 (238). Our DNA microarray analysis demonstrates that 50 µM UCB affects the transcription of catalase some time between 1-6 h, however our R2D-PAGE data suggest that there is sufficient intracellular catalase activity to detoxify H_2O_2 up to 6 h as Prx 1, in cells treated with 50 µM UCB for 6 h, exists as a disulfide monomer, demonstrating that it is not being activated (238). Had it been activated, it would become hyperoxidized into sulfinic Prx 1 as was found to occur in the 50 µM for 18 h treatment, and would no longer appear as its disulfide, below the diagonal line after reduction. Prx 1 was activated in the 50 µM for 18 h treatment, in part because by this point in time catalase activity was decreased, facilitating activation of the Prx 1 catalytic cycle (238). This parallels results from our earlier studies in oxidized HEK 293 cells described in 5.5.1.1.

The significant increase in Prx 2 in Hepa 1c1c7 cells treated with 70 nM UCB for 6 or 18 h demonstrates the antioxidant effect of UCB. As reduction of sulfinic-Prx back into the disulfide-linked intermediary can only be carried out by Srx, 70 nM UCB appears to have an indirect effect on the reduction of sulfinic Prx, presumably through a mechanism that increases the rate of reaction carried out by Srx (238). The intensity of Prx 2 does not change in the 50 µM UCB for 6 and 18 h treated cells, as Prx 2 remains

inactivated. This demonstrates that despite the sufficiently low levels of catalase present in the system at this point in time, Prx 2 unlike Prx 1 remains inactivated. Prx 2 activation during levels of high oxidative stress appears to occur only if (1) catalase is not inactivated during the oxidative insult (238) or (2) the ROS is in the form of an organic peroxide like TBHP which is not a substrate for catalase (238).

M3 was identified in our cytosolic fraction by MS analysis to be albumin and serum albumin precursor. The intensity of M3 decreased in cells treated for 18 h with either 50 μM or 70 nM UCB. Mouse albumin is a 69 kDa, 584 amino acid protein with 36 reactive Cys thiol residues, 17 of which form intramolecular (PSS) disulfide bridges with one another, and the remaining two exist as free thiols (Cys 36 and Cys 578) (UniProt sequence http://www.uniprot.org/uniprot/P07724). The serum albumin precursor shows no difference from albumin in primary structure other than the presence of the NH$_2$-terminal hexapeptide which is cleaved forming albumin (242). Both of these proteins form intramolecular disulfide bonds (PSS) readily, as completely reduced albumin and serum albumin precursor regenerate native disulfide bonding patterns during a period of a few hours *in vitro* (242). As both of these proteins have PSS, they appear above the prominent diagonal line, and because the difference in the mol wt of both of these proteins is less than 2 kDa, these proteins appear together on the same protein spot (Swiss Institute of Bioinformatics http://www.expasy.org/cgi-bin/peptide-mass.pl).

A high sequence homology between mammals is present in albumin, whereby the 17 intramolecular disulfide bridges which form a nine loop-link-look structure centered around eight sequential Cys-Cys pairs has been conserved in all mammals (243). Despite the presence of only one available PSH (Cys34) in rats, humans, and cows instead of the

two found in mice (Cys35 and Cys578), a high sequence homology of 89%, 72%, and 69% is present between mice, and rats and humans (UniProt BLAST http://services.uniprot.org/blast/blast-20100728-0005075592). Albumin is a powerful antioxidant, with the free PSH able to scavenge HO^- forming PSOH (reversible oxidation), or PSH can become irreversibly oxidized and form PSO_2H, or PSO_3H (244). Seventy-eighty percent human serum albumin (HSA) in healthy human adults is found in its reduced form (PSH), the rest forms a disulfide with low molecular compounds like GSH or cysteine (244). HSA in its PSH form steadily decreases as humans age, and has been documented to be significantly lower in patients with respiratory diseases (244).

We postulate that in the 50 μM UCB for 18 h (a pro-oxidant treatment), the decrease in the intensity of the protein spot could be due to the formation of a homodimeric albumin disulfide (PSSP). The presence of this disulfide is further supported by the presence of a large protein spot with an apparent mol wt of 64 kDa (observed mol wt of mouse albumin is 69 kDa) (Fig. 4.8; UCB Cytosol 50 μM for 18 h R2D-PAGE gel) directly below the prominent diagonal line at a location with an apparent mol wt of 125 kDa (observed mol wt of mouse albumin homodimer is 138 kDa) between M7 and M10. As this protein spot has an apparent mol wt that is very similar to the observed mol wt of mouse albumin and albumin dimer, and as this protein spot is only present in significant amounts in the 50 μM for 18 h UCB treatment, we postulate that this protein spot is an albumin monomer that was originally an albumin dimer and was reduced and separated during R2D-PAGE.

Additionally, albumin has been found to form dimers upon oxidation in mammals. Work in this thesis confirms that this occurs with bovine albumin (Fig. 4.1A),

validating earlier work with albumin from cows (245). Despite the discovery of HSA dimers as early as 1985 (246) some researchers argued, based on the three dimensional structure of HSA determined by He et al. in 1992 (247, 248) that HSA can only form disulfide bonds with small molecules, as steric restrictions and the location of the single thiol (Cys35) of albumin in a crevice preclude dimer formation. Using R1D-PAGE, Ogasawara et al (249) demonstrated that HSA can be used as a marker for oxidative stress, because it dimerizes a concentration-dependent manner when oxidized with TBHP. Additionally, Ogasawara and his colleagues (249) confirmed that HSA PSSP are present in healthy humans at very low levels, but are present at higher concentrations in plasma of humans suffering from respiratory diseases.

In the case of the antioxidant 70 nM for 18 h UCB treatment, a possible explanation for the decrease in the intensity of the protein spot is that less albumin (which is also an antioxidant protein) is being produced by the cell. As the half-life of mouse albumin is only 2 days (250), a decrease in the amount of protein produced would be detected by this procedure.

The intensity of cytosolic protein spot M4 (identified to be transferrin) does not change in any of the treatments as compared to the vehicle treated control. Of the 38 Cys residues present in transferrin, 36 form PSSP consistent with its presence above the diagonal line in our R2D gels (UniProt http://www.uniprot.org/uniprot/Q921I1). The disulfide bonds of transferrin, however, are not in orderly sequence as are those of albumin, but overlap heavily within the two domains of the transferrin chain, 8 in one domain and 11 in the other (251). Furthermore, unlike albumin, transferrin does not refold spontaneously to yield native properties such as binding of iron, binding of

antibodies, or binding to reticulocytes following reduction of its disulfide bonds *in vitro* (252). As transferrin is not affected by 50 μM or 70 nM concentrations of UCB (pro-oxidant or antioxidant treatments), it appears that the tertiary structure of transferrin is resistant to oxidation/reduction under our exposure conditions.

M5, identified to be protein kinase C substrate 80K-H (PKCη) is significantly decreased in Hepa 1c1c7 cells treated with 70 nM UCB for 18 h. PKC isoforms usually exist as inactive forms in the cytosol and become activated upon translocation to membranes in the presence of isoform-specific second messengers (253). Although disulfide bonding has yet to be shown in PKCη, disulfide bonding has been found to activate PKCδ and to inactivate PKCε, and PKCα (254). Furthermore, treatment of cells with cysteamine or a metabolic cysteine precursor activates PKCδ and inactivates PKCε in a concentration-dependent and thiol-reversible manner (254). In a recent study, it was found that reducing PKCε with DTT almost doubled its activity and that Cys452 is a disulfide-regulated PKCε inactivating switch (254). This study established that disulfide inactivation of PKCε involves covalent modification of one or more Cys residues in the catalytic domain of the protein (254). Although this group was unable to deduce the exact disulfide modification of Cys452, their studies demonstrate that it could be due to either (1) PSS formation or (2) stable conjugation of a small molecule to Cys452, such as S-glutathionylation (254). Recent developments have demonstrated that the structure of PKCη is similar to that of PKCε (255). Furthermore, PKCη is located above the prominent diagonal line in its native state, providing direct evidence for a PSS form as proposed for PKCε. In the context of these reports, our data suggest it is possible that PKCη is also in an inactivated state due to the formation of PSS. Just as the DTT

treatment in PKCε results in an activation of the protein by reduction of the disulfide bond, it is possible that treatment of Hepa 1c1c7 cells with 70 nM UCB for 18 h and the resulting decreased oxidation/reduction ratio of the cytosol facilitates the reduction of the PSS form of PKCη to its PS⁻ or PSH. To be determined is whether or not this reduction of PKCη results in activation or inhibiton of this PKC isozyme. This is also a plausible explanation of why the intensity of protein spot M5 decreases significantly following cell treatment with 70 nM UCB for 18 h (i.e. reduction of PSSP tp PSH).

The intensity of protein spots M6, M8, and M10 was found to be significantly affected by oxidation with 50 μM UCB for 18 h with little or no change following all other treatments. M6, M8 and M10 each occurred as intermolecular protein disulfides because all of these proteins spots are situated below the diagonal line in the R2D gels. The intensity of the protein spot in M6 more than doubled in Hepa 1c1c7 cells treated with 50 μM UCB compared to the vehicle control, indicating that these proteins are protected during oxidation by reversible disulfide formation: i.e. P^1SSP^2. M6 forms a P^1SSP^2 with a significantly smaller protein as it is located slightly below the diagonal line. Protein spots M8 and M10 disappear entirely after the 50 μM UCB for 18 h treatment, indicating further oxidation of these proteins to the irreversible PSO_2H or PSO_3H form, which would appear on the diagonal line.

M9 reacts rapidly to changes in the oxidative environment in as little as 6 h. When Hepa 1c1c7 cells were treated with 50 μM UCB for 6 h, M9 was rapidly oxidized, and the intensity of the protein spot was significantly decreased. However within 18 h, the cell's antioxidant defense mechanisms are apparently capable of reducing the protein back to its biologically "normal" protein disulfide levels, as the intensity of the protein

spot in 50 µM UCB / 18 h treated cells is no different than that of the control. M9 is rapidly reduced by 70 nM UCB as is evident by the massive increase and then decrease in the intensity of that protein spot. First, the intensity of the protein spot in M6 increased after cell treatment with 70 nM UCB for 6 h, presumably because proteins that were going to be oxidized to PSO_2H and PSO_3H are arrested at the PSOH stage, resulting in increased formation of PSSP. At 18 h, the antioxidant effects of UCB become more apparent as the PSSP in M9 become reduced even further into PS⁻ or PSH, causing the protein to appear on the diagonal line, which is evident in the substantial decrease in the intensity of the protein spot at 70 nM UCB treatment for 18 h. M7 appears to be shielded from the pro-oxidant and antioxidant effects of UCB as its intensity does not change in any of the treatments.

5.6.2 Proteomic Signature of the Mitochondrial Fraction

A distinct proteomic signature resulted from the oxidizing effect of 50 µM UCB on proteins in the mitochondrial fraction because M15 was completely absent in cells treated for 6 or 18 h. Furthermore, M12, M13, and M15 decreased in intensity as time increases, with the complete disappearance of M13 and M15 by 18 h. We believe that the absence of all protein spots is indicative of the irreversible oxidation into either PSO_2H or PSO_3H. The antioxidant effect of UCB is not apparent as 70 nM UCB had little effect on the disulfide proteome at 6 h, with almost no effect at 18 h. Interestingly, M11 is the only protein spot which increased in intensity in the 70 nM UCB for 18 h treatment, demonstrating the sensitivity of this protein to any changes in the redox environment. It is important to note that the antioxidant effects of UCB using roGFP2 could only be measured in the cytosol. To better understand the effects of UCB on the

redox environment of the mitochondria, an roGFP2 plasmid that is localized to the mitochondria might have been employed (205).

We believe that M13 and M15 form heterodimers with one another as they are on the same vertical plane, and more importantly their decrease in 50 μM UCB for 6 h and complete absence in 50 μM UCB for 18 h treatments occurs simultaneously. It is probable that M13 and M14 are the same proteins as they are both on the same horizontal plane and have the same apparent MW. As the sum of twice the MW of M13 (190 kDa) would place it on the diagonal line, it is therefore probable that this protein exists as a homodimer in M13, or less likely as a heterodimeric complex compromising a single M13 protein and two M15 proteins whose sum would be 190 kDa. M14 is the only protein spot whose intensity does not change in any of the treatments. This demonstrates that the strong interaction of the disulfide bonds in that PSSP cause it to be shielded form the pro-oxidant and antioxidant effects of UCB.

Whereas 70 nM UCB had an effect on the intensity of PSSP in the cytosol, we noted that UCB had little effect on the mitochondrial fraction. The cytosol is a very reducing environment with a GSH:GSSG ratio of ~3000:1, whereas the mitochondria and ER by comparison are far more oxidizing with GSH:GSSG ratios of 20:1-40:1, and 1:1– 3:1, respectively (240). Like NADPH, the GSH:GSSG pools of each of these subcellular components is independent, and studies have suggested that redox states of the cytosol, mitochondria, and ER are influenced by factors that are specifically targeted to these components (240).

Our DNA microarray analysis demonstrated the down-regulation of *Cat, Gsta4,*

Gstk1, Gstm1, and Idpm, which code for proteins located in the mitochondria, and are associated with disulfide bonding (with the exception of catalase which does not form disulfide bonds). However we were unable to attribute any particular protein spot in our R2D-PAGE, with any protein whose genes were down-regulated. This was immediately apparent from the proteomic signature, as we did not find any protein spot below 50 kDa, and the monomeric form of all these protein spots is ~ 25 kDa with the exception of catalase which is 60 kDa (MW of proteins obtained from http://www.uniprot.org). The effect of UCB on catalase could not be detected in our R2D-PAGE gels as this protein would only be located on the diagonal line. Catalase does not form disulfide bonds when oxidized (231). Idpm undergoes *S*-glutathionylation at Cys 269 so one would expect a PSSP upon oxidation with UCB. We speculate there was too little PSSP formed from Idpm to be detected by our analysis (234). Although Gsta4, Gstk1, and Gstm1 exist as homodimers in their native state, they were not found in their monomeric form in any of the treatments or the control (256). We postulate that the Gst isoenzymes in the mitochondrial fraction were not found as they (1) were not present at high enough concentration and therefore could not be visualized or less likely, (2) they migrated off the R2D-PAGE gel during separation.

5.6.3 Proteomic Signature of the Endoplasmic Reticulum (ER) Fraction

UCB does not have a recognizable proteomic signature on any PSSP in the ER fraction. With the exception of M17, both the pro-oxidant (50 μM UCB) and antioxidant (70 nM UCB) treatments of UCB had little affect on any of the proteins within 6 h. However, after treatment for 18 h, the intensity of protein spots M18-M21 increased. There was no substantial change in M16 in any of the fractions. As both the pro-oxidant

and antioxidant concentrations of UCB affect the PSSP content, we believe that UCB affects the ER indirectly through an unidentified mechanism at 18 h, but not at 6 h.

We were unable to determine whether microsomal glutathione S-transferase, the protein product of *Gstm2*, shown by our DNA microarray experiments to be down regulated, was effected by 50 μM UCB treatment. This is because our procedure id not resolve troteins with a Mol Wt less that 21 kD and the MW of Gstm2 is less than 17 kD.

Our DNA microarray analysis also demonstrated the down-regulation of *Hmox1, and Prdx4,* genes whose proteins are located in the microsomes. *Hmox1* codes for heme oygenase 1 (HO-1), the inducible form of heme oxygenase, and is found on the diagonal line as it does not form any PSS/PSSP. Unlike HO-1, whose transcription is redox regulated at the transcriptional level, the constitutively expressed form of HO, HO-2 coded by *Hmox2*, is redox-regulated at the protein level (257). Upon oxidation, HO-2 forms an intermolecular PSS at Cys 265 and Cys 282 which increases its ability to bind to heme (a prominent antioxidant) (257). However, we were unable to determine the presence of HO-2 in any of our R2D-PAGE gels as we did not find any protein spot above the diagonal line near ~36 kDa, the MW of HO-2.

We believe that Prx4 could be either M19 or M20, as the apparent molecular mass of these protein spots is 30 and 31 kDa, which matches 31 kDa, the theoretical weight of Prx4. Additionally, the 2-cys peroxiredoxin Prdx4, is the only peroxiredoxin found in the ER (224). If M19 or M20 is found to be Prd4, it would demonstrate that in its "normal" state in the transformed cell line Hepa 1c1c, Prd4 is oxidized into $Prx-SO_2H$ or $Prx-SO_3H$, the latter incapable of activation, and is not present as a dimer. This could be plausible as the ER has a very oxidizing redox environment even in normal, non-

transformed cells (GSH:GSSG ratio between 1:1-1:3), so that very little Prx4 might be in the dimeric form, consistent with spots M19 or M20 in the untreated Hepa 1c1c7 cells (Fig. 4.13) (240).

5.7   Conclusion

Our results demonstrate that R2D-PAGE is an accurate method for identifying proteins in the disulfide proteome that are affected by oxidation or reduction with one major limitation. We were only able to identify proteins present in the cells in relatively large amounts, i.e. "high copy number" by means of mass spectrometry. Silver staining is considered to be the most sensitive technique for visualizing proteins in PAGE (204). One of the drawbacks of using this technique, however, is that the user is unable to approximate the amount of protein present in any given protein spot. This results in protein spots with very low concentration being picked for MS analysis, which could not be identified by the MALDI instrumentation that we used.

5.7.1   Proteomic Signature and Proteins identified in HEK 293 and Hepa1c1c7 cells

The differences in the proteomic signature of HEK 293 and Hepa1c1c7 cells is due to differences in (1) cell types (species) (213, 215), (2) subcellular fractions used (215), and (3) different pro-oxidant and antioxidant treatments that were employed (202). Not surprisingly, different species and tissues have different redox regulated proteins that undergo formation of PSSP (213, 215) as we noted when PSSP in control and oxidized HEK 293 and Hepa1c1c7 cells were analyzed by RD-PAGE. Proteins are also localized to specific organelles therefore it was not surprising that our R2D-PAGE data with cell

lysates from HEK 293 cells contained PRX3 (a mitochondrial protein) present within them that was not found in the cytosolic fraction of Hepa 1c1c7 cells (215).

The pro-oxidant compounds used in our studies (50 μM UCB and 50 μM TBHP for the Heoa1c1c7 and HEK 293 cells, respectively), had an effect on the cells antioxidant defense mechanism. Although 50 μM UCB is roughly equivalent to treating cells with 100 μM H_2O_2 in terms of intracellular ROS content, Hepa 1c1c7 cells treated with 50 μM UCB led to hyperoxidation of Prx 1 after 18 h, with no apparent effect on Prx 2, whereas HEK 293 cells treated with 50 μM TBHP resulted in hyperoxidation of both Prx 1 and 2 within 30 min. Furthermore, our study validates work demonstrating that 70 nM UCB is an antioxidant treatment because it increases the PSSP form of Prx 2 whereas 10 μM of the antioxidant BE, a concentration shown to slightly attenuate the toxicity of some oxidants, had no effect on on the PSSP form of Prx 2. 50 μM UCB is a pro-oxidant that affects both cytosolic and mitochondrial proteins in Hepa1c1c7 cells. We found that Hepa 1c1c7 cells treated with 50 μM UCB had a significant decrease or even the complete disappearance of disulfide bonded proteins at both 6 and 18 h. The reduction in the intensity of these disulfide spots is indicative of hyperoxidation of the disulfide bonded proteins into either sulfenic (PSOH), sulfinic (PSO2H), or sulphonic (PSO_3H) acid derivatives. We believe that the latter two irreversibly oxidized forms of these proteins (PSO_2H and PSO_3H derivatives) occurred because the GSH:GSSG levels in cells treated with 50 μM UCB is quite low.

70 nM UCB proved to be an effective antioxidant in the cytosol of Hepa 1c1c7 cells bud had no discernible effect on proteins in the mitochondrial fraction. This was not especially surprising because previous studies have suggested that redox states of the

cytosol, mitochondria and ER are influenced separately by factors specific to these organelles (240).

CHAPTER 6: FUTURE DIRECTIONS

Previous reports from our laboratory demonstrate that pro-oxidant (50 μM) and antioxidant (70 nM) concentrations of UCB result in the up or down-regulation of a variety of different genes (47). It would be interesting to evaluate the changes in the transcription of these proteins over time, by performing densitometry studies from Western Blots on proteins separated by R2D-PAGE. In this regard it would be particularly relevant to analyze the relative amounts of the various forms of proteins identified in this thesis to form disulfides that are quantitatively altered by exposure to UCB in Hepa1c1c7 cells to determine the earliest changes in protein that occur during the development of UCB-mediated toxicity. Immuunochemical based methods of detection would be employed wherever possible to verify protein identification (e.g. anti-GSH and anti-Prx1 and anti-Prx2 antibodies)

Secondly, it would be interesting to perform our R2D-PAGE experiments with a GSH specific fluorescent dye. This would allow us to determine the degree of S-glutathionylation that occurs in cells before and after treatment with pro-oxidant and antioxidant concentrations of UCB This technology could also assist in identification of proteins that are S-glutathionylated before and after treatments, by allowing us to readily pick and excise spots on the prominent diagonal line for MS analysis.

It would also be interesting to artificially alter the GSH:GSSG ratio in Hepa 1c1c7 cells and subsequently perform R2D-PAGE analysis. This would allow us to compare the proteomic signature from UCB treated and altered GSH:GSSG ratios which would allow us to determine if there are proteins that undergo disulfide bonding

specifically because of treatment with UCB or if all such changes observed occur solely as a result of perturbations cell's redox status.

Finally, it would be worthwhile to compare the changes to the disulfide proteome in transformed mouse hepatocytes (Hepa 1c1c7 cells) exposed to antioxidant and pro-oxidant concentrations of UCB compared to the changes in primary mouse hepatocytes that are well differentiated, compared to the transformed cells.

CHAPTER 7: REFERENCES

1.   Shapiro, S. M. Bilirubin toxicity in the developing nervous system. *Pediatr. Neurol.* **29,** 410-421 (2003).

2.   Kirk, J. M. Neonatal jaundice: a critical review of the role and practice of bilirubin analysis. *Ann. Clin. Biochem.* **45,** 452-462 (2008).

3.   Schipper, H. M., Song, W., Zukor, H., Hascalovici, J. R. & Zeligman, D. Heme oxygenase-1 and neurodegeneration: expanding frontiers of engagement. *J. Neurochem.* **110,** 469-485 (2009).

4.   Maines, M. D. The heme oxygenase system: a regulator of second messenger gases. *Annu. Rev. Pharmacol. Toxicol.* **37,** 517-554 (1997).

5.   Durante, W., Kroll, M. H., Christodoulides, N., Peyton, K. J. & Schafer, A. I. Nitric oxide induces heme oxygenase-1 gene expression and carbon monoxide production in vascular smooth muscle cells. *Circ. Res.* **80,** 557-564 (1997).

6.   Keyse, S. M. & Tyrrell, R. M. Heme oxygenase is the major 32-kDa stress protein induced in human skin fibroblasts by UVA radiation, hydrogen peroxide, and sodium arsenite. *Proc. Natl. Acad. Sci. U. S. A.* **86,** 99-103 (1989).

7.   Sedlak, T. W. *et al.* Bilirubin and glutathione have complementary antioxidant and cytoprotective roles. *Proc. Natl. Acad. Sci. U. S. A.* **106,** 5171-5176 (2009).

8.   Kutty, R. K. & Maines, M. D. Purification and characterization of biliverdin reductase from rat liver. *J. Biol. Chem.* **256,** 3956-3962 (1981).

9.   Shapiro, S. M. Definition of the clinical spectrum of kernicterus and bilirubin-induced neurologic dysfunction (BIND). *J. Perinatol.* **25,** 54-59 (2005).

10.   Kaplan, M. & Hammerman, C. Understanding severe hyperbilirubinemia and preventing kernicterus: adjuncts in the interpretation of neonatal serum bilirubin. *Clin. Chim. Acta* **356,** 9-21 (2005).

11.   Sedlak, T. W. & Snyder, S. H. Bilirubin benefits: cellular protection by a biliverdin reductase antioxidant cycle. *Pediatrics* **113,** 1776-1782 (2004).

12.   Abboud, S. & Haile, D. J. A novel mammalian iron-regulated protein involved in intracellular iron metabolism. *J. Biol. Chem.* **275,** 19906-19912 (2000).

13.   Baranano, D. E. *et al.* A mammalian iron ATPase induced by iron. *J. Biol. Chem.* **275,** 15166-15173 (2000).

14. Rohrer, J. S. *et al*. Stabilization of iron in a ferrous form by ferritin. A study using dispersive and conventional x-ray absorption spectroscopy. *J. Biol. Chem.* **262**, 13385-13387 (1987).

15. Estrella, B. *et al*. Acute respiratory diseases and carboxyhemoglobin status in school children of Quito, Ecuador. *Environ. Health Perspect.* **113**, 607-611 (2005).

16. Zakhary, R. *et al*. Targeted gene deletion of heme oxygenase 2 reveals neural role for carbon monoxide. *Proc. Natl. Acad. Sci. U. S. A.* **94**, 14848-14853 (1997).

17. Morse, D. & Choi, A. M. Heme oxygenase-1: from bench to bedside. *Am. J. Respir. Crit. Care Med.* **172**, 660-670 (2005).

18. Yasuda, S., Itoh, S., Imai, T., Isobe, K. & Onishi, S. Cyclobilirubin formation by in vitro photoirradiation with neonatal phototherapy light. *Pediatr. Int.* **43**, 270-275 (2001).

19. Maisels, M. J. & McDonagh, A. F. Phototherapy for neonatal jaundice. *N. Engl. J. Med.* **358**, 920-928 (2008).

20. Maisels, M. J. & Kring, E. The contribution of hemolysis to early jaundice in normal newborns. *Pediatrics* **118**, 276-279 (2006).

21. Kaplan, M. *et al*. Imbalance between production and conjugation of bilirubin: a fundamental concept in the mechanism of neonatal jaundice. *Pediatrics* **110**, e47 (2002).

22. Wennberg, R. P. The blood-brain barrier and bilirubin encephalopathy. *Cell. Mol. Neurobiol.* **20**, 97-109 (2000).

23. Fay, D. L., Schellhase, K. G. & Suresh, G. K. Bilirubin screening for normal newborns: a critique of the hour-specific bilirubin nomogram. *Pediatrics* **124**, 1203-1205 (2009).

24. Abdel Fattah, M., Abdel Ghany, E., Adel, A., Mosallam, D. & Kamal, S. Glucose-6-phosphate dehydrogenase and red cell pyruvate kinase deficiency in neonatal jaundice cases in egypt. *Pediatr. Hematol. Oncol.* **27**, 262-271 (2010).

25. Valaes, T. Severe neonatal jaundice associated with glucose-6-phosphate dehydrogenase deficiency: pathogenesis and global epidemiology. *Acta Paediatr. Suppl.* **394**, 58-76 (1994).

26. Watchko, J. F. Kernicterus and the molecular mechanisms of bilirubin-induced CNS injury in newborns. *Neuromolecular Med.* **8**, 513-529 (2006).

27. Ostrow, J. D., Pascolo, L., Shapiro, S. M. & Tiribelli, C. New concepts in bilirubin encephalopathy. *Eur. J. Clin. Invest.* **33**, 988-997 (2003).

28. De Luca, D., Jackson, G. L., Tridente, A., Carnielli, V. P. & Engle, W. D. Transcutaneous bilirubin nomograms: a systematic review of population differences and analysis of bilirubin kinetics. *Arch. Pediatr. Adolesc. Med.* **163**, 1054-1059 (2009).

29. Bhutani, V. K., Johnson, L. H., Schwoebel, A. & Gennaro, S. A systems approach for neonatal hyperbilirubinemia in term and near-term newborns. *J. Obstet. Gynecol. Neonatal Nurs.* **35**, 444-455 (2006).

30. Bhutani, V. K. & Johnson, L. H. Urgent clinical need for accurate and precise bilirubin measurements in the United States to prevent kernicterus. *Clin. Chem.* **50**, 477-480 (2004).

31. Ebbesen, F. & Nyboe, J. Postnatal changes in the ability of plasma albumin to bind bilirubin. *Acta Paediatr. Scand.* **72**, 665-670 (1983).

32. Ahlfors, C. E. Criteria for exchange transfusion in jaundiced newborns. *Pediatrics* **93**, 488-494 (1994).

33. Nilsen, S. T., Finne, P. H.; Bergsjo, P. & Stamnes, O. Males with neonatal hyperbilirubinemia examined at 18 years of age. *Acta Paediatr. Scand.* **73**, 176-180 (1984).

34. Ozmert, E. *et al.* Long-term follow-up of indirect hyperbilirubinemia in full-term Turkish infants. *Acta Paediatr.* **85**, 1440-1444 (1996).

35. Hanko, E., Hansen, T. W., Almaas, R., Lindstad, J. & Rootwelt, T. Bilirubin induces apoptosis and necrosis in human NT2-N neurons. *Pediatr. Res.* **57**, 179-184 (2005).

36. Silva, R. F., Rodrigues, C. M. & Brites, D. Bilirubin-induced apoptosis in cultured rat neural cells is aggravated by chenodeoxycholic acid but prevented by ursodeoxycholic acid. *J. Hepatol.* **34**, 402-408 (2001).

37. Cashore, W. J. Free bilirubin concentrations and bilirubin-binding affinity in term and preterm infants. *J. Pediatr.* **96**, 521-527 (1980).

38. Zucker, S. D., Goessling, W., Bootle, E. J. & Sterritt, C. Localization of bilirubin in phospholipid bilayers by parallax analysis of fluorescence quenching. *J. Lipid Res.* **42**, 1377-1388 (2001).

39. Cestaro, B. *et al.* Interaction of bilirubin with small unilamellar vesicles of dipalmitoylphosphatidylcholine. *Ital. J. Biochem.* **32**, 318-329 (1983).

40. Rodrigues, C. M., Sola, S. & Brites, D. Bilirubin induces apoptosis via the mitochondrial pathway in developing rat brain neurons. *Hepatology* **35**, 1186-1195 (2002).

41. Grojean, S., Koziel, V., Vert, P. & Daval, J. L. Bilirubin induces apoptosis via activation of NMDA receptors in developing rat brain neurons. *Exp. Neurol.* **166**, 334-341 (2000).

42. Schiff, D., Chan, G. & Poznansky, M. J. Bilirubin toxicity in neural cell lines N115 and NBR10A. *Pediatr. Res.* **19**, 908-911 (1985).

43. Silva, R. *et al*. Inhibition of glutamate uptake by unconjugated bilirubin in cultured cortical rat astrocytes: role of concentration and pH. *Biochem. Biophys. Res. Commun.* **265**, 67-72 (1999).

44. Chuniaud, L. *et al*. Cytotoxicity of bilirubin for human fibroblasts and rat astrocytes in culture. Effect of the ratio of bilirubin to serum albumin. *Clin. Chim. Acta* **256**, 103-114 (1996).

45. Seubert, J. M., Darmon, A. J., El-Kadi, A. O., D'Souza, S. J. & Bend, J. R. Apoptosis in murine hepatoma hepa 1c1c7 wild-type, C12, and C4 cells mediated by bilirubin. *Mol. Pharmacol.* **62**, 257-264 (2002).

46. Oakes, G. H. & Bend, J. R. Early steps in bilirubin-mediated apoptosis in murine hepatoma (Hepa 1c1c7) cells are characterized by aryl hydrocarbon receptor-independent oxidative stress and activation of the mitochondrial pathway. *J. Biochem. Mol. Toxicol.* **19**, 244-255 (2005).

47. Oakes, G. H. & Bend, J. R. Global changes in gene regulation demonstrate that unconjugated bilirubin is able to upregulate and activate select components of the endoplasmic reticulum stress response pathway. *J. Biochem. Mol. Toxicol.* **24**, 73-88 (2010).

48. Passamonti, S. *et al*. Uptake of bilirubin into HepG2 cells assayed by thermal lens spectroscopy. Function of bilitranslocase. *FEBS J.* **272**, 5522-5535 (2005).

49. Lathe, G. H. & Walker, M. The synthesis of bilirubin glucuronide in animal and human liver. *Biochem. J.* **70**, 705-712 (1958).

50. Bosma, P. J. *et al*. Bilirubin UDP-glucuronosyltransferase 1 is the only relevant bilirubin glucuronidating isoform in man. *J. Biol. Chem.* **269**, 17960-17964 (1994).

51. Schmid, R. The identification of direct-reacting bilirubin as bilirubin glucuronide. *J. Biol. Chem.* **229**, 881-888 (1957).

52. Fevery, J., Van de Vijver, M., Michiels, R. & Heirwegh, K. P. Comparison in different species of biliary bilirubin-IX alpha conjugates with the activities of hepatic and renal bilirubin-IX alpha-uridine diphosphate glycosyltransferases. *Biochem. J.* **164**, 737-746 (1977).

53. Blanckaert, N. Analysis of bilirubin and bilirubin mono- and di-conjugates. Determination of their relative amounts in biological samples. *Biochem. J.* **185**, 115-128 (1980).

54. Jedlitschky, G. *et al*. ATP-dependent transport of bilirubin glucuronides by the multidrug resistance protein MRP1 and its hepatocyte canalicular isoform MRP2. *Biochem. J.* **327 (Pt 1)**, 305-310 (1997).

55. Ho, K. J., Hsu, S. C., Chen, J. S. & Ho, L. H. Human biliary beta-glucuronidase: correlation of its activity with deconjugation of bilirubin in the bile. *Eur. J. Clin. Invest.* **16**, 361-367 (1986).

56. Gadelle, D., Raibaud, P. & Sacquet, E. beta-Glucuronidase activities of intestinal bacteria determined both in vitro and in vivo in gnotobiotic rats. *Appl. Environ. Microbiol.* **49**, 682-685 (1985).

57. Fahmy, K., Gray, C. H. & Nicholson, D. C. The reduction of bile pigments by faecal and intestinal bacteria. *Biochim. Biophys. Acta* **264**, 85-97 (1972).

58. Vitek, L. *et al*. Identification of bilirubin reduction products formed by Clostridium perfringens isolated from human neonatal fecal flora. *J. Chromatogr. B. Analyt Technol. Biomed. Life. Sci.* **833**, 149-157 (2006).

59. Vitek, L. & Carey, M. C. Enterohepatic cycling of bilirubin as a cause of 'black' pigment gallstones in adult life. *Eur. J. Clin. Invest.* **33**, 799-810 (2003).

60. Vitek, L. *et al*. Intestinal colonization leading to fecal urobilinoid excretion may play a role in the pathogenesis of neonatal jaundice. *J. Pediatr. Gastroenterol. Nutr.* **30**, 294-298 (2000).

61. Gourley, G. R. & Arend, R. A. beta-Glucuronidase and hyperbilirubinaemia in breast-fed and formula-fed babies. *Lancet* **1**, 644-646 (1986).

62. Brink, M. A. *et al*. Enterohepatic cycling of bilirubin: a putative mechanism for pigment gallstone formation in ileal Crohn's disease. *Gastroenterology* **116**, 1420-1427 (1999).

63. McDonagh, A. F. in *The Porphyrins* 293-491 (Academic Press, New York, NY, 1979).

64. Tenhunen, R., Ross, M. E., Marver, H. S. & Schmid, R. Reduced nicotinamide-adenine dinucleotide phosphate dependent biliverdin reductase: partial purification and characterization. *Biochemistry* **9**, 298-303 (1970).

65. Stocker, R., Glazer, A. N. & Ames, B. N. Antioxidant activity of albumin-bound bilirubin. *Proc. Natl. Acad. Sci. U. S. A.* **84**, 5918-5922 (1987).

66. Stocker, R., Yamamoto, Y., McDonagh, A. F., Glazer, A. N. & Ames, B. N. Bilirubin is an antioxidant of possible physiological importance. *Science* **235**, 1043-1046 (1987).

67. Baranano, D. E., Rao, M., Ferris, C. D. & Snyder, S. H. Biliverdin reductase: a major physiologic cytoprotectant. *Proc. Natl. Acad. Sci. U. S. A.* **99**, 16093-16098 (2002).

68. Ohnaka, K. *et al.* Inverse associations of serum bilirubin with high sensitivity C-reactive protein, glycated hemoglobin, and prevalence of type 2 diabetes in middle-aged and elderly Japanese men and women. *Diabetes Res. Clin. Pract.* **88**, 103-110 (2010).

69. Giustarini, D., Rossi, R., Milzani, A., Colombo, R. & Dalle-Donne, I. S-glutathionylation: from redox regulation of protein functions to human diseases. *J. Cell. Mol. Med.* **8**, 201-212 (2004).

70. D'Autreaux, B. & Toledano, M. B. ROS as signalling molecules: mechanisms that generate specificity in ROS homeostasis. *Nat. Rev. Mol. Cell Biol.* **8**, 813-824 (2007).

71. Kohchi, C., Inagawa, H., Nishizawa, T. & Soma, G. ROS and innate immunity. *Anticancer Res.* **29**, 817-821 (2009).

72. Hensley, K., Robinson, K. A., Gabbita, S. P., Salsman, S. & Floyd, R. A. Reactive oxygen species, cell signaling, and cell injury. *Free Radic. Biol. Med.* **28**, 1456-1462 (2000).

73. Halliwell, B. Oxygen and nitrogen are pro-carcinogens. Damage to DNA by reactive oxygen, chlorine and nitrogen species: measurement, mechanism and the effects of nutrition. *Mutat. Res.* **443**, 37-52 (1999).

74. Gille, J. J., van Berkel, C. G. & Joenje, H. Mutagenicity of metabolic oxygen radicals in mammalian cell cultures. *Carcinogenesis* **15**, 2695-2699 (1994).

75. Floyd, R. A. The role of 8-hydroxyguanine in carcinogenesis. *Carcinogenesis* **11**, 1447-1450 (1990).

76. Barnham, K. J., Masters, C. L. & Bush, A. I. Neurodegenerative diseases and oxidative stress. *Nat. Rev. Drug Discov.* **3**, 205-214 (2004).

77. Finkel, T. & Holbrook, N. J. Oxidants, oxidative stress and the biology of ageing. *Nature* **408**, 239-247 (2000).

78. Colavitti, R. & Finkel, T. Reactive oxygen species as mediators of cellular senescence. *IUBMB Life* **57**, 277-281 (2005).

79. Pedersen, W. A. *et al.* Protein modification by the lipid peroxidation product 4-hydroxynonenal in the spinal cords of amyotrophic lateral sclerosis patients. *Ann. Neurol.* **44**, 819-824 (1998).

80. Dexter, D. T. *et al.* Basal lipid peroxidation in substantia nigra is increased in Parkinson's disease. *J. Neurochem.* **52**, 381-389 (1989).

81. Butterfield, D. A., Castegna, A., Lauderback, C. M. & Drake, J. Evidence that amyloid beta-peptide-induced lipid peroxidation and its sequelae in Alzheimer's disease brain contribute to neuronal death. *Neurobiol. Aging* **23**, 655-664 (2002).

82. Selley, M. L., Close, D. R. & Stern, S. E. The effect of increased concentrations of homocysteine on the concentration of (E)-4-hydroxy-2-nonenal in the plasma and cerebrospinal fluid of patients with Alzheimer's disease. *Neurobiol. Aging* **23**, 383-388 (2002).

83. Burdon, R. H., Alliangana, D. & Gill, V. Endogenously generated active oxygen species and cellular glutathione levels in relation to BHK-21 cell proliferation. *Free Radic. Res.* **21**, 121-133 (1994).

84. Halliwell, B. & Aruoma, O. I. DNA damage by oxygen-derived species. Its mechanism and measurement in mammalian systems. *FEBS Lett.* **281**, 9-19 (1991).

85. Chaudhary, A. K. *et al.* Detection of endogenous malondialdehyde-deoxyguanosine adducts in human liver. *Science* **265**, 1580-1582 (1994).

86. Ghissassi, F., Barbin, A., Nair, J. & Bartsch, H. Formation of 1,N6-ethenoadenine and 3,N4-ethenocytosine by lipid peroxidation products and nucleic acid bases. *Chem. Res. Toxicol.* **8**, 278-283 (1995).

87. Feig, D. I. & Loeb, L. A. Mechanisms of mutation by oxidative DNA damage: reduced fidelity of mammalian DNA polymerase beta. *Biochemistry* **32**, 4466-4473 (1993).

88. Taguchi, T. & Ohashi, M. Changes in fidelity levels of DNA polymerases alpha-1, alpha-2, and beta during ageing in rats. *Mech. Ageing Dev.* **99**, 33-47 (1997).

89. Poole, L. B., Karplus, P. A. & Claiborne, A. Protein sulfenic acids in redox signaling. *Annu. Rev. Pharmacol. Toxicol.* **44**, 325-347 (2004).

90. Gilbert, H. F. Molecular and cellular aspects of thiol-disulfide exchange. *Adv. Enzymol. Relat. Areas Mol. Biol.* **63**, 69-172 (1990).

91. Townsend, D. M. S-glutathionylation: indicator of cell stress and regulator of the unfolded protein response. *Mol. Interv.* **7**, 313-324 (2007).

92. Riemer, J., Bulleid, N. & Herrmann, J. M. Disulfide formation in the ER and mitochondria: two solutions to a common process. *Science* **324**, 1284-1287 (2009).

93. Boveris, A. & Chance, B. The mitochondrial generation of hydrogen peroxide. General properties and effect of hyperbaric oxygen. *Biochem. J.* **134**, 707-716 (1973).

94. Chae, H. Z., Kang, S. W. & Rhee, S. G. Isoforms of mammalian peroxiredoxin that reduce peroxides in presence of thioredoxin. *Methods Enzymol.* **300**, 219-226 (1999).

95. Dickinson, D. A. & Forman, H. J. Glutathione in defense and signaling: lessons from a small thiol. *Ann. N. Y. Acad. Sci.* **973**, 488-504 (2002).

96. Valko, M. *et al.* Free radicals and antioxidants in normal physiological functions and human disease. *Int. J. Biochem. Cell Biol.* **39**, 44-84 (2007).

97. Schafer, F. Q. & Buettner, G. R. Redox environment of the cell as viewed through the redox state of the glutathione disulfide/glutathione couple. *Free Radic. Biol. Med.* **30**, 1191-1212 (2001).

98. Ballatori, N. *et al.* Glutathione dysregulation and the etiology and progression of human diseases. *Biol. Chem.* **390**, 191-214 (2009).

99. Pool-Zobel, B., Veeriah, S. & Bohmer, F. D. Modulation of xenobiotic metabolising enzymes by anticarcinogens -- focus on glutathione S-transferases and their role as targets of dietary chemoprevention in colorectal carcinogenesis. *Mutat. Res.* **591**, 74-92 (2005).

100. Motohashi, H. & Yamamoto, M. Nrf2-Keap1 defines a physiologically important stress response mechanism. *Trends Mol. Med.* **10**, 549-557 (2004).

101. Waleh, N. S. *et al.* The redox-sensitive human antioxidant responsive element induces gene expression under low oxygen conditions. *Carcinogenesis* **19**, 1333-1337 (1998).

102. Rushmore, T. H., Morton, M. R. & Pickett, C. B. The antioxidant responsive element. Activation by oxidative stress and identification of the DNA consensus sequence required for functional activity. *J. Biol. Chem.* **266**, 11632-11639 (1991).

103. Nguyen, T., Sherratt, P. J. & Pickett, C. B. Regulatory mechanisms controlling gene expression mediated by the antioxidant response element. *Annu. Rev. Pharmacol. Toxicol.* **43**, 233-260 (2003).

104. Sasaki, H. *et al.* Electrophile response element-mediated induction of the cystine/glutamate exchange transporter gene expression. *J. Biol. Chem.* **277**, 44765-44771 (2002).

105. Hayashi, A., Suzuki, H., Itoh, K., Yamamoto, M. & Sugiyama, Y. Transcription factor Nrf2 is required for the constitutive and inducible expression of multidrug resistance-associated protein 1 in mouse embryo fibroblasts. *Biochem. Biophys. Res. Commun.* **310**, 824-829 (2003).

106. Motohashi, H., Katsuoka, F., Shavit, J. A., Engel, J. D. & Yamamoto, M. Positive or negative MARE-dependent transcriptional regulation is determined by the abundance of small Maf proteins. *Cell* **103**, 865-875 (2000).

107. Zhang, D. D., Lo, S. C., Cross, J. V., Templeton, D. J. & Hannink, M. Keap1 is a redox-regulated substrate adaptor protein for a Cul3-dependent ubiquitin ligase complex. *Mol. Cell. Biol.* **24**, 10941-10953 (2004).

108. Cullinan, S. B., Gordan, J. D., Jin, J., Harper, J. W. & Diehl, J. A. The Keap1-BTB protein is an adaptor that bridges Nrf2 to a Cul3-based E3 ligase: oxidative stress sensing by a Cul3-Keap1 ligase. *Mol. Cell. Biol.* **24**, 8477-8486 (2004).

109. Furukawa, M. & Xiong, Y. BTB protein Keap1 targets antioxidant transcription factor Nrf2 for ubiquitination by the Cullin 3-Roc1 ligase. *Mol. Cell. Biol.* **25**, 162-171 (2005).

110. Itoh, K. *et al.* Keap1 represses nuclear activation of antioxidant responsive elements by Nrf2 through binding to the amino-terminal Neh2 domain. *Genes Dev.* **13**, 76-86 (1999).

111. Zhang, D. D. & Hannink, M. Distinct cysteine residues in Keap1 are required for Keap1-dependent ubiquitination of Nrf2 and for stabilization of Nrf2 by chemopreventive agents and oxidative stress. *Mol. Cell. Biol.* **23**, 8137-8151 (2003).

112. Wakabayashi, N. *et al.* Protection against electrophile and oxidant stress by induction of the phase 2 response: fate of cysteines of the Keap1 sensor modified by inducers. *Proc. Natl. Acad. Sci. U. S. A.* **101**, 2040-2045 (2004).

113. Kobayashi, A. *et al*. Oxidative stress sensor Keap1 functions as an adaptor for Cul3-based E3 ligase to regulate proteasomal degradation of Nrf2. *Mol. Cell. Biol.* **24**, 7130-7139 (2004).

114. Kraft, A. D., Johnson, D. A. & Johnson, J. A. Nuclear factor E2-related factor 2-dependent antioxidant response element activation by tert-butylhydroquinone and sulforaphane occurring preferentially in astrocytes conditions neurons against oxidative insult. *J. Neurosci.* **24**, 1101-1112 (2004).

115. Chan, K. & Kan, Y. W. Nrf2 is essential for protection against acute pulmonary injury in mice. *Proc. Natl. Acad. Sci. U. S. A.* **96**, 12731-12736 (1999).

116. Enomoto, A. *et al*. High sensitivity of Nrf2 knockout mice to acetaminophen hepatotoxicity associated with decreased expression of ARE-regulated drug metabolizing enzymes and antioxidant genes. *Toxicol. Sci.* **59**, 169-177 (2001).

117. Goldring, C. E. *et al*. Activation of hepatic Nrf2 in vivo by acetaminophen in CD-1 mice. *Hepatology* **39**, 1267-1276 (2004).

118. Aoki, Y. *et al*. Accelerated DNA adduct formation in the lung of the Nrf2 knockout mouse exposed to diesel exhaust. *Toxicol. Appl. Pharmacol.* **173**, 154-160 (2001).

119. Dalle-Donne, I. *et al*. Molecular mechanisms and potential clinical significance of S-glutathionylation. *Antioxid. Redox Signal.* **10**, 445-473 (2008).

120. Chai, Y. C., Hoppe, G. & Sears, J. Reversal of protein S-glutathiolation by glutaredoxin in the retinal pigment epithelium. *Exp. Eye Res.* **76**, 155-159 (2003).

121. Lind, C. *et al*. Identification of S-glutathionylated cellular proteins during oxidative stress and constitutive metabolism by affinity purification and proteomic analysis. *Arch. Biochem. Biophys.* **406**, 229-240 (2002).

122. Reynaert, N. L. *et al*. In situ detection of S-glutathionylated proteins following glutaredoxin-1 catalyzed cysteine derivatization. *Biochim. Biophys. Acta* **1760**, 380-387 (2006).

123. Pastore, A. *et al*. Actin glutathionylation increases in fibroblasts of patients with Friedreich's ataxia: a potential role in the pathogenesis of the disease. *J. Biol. Chem.* **278**, 42588-42595 (2003).

124. Biswas, S., Chida, A. S. & Rahman, I. Redox modifications of protein-thiols: emerging roles in cell signaling. *Biochem. Pharmacol.* **71**, 551-564 (2006).

125. Gallogly, M. M. & Mieyal, J. J. Mechanisms of reversible protein glutathionylation in redox signaling and oxidative stress. *Curr. Opin. Pharmacol.* **7**, 381-391 (2007).

126. Di Simplicio, P., Franconi, F., Frosali, S. & Di Giuseppe, D. Thiolation and nitrosation of cysteines in biological fluids and cells. *Amino Acids* **25**, 323-339 (2003).

127. Meyer, A. J. The integration of glutathione homeostasis and redox signaling. *J. Plant Physiol.* **165**, 1390-1403 (2008).

128. Martinez-Ruiz, A. & Lamas, S. Signalling by NO-induced protein S-nitrosylation and S-glutathionylation: convergences and divergences. *Cardiovasc. Res.* **75**, 220-228 (2007).

129. Townsend, D. M. *et al.* Novel role for glutathione S-transferase pi. Regulator of protein S-Glutathionylation following oxidative and nitrosative stress. *J. Biol. Chem.* **284**, 436-445 (2009).

130. Mieyal, J. J., Gallogly, M. M., Qanungo, S., Sabens, E. A. & Shelton, M. D. Molecular mechanisms and clinical implications of reversible protein S-glutathionylation. *Antioxid. Redox Signal.* **10**, 1941-1988 (2008).

131. Tew, K. D. Redox in redux: Emergent roles for glutathione S-transferase P (GSTP) in regulation of cell signaling and S-glutathionylation. *Biochem. Pharmacol.* **73**, 1257-1269 (2007).

132. Peltoniemi, M. J., Karala, A. R., Jurvansuu, J. K., Kinnula, V. L. & Ruddock, L. W. Insights into deglutathionylation reactions. Different intermediates in the glutaredoxin and protein disulfide isomerase catalyzed reactions are defined by the gamma-linkage present in glutathione. *J. Biol. Chem.* **281**, 33107-33114 (2006).

133. Findlay, V. J. *et al.* A novel role for human sulfiredoxin in the reversal of glutathionylation. *Cancer Res.* **66**, 6800-6806 (2006).

134. Chrestensen, C. A., Starke, D. W. & Mieyal, J. J. Acute cadmium exposure inactivates thioltransferase (Glutaredoxin), inhibits intracellular reduction of protein-glutathionyl-mixed disulfides, and initiates apoptosis. *J. Biol. Chem.* **275**, 26556-26565 (2000).

135. Chang, T. S. *et al.* Characterization of mammalian sulfiredoxin and its reactivation of hyperoxidized peroxiredoxin through reduction of cysteine sulfinic acid in the active site to cysteine. *J. Biol. Chem.* **279**, 50994-51001 (2004).

136. Jonsson, T. J., Tsang, A. W., Lowther, W. T. & Furdui, C. M. Identification of intact protein thiosulfinate intermediate in the reduction of cysteine sulfinic acid in peroxiredoxin by human sulfiredoxin. *J. Biol. Chem.* **283**, 22890-22894 (2008).

137. Sommer, A. & Traut, R. R. Diagonal polyacrylamide-dodecyl sulfate gel electrophoresis for the identification of ribosomal proteins crosslinked with methyl-4-mercaptobutyrimidate. *Proc. Natl. Acad. Sci. U. S. A.* **71**, 3946-3950 (1974).

138. Leichert, L. I. & Jakob, U. Global methods to monitor the thiol-disulfide state of proteins in vivo. *Antioxid. Redox Signal.* **8**, 763-772 (2006).

139. Stadtman, E. R. Protein oxidation in aging and age-related diseases. *Ann. N. Y. Acad. Sci.* **928**, 22-38 (2001).

140. Jaffrey, S. R. & Snyder, S. H. The biotin switch method for the detection of S-nitrosylated proteins. *Sci. STKE* **2001**, PL1 (2001).

141. Cumming, R. C. & Schubert, D. Amyloid-beta induces disulfide bonding and aggregation of GAPDH in Alzheimer's disease. *FASEB J.* **19**, 2060-2062 (2005).

142. Rinalducci, S., Murgiano, L. & Zolla, L. Redox proteomics: basic principles and future perspectives for the detection of protein oxidation in plants. *J. Exp. Bot.* **59**, 3781-3801 (2008).

143. Grimm, L. M., Collison, M. W., Fisher, R. A. & Thomas, J. A. Protein mixed-disulfides in cardiac cells. S-thiolation of soluble proteins in response to diamide. *Biochim. Biophys. Acta* **844**, 50-54 (1985).

144. Dalle-Donne, I., Rossi, R., Colombo, G., Giustarini, D. & Milzani, A. Protein S-glutathionylation: a regulatory device from bacteria to humans. *Trends Biochem. Sci.* **34**, 85-96 (2009).

145. Rinna, A., Torres, M. & Forman, H. J. Stimulation of the alveolar macrophage respiratory burst by ADP causes selective glutathionylation of protein tyrosine phosphatase 1B. *Free Radic. Biol. Med.* **41**, 86-91 (2006).

146. Cross, J. V. & Templeton, D. J. Oxidative stress inhibits MEKK1 by site-specific glutathionylation in the ATP-binding domain. *Biochem. J.* **381**, 675-683 (2004).

147. Pineda-Molina, E. *et al.* Glutathionylation of the p50 subunit of NF-kappaB: a mechanism for redox-induced inhibition of DNA binding. *Biochemistry* **40**, 14134-14142 (2001).

148. Stamler, J. S. & Hausladen, A. Oxidative modifications in nitrosative stress. *Nat. Struct. Biol.* **5**, 247-249 (1998).

149. Fratelli, M. *et al.* Identification of proteins undergoing glutathionylation in oxidatively stressed hepatocytes and hepatoma cells. *Proteomics* **3**, 1154-1161 (2003).

150. Abate, C., Patel, L., Rauscher, F. J.,3rd & Curran, T. Redox regulation of fos and jun DNA-binding activity in vitro. *Science* **249**, 1157-1161 (1990).

151. Klatt, P., Molina, E. P. & Lamas, S. Nitric oxide inhibits c-Jun DNA binding by specifically targeted S-glutathionylation. *J. Biol. Chem.* **274**, 15857-15864 (1999).

152. Michelet, L. *et al.* Glutathionylation of chloroplast thioredoxin f is a redox signaling mechanism in plants. *Proc. Natl. Acad. Sci. U. S. A.* **102**, 16478-16483 (2005).

153. Wang, W. *et al.* Reversible silencing of CFTR chloride channels by glutathionylation. *J. Gen. Physiol.* **125**, 127-141 (2005).

154. Demasi, M. *et al.* Oligomerization of the cysteinyl-rich oligopeptidase EP24.15 is triggered by S-glutathionylation. *Free Radic. Biol. Med.* **44**, 1180-1190 (2008).

155. DalleDonne, I., Milzani, A. & Colombo, R. The tert-butyl hydroperoxide-induced oxidation of actin Cys-374 is coupled with structural changes in distant regions of the protein. *Biochemistry* **38**, 12471-12480 (1999).

156. Dalle-Donne, I., Giustarini, D., Rossi, R., Colombo, R. & Milzani, A. Reversible S-glutathionylation of Cys 374 regulates actin filament formation by inducing structural changes in the actin molecule. *Free Radic. Biol. Med.* **34**, 23-32 (2003).

157. Wang, J. *et al.* Reversible glutathionylation regulates actin polymerization in A431 cells. *J. Biol. Chem.* **276**, 47763-47766 (2001).

158. Fiaschi, T. *et al.* Redox regulation of beta-actin during integrin-mediated cell adhesion. *J. Biol. Chem.* **281**, 22983-22991 (2006).

159. Zhang, Q. & Kelly, J. W. Cys10 mixed disulfides make transthyretin more amyloidogenic under mildly acidic conditions. *Biochemistry* **42**, 8756-8761 (2003).

160. Forloni, G. *et al.* Protein misfolding in Alzheimer's and Parkinson's disease: genetics and molecular mechanisms. *Neurobiol. Aging* **23**, 957-976 (2002).

161. Zhang, Q. & Kelly, J. W. Cys-10 mixed disulfide modifications exacerbate transthyretin familial variant amyloidogenicity: a likely explanation for variable clinical expression of amyloidosis and the lack of pathology in C10S/V30M transgenic mice? *Biochemistry* **44**, 9079-9085 (2005).

162. Monteiro, G., Horta, B. B., Pimenta, D. C., Augusto, O. & Netto, L. E. Reduction of 1-Cys peroxiredoxins by ascorbate changes the thiol-specific antioxidant paradigm, revealing another function of vitamin C. *Proc. Natl. Acad. Sci. U. S. A.* **104**, 4886-4891 (2007).

163. Lim, J. C. *et al.* Irreversible oxidation of the active-site cysteine of peroxiredoxin to cysteine sulfonic acid for enhanced molecular chaperone activity. *J. Biol. Chem.* **283**, 28873-28880 (2008).

164. Rhee, S. G., Chae, H. Z. & Kim, K. Peroxiredoxins: a historical overview and speculative preview of novel mechanisms and emerging concepts in cell signaling. *Free Radic. Biol. Med.* **38**, 1543-1552 (2005).

165. Wood, Z. A., Schroder, E., Robin Harris, J. & Poole, L. B. Structure, mechanism and regulation of peroxiredoxins. *Trends Biochem. Sci.* **28**, 32-40 (2003).

166. Yang, K. S. *et al.* Inactivation of human peroxiredoxin I during catalysis as the result of the oxidation of the catalytic site cysteine to cysteine-sulfinic acid. *J. Biol. Chem.* **277**, 38029-38036 (2002).

167. Parsonage, D. *et al.* Analysis of the link between enzymatic activity and oligomeric state in AhpC, a bacterial peroxiredoxin. *Biochemistry* **44**, 10583-10592 (2005).

168. Wood, Z. A., Poole, L. B., Hantgan, R. R. & Karplus, P. A. Dimers to doughnuts: redox-sensitive oligomerization of 2-cysteine peroxiredoxins. *Biochemistry* **41**, 5493-5504 (2002).

169. Wagner, E. *et al.* A method for detection of overoxidation of cysteines: peroxiredoxins are oxidized in vivo at the active-site cysteine during oxidative stress. *Biochem. J.* **366**, 777-785 (2002).

170. Rabilloud, T. *et al.* Proteomics analysis of cellular response to oxidative stress. Evidence for in vivo overoxidation of peroxiredoxins at their active site. *J. Biol. Chem.* **277**, 19396-19401 (2002).

171. Chae, H. Z., Uhm, T. B. & Rhee, S. G. Dimerization of thiol-specific antioxidant and the essential role of cysteine 47. *Proc. Natl. Acad. Sci. U. S. A.* **91**, 7022-7026 (1994).

172. Chae, H. Z., Chung, S. J. & Rhee, S. G. Thioredoxin-dependent peroxide reductase from yeast. *J. Biol. Chem.* **269**, 27670-27678 (1994).

173. Seo, M. S. *et al.* Identification of a new type of mammalian peroxiredoxin that forms an intramolecular disulfide as a reaction intermediate. *J. Biol. Chem.* **275**, 20346-20354 (2000).

174. Declercq, J. P. *et al.* Crystal structure of human peroxiredoxin 5, a novel type of mammalian peroxiredoxin at 1.5 A resolution. *J. Mol. Biol.* **311**, 751-759 (2001).

175. Choi, H. J., Kang, S. W., Yang, C. H., Rhee, S. G. & Ryu, S. E. Crystal structure of a novel human peroxidase enzyme at 2.0 A resolution. *Nat. Struct. Biol.* **5**, 400-406 (1998).

176. Kleinman, W. A. *et al*. Protein glutathiolation in human blood. *Biochem. Pharmacol.* **65**, 741-746 (2003).

177. Bursell, S. E. & King, G. L. The potential use of glutathionyl hemoglobin as a clinical marker of oxidative stress. *Clin. Chem.* **46**, 145-146 (2000).

178. Garel, M. C. *et al*. Covalent binding of glutathione to hemoglobin. I. Inhibition of hemoglobin S polymerization. *J. Biol. Chem.* **261**, 14704-14709 (1986).

179. Craescu, C. T. *et al*. Covalent binding of glutathione to hemoglobin. II. Functional consequences and structural changes reflected in NMR spectra. *J. Biol. Chem.* **261**, 14710-14716 (1986).

180. Piemonte, F. *et al*. Glutathione in blood of patients with Friedreich's ataxia. *Eur. J. Clin. Invest.* **31**, 1007-1011 (2001).

181. Niwa, T., Naito, C., Mawjood, A. H. & Imai, K. Increased glutathionyl hemoglobin in diabetes mellitus and hyperlipidemia demonstrated by liquid chromatography/electrospray ionization-mass spectrometry. *Clin. Chem.* **46**, 82-88 (2000).

182. Muscat, J. E. *et al*. Enhanced protein glutathiolation and oxidative stress in cigarette smokers. *Free Radic. Biol. Med.* **36**, 464-470 (2004).

183. Giustarini, D. *et al*. Protein glutathionylation in erythrocytes. *Clin. Chem.* **49**, 327-330 (2003).

184. Lou, M. F. Thiol regulation in the lens. *J. Ocul. Pharmacol. Ther.* **16**, 137-148 (2000).

185. Lou, M. F. Redox regulation in the lens. *Prog. Retin. Eye Res.* **22**, 657-682 (2003).

186. Ghezzi, P. *et al*. Protein glutathionylation: coupling and uncoupling of glutathione to protein thiol groups in lymphocytes under oxidative stress and HIV infection. *Mol. Immunol.* **38**, 773-780 (2002).

187. Herzenberg, L. A. *et al*. Glutathione deficiency is associated with impaired survival in HIV disease. *Proc. Natl. Acad. Sci. U. S. A.* **94**, 1967-1972 (1997).

188. Dinoto, L., Deture, M. A. & Purich, D. L. Structural insights into Alzheimer filament assembly pathways based on site-directed mutagenesis and S-

glutathionylation of three-repeat neuronal Tau protein. *Microsc. Res. Tech.* **67**, 156-163 (2005).

189. Soto, C. Alzheimer's and prion disease as disorders of protein conformation: implications for the design of novel therapeutic approaches. *J. Mol. Med.* **77**, 412-418 (1999).

190. Chau, M. F. *et al.* The microtubule-associated protein tau cross-links to two distinct sites on each alpha and beta tubulin monomer via separate domains. *Biochemistry* **37**, 17692-17703 (1998).

191. Barghorn, S. *et al.* Structure, microtubule interactions, and paired helical filament aggregation by tau mutants of frontotemporal dementias. *Biochemistry* **39**, 11714-11721 (2000).

192. Aksenov, M. Y. & Markesbery, W. R. Changes in thiol content and expression of glutathione redox system genes in the hippocampus and cerebellum in Alzheimer's disease. *Neurosci. Lett.* **302**, 141-145 (2001).

193. Nakajima, H. *et al.* The active site cysteine of the proapoptotic protein glyceraldehyde-3-phosphate dehydrogenase is essential in oxidative stress-induced aggregation and cell death. *J. Biol. Chem.* **282**, 26562-26574 (2007).

194. Ishii, T. & Uchida, K. Induction of reversible cysteine-targeted protein oxidation by an endogenous electrophile 15-deoxy-delta12,14-prostaglandin J2. *Chem. Res. Toxicol.* **17,** 1313-1322 (2004).

195. Newman, S. F. *et al.* An increase in S-glutathionylated proteins in the Alzheimer's disease inferior parietal lobule, a proteomics approach. *J. Neurosci. Res.* **85**, 1506-1514 (2007).

196. Yano, H., Kuroda, S. & Buchanan, B. B. Disulfide proteome in the analysis of protein function and structure. *Proteomics* **2**, 1090-1096 (2002).

197. Sitia, R. & Molteni, S. N. Stress, protein (mis)folding, and signaling: the redox connection. *Sci. STKE* **2004**, pe27 (2004).

198. Mazzola, J. L. & Sirover, M. A. Subcellular alteration of glyceraldehyde-3-phosphate dehydrogenase in Alzheimer's disease fibroblasts. *J. Neurosci. Res.* **71**, 279-285 (2003).

199. Tsuchiya, K. *et al.* Pro-apoptotic protein glyceraldehyde-3-phosphate dehydrogenase promotes the formation of Lewy body-like inclusions. *Eur. J. Neurosci.* **21**, 317-326 (2005).

200. Senatorov, V. V., Charles, V., Reddy, P. H., Tagle, D. A. & Chuang, D. M. Overexpression and nuclear accumulation of glyceraldehyde-3-phosphate dehydrogenase in a transgenic mouse model of Huntington's disease. *Mol. Cell. Neurosci.* **22**, 285-297 (2003).

201. Sawa, A., Khan, A. A., Hester, L. D. & Snyder, S. H. Glyceraldehyde-3-phosphate dehydrogenase: nuclear translocation participates in neuronal and nonneuronal cell death. *Proc. Natl. Acad. Sci. U. S. A.* **94**, 11669-11674 (1997).

202. Cumming, R. C. *et al.* Protein disulfide bond formation in the cytoplasm during oxidative stress. *J. Biol. Chem.* **279**, 21749-21758 (2004).

203. Motohashi, K., Kondoh, A., Stumpp, M. T. & Hisabori, T. Comprehensive survey of proteins targeted by chloroplast thioredoxin. *Proc. Natl. Acad. Sci. U. S. A.* **98**, 11224-11229 (2001).

204. Shevchenko, A., Wilm, M., Vorm, O. & Mann, M. Mass spectrometric sequencing of proteins silver-stained polyacrylamide gels. *Anal. Chem.* **68**, 850-858 (1996).

205. Dooley, C. T. *et al.* Imaging dynamic redox changes in mammalian cells with green fluorescent protein indicators. *J. Biol. Chem.* **279**, 22284-22293 (2004).

206. Hanson, G. T. *et al.* Investigating mitochondrial redox potential with redox-sensitive green fluorescent protein indicators. *J. Biol. Chem.* **279**, 13044-13053 (2004).

207. Hayes, J. D. & Pulford, D. J. The glutathione S-transferase supergene family: regulation of GST and the contribution of the isoenzymes to cancer chemoprotection and drug resistance. *Crit. Rev. Biochem. Mol. Biol.* **30**, 445-600 (1995).

208. Bai, J. & Cederbaum, A. I. Mitochondrial catalase and oxidative injury. *Biol. Signals Recept.* **10**, 189-199 (2001).

209. Morel, F. *et al.* Gene and protein characterization of the human glutathione S-transferase kappa and evidence for a peroxisomal localization. *J. Biol. Chem.* **279**, 16246-16253 (2004).

210. Carolan, B. J. *et al.* Disparate oxidant gene expression of airway epithelium compared to alveolar macrophages in smokers. *Respir. Res.* **10**, 111 (2009).

211. Giles, N. M., Giles, G. I. & Jacob, C. Multiple roles of cysteine in biocatalysis. *Biochem. Biophys. Res. Commun.* **300**, 1-4 (2003).

212. Linke, K. & Jakob, U. Not every disulfide lasts forever: disulfide bond formation as a redox switch. *Antioxid. Redox Signal.* **5**, 425-434 (2003).

213. Xia, K. *et al*. Identifying the subproteome of kinetically stable proteins via diagonal 2D SDS/PAGE. *Proc. Natl. Acad. Sci. U. S. A.* **104**, 17329-17334 (2007).

214. Lindahl, M. & Florencio, F. J. Thioredoxin-linked processes in cyanobacteria are as numerous as in chloroplasts, but targets are different. *Proc. Natl. Acad. Sci. U. S. A.* **100**, 16107-16112 (2003).

215. Winger, A. M., Taylor, N. L., Heazlewood, J. L., Day, D. A. & Millar, A. H. Identification of intra- and intermolecular disulphide bonding in the plant mitochondrial proteome by diagonal gel electrophoresis. *Proteomics* **7**, 4158-4170 (2007).

216. Brennan, J. P. *et al*. Detection and mapping of widespread intermolecular protein disulfide formation during cardiac oxidative stress using proteomics with diagonal electrophoresis. *J. Biol. Chem.* **279**, 41352-41360 (2004).

217. Cumming, R. C. Analysis of global and specific changes in the disulfide proteome using redox two-dimensional polyacrylamide gel electrophoresis. *Methods Mol. Biol.* **476**, 160-174 (2009).

218. Samelson, L. E. Diagonal gel electrophoresis. *Curr. Protoc. Immunol.* **Chapter 8**, Unit 8.6 (2001).

219. McDonagh, B. Diagonal electrophoresis for detection of protein disulphide bridges. *Methods Mol. Biol.* **519**, 305-310 (2009).

220. Dinkova-Kostova, A. T. *et al*. Direct evidence that sulfhydryl groups of Keap1 are the sensors regulating induction of phase 2 enzymes that protect against carcinogens and oxidants. *Proc. Natl. Acad. Sci. U. S. A.* **99**, 11908-11913 (2002).

221. McMahon, M., Itoh, K., Yamamoto, M. & Hayes, J. D. Keap1-dependent proteasomal degradation of transcription factor Nrf2 contributes to the negative regulation of antioxidant response element-driven gene expression. *J. Biol. Chem.* **278**, 21592-21600 (2003).

222. He, X., Chen, M. G., Lin, G. X. & Ma, Q. Arsenic induces NAD(P)H-quinone oxidoreductase I by disrupting the Nrf2 x Keap1 x Cul3 complex and recruiting Nrf2 x Maf to the antioxidant response element enhancer. *J. Biol. Chem.* **281**, 23620-23631 (2006).

223. Wang, H. Q. *et al*. TNF-related apoptosis-inducing ligand suppresses PRDX4 expression. *FEBS Lett.* **583**, 1511-1515 (2009).

224. Brixius, K. *et al*. Isoform-specific downregulation of peroxiredoxin in human failing myocardium. *Life Sci.* **81**, 823-831 (2007).

225. Clapham, D. E. Calcium signaling. *Cell* **80**, 259-268 (1995).

226. Geraldes, P. *et al.* Selective regulation of heme oxygenase-1 expression and function by insulin through IRS1/phosphoinositide 3-kinase/Akt-2 pathway. *J. Biol. Chem.* **283**, 34327-34336 (2008).

227. Lee, C. J., Lee, S. S., Chen, S. C., Ho, F. M. & Lin, W. W. Oregonin inhibits lipopolysaccharide-induced iNOS gene transcription and upregulates HO-1 expression in macrophages and microglia. *Br. J. Pharmacol.* **146**, 378-388 (2005).

228. Immenschuh, S. & Ramadori, G. Gene regulation of heme oxygenase-1 as a therapeutic target. *Biochem. Pharmacol.* **60**, 1121-1128 (2000).

229. Vijayan, V., Mueller, S., Baumgart-Vogt, E. & Immenschuh, S. Heme oxygenase-1 as a therapeutic target in inflammatory disorders of the gastrointestinal tract. *World J. Gastroenterol.* **16**, 3112-3119 (2010).

230. Takahashi, K., Nakayama, M., Takeda, K., Fujia, H. & Shibahara, S. Suppression of heme oxygenase-1 mRNA expression by interferon-gamma in human glioblastoma cells. *J. Neurochem.* **72**, 2356-2361 (1999).

231. Schriner, S. E. *et al.* Extension of murine life span by overexpression of catalase targeted to mitochondria. *Science* **308**, 1909-1911 (2005).

232. Yu, L. *et al.* Autophagic programmed cell death by selective catalase degradation. *Proc. Natl. Acad. Sci. U. S. A.* **103**, 4952-4957 (2006).

233. Ogawa, F. *et al.* The repair enzyme peptide methionine-S-sulfoxide reductase is expressed in human epidermis and upregulated by UVA radiation. *J. Invest. Dermatol.* **126**, 1128-1134 (2006).

234. Kil, I. S. & Park, J. W. Regulation of mitochondrial NADP+-dependent isocitrate dehydrogenase activity by glutathionylation. *J. Biol. Chem.* **280**, 10846-10854 (2005).

235. Xiao, Z., Prieto, D., Conrads, T. P., Veenstra, T. D. & Issaq, H. J. Proteomic patterns: their potential for disease diagnosis. *Mol. Cell. Endocrinol.* **230**, 95-106 (2005).

236. Wulfkuhle, J. D., Liotta, L. A. & Petricoin, E. F. Proteomic applications for the early detection of cancer. *Nat. Rev. Cancer.* **3**, 267-275 (2003).

237. Prevodnik, A. *et al.* Oxidative stress in response to xenobiotics in the blue mussel Mytilus edulis L.: evidence for variation along a natural salinity gradient of the Baltic Sea. *Aquat. Toxicol.* **82**, 63-71 (2007).

238. Cho, C. S. *et al*. Irreversible inactivation of glutathione peroxidase 1 and reversible inactivation of peroxiredoxin II by H2O2 in red blood cells. *Antioxid. Redox Signal.* **12**, 1235-1246 (2010).

239. Reifschneider, N. H. *et al*. Defining the mitochondrial proteomes from five rat organs in a physiologically significant context using 2D blue-native/SDS-PAGE. *J. Proteome Res.* **5**, 1117-1132 (2006).

240. Hu, J., Dong, L. & Outten, C. E. The redox environment in the mitochondrial intermembrane space is maintained separately from the cytosol and matrix. *J. Biol. Chem.* **283**, 29126-29134 (2008).

241. Ghezzi, P. & Bonetto, V. Redox proteomics: identification of oxidatively modified proteins. *Proteomics* **3**, 1145-1153 (2003).

242. Peters, T.,Jr & Reed, R. G. The biosynthesis of rat serum albumin. Composition and properties of the intracellular precursor, proalbumin. *J. Biol. Chem.* **255**, 3156-3163 (1980).

243. He, X. M. & Carter, D. C. Atomic structure and chemistry of human serum albumin. *Nature* **358**, 209-215 (1992).

244. Roche, M., Rondeau, P., Singh, N. R., Tarnus, E. & Bourdon, E. The antioxidant properties of serum albumin. *FEBS Lett.* **582**, 1783-1787 (2008).

245. Andersson, L. The heterogeneity of bovine serum albumin. *Biochimica et Biophysica Acta (BBA) - General Subjects* **117**, 115-133 (1966).

246. Beilby, J. P., Chin, C., Garcia-Webb, P. & Bhagat, C. I. An albumin dimer in urine. *Clin. Chem.* **31**, 478-479 (1985).

247. Carballal, S. *et al*. Sulfenic acid formation in human serum albumin by hydrogen peroxide and peroxynitrite. *Biochemistry* **42**, 9906-9914 (2003).

248. Carballal, S. *et al*. Sulfenic acid in human serum albumin. *Amino Acids* **32**, 543-551 (2007).

249. Ogasawara, Y., Namai, T., Togawa, T. & Ishii, K. Formation of albumin dimers induced by exposure to peroxides in human plasma: a possible biomarker for oxidative stress. *Biochem. Biophys. Res. Commun.* **340**, 353-358 (2006).

250. Nguyen, A. *et al*. The pharmacokinetics of an albumin-binding Fab (AB.Fab) can be modulated as a function of affinity for albumin. *Protein Eng. Des. Sel.* **19**, 291-297 (2006).

251. MacGillivray, R. T. *et al*. The complete amino acid sequence of human serum transferrin. *Proc. Natl. Acad. Sci. U. S. A.* **79**, 2504-2508 (1982).

252. Schreiber, G. *et al*. The synthesis and secretion of rat transferrin. *J. Biol. Chem.* **254**, 12013-12019 (1979).

253. Noble, M. E., Endicott, J. A. & Johnson, L. N. Protein kinase inhibitors: insights into drug design from structure. *Science* **303**, 1800-1805 (2004).

254. Chu, F., Koomen, J. M., Kobayashi, R. & O'Brian, C. A. Identification of an inactivating cysteine switch in protein kinase Cepsilon, a rational target for the design of protein kinase Cepsilon-inhibitory cancer therapeutics. *Cancer Res.* **65**, 10478-10485 (2005).

255. Littler, D. R. *et al*. Structure of human protein kinase C eta (PKCeta) C2 domain and identification of phosphorylation sites. *Biochem. Biophys. Res. Commun.* **349**, 1182-1189 (2006). `

256. Wilce, M. C. & Parker, M. W. Structure and function of glutathione S-transferases. *Biochim. Biophys. Acta* **1205**, 1-18 (1994).

257. Yi, L. *et al*. Heme regulatory motifs in heme oxygenase-2 form a thiol/disulfide redox switch that responds to the cellular redox state. *J. Biol. Chem.* **284**, 20556-20561 (2009).

APPENDIX I: COMPOSITION AND SUPPLIERS FOR SOLUTIONS AND REAGENTS

AI.1 Chemicals and Reagents

All solutions and regents were prepared using Milli Q water unless otherwise indicated.

AI.2 Cell Culture, Treatment, and Lysis

- Mouse hepatoma Hepa 1c1c7 line (ATCC No. CRL-2026) generously provided by Dr. O. Hankinson (University of California, Los Angeles, CA).

- Minimum essential medium (Invitrogen, Grand Island, NY) supplemented with 10% FBS (Gibco, Grand Island, NY) (final concentration of 40 µM prepared according to manufacturer's instructions), 20 µM L-glutamine (Gibco, Grand Island, NY), 50 µg/mL gentamycin sulfate (Gibco), 100 IU/mL penicillin (Gibco), 10 µg/mL streptomycin (Gibco, Grand Island, NY), and 25 ng/mL amphotorecin B (ICN Biomedicals, Aurora, OH). Solution was stored at -20 °C prior to use.

- 4 mM UCB: UCB stock solution prepared by dissolving 2.3 mg UCB (Poryphyrin Products, Logan, UT) in 0.2 mL 0.1 N NaOH, followed by adding of 0.8 mL PBS. Solution freshly prepared prior to use.

- 0.5 M Potassium Phosphate (monobasic): 34.02 g potassium phosphate (monobasic) (EMD Science, Gibbstown, NJ) dissolved in 425 mL of water, and adjusted to a final volume of 500 mL with water. Solution stored at 4 °C prior to use.

- 0.5 M Potassium Phosphate (dibasic): 43.54 g potassium phosphate (dibasic) (EMD Science, Gibbstown, NJ) dissolved in 425 mL of water and adjusted to a final volume of 500 mL with water. Solution stored at 4 °C prior to use.

- 0.5 M KP Buffer, ph 7.4: 0.5 M monobasic potassium phosphate was added to 0.5 M dibasic potassium phosphate until a final pH of 7.4 was achieved. Solution stored at 4 °C prior to use.

- 0.01 M Phosphate-Buffered Saline (PBS), pH 7.4: 1 pouch PBS powder (Sigma, St. Louis, MO) dissolved in 1 L water.

- 2.16 M IA Stock: 0.5 g IA (EMD Chemicals, Gibbstown, NJ) dissolved in 1.25 mL water. Solution prepared fresh prior to use.

- 40 mM IA PBS: 925 μL IA stock added to 49.1 mL of PBS. Solution prepared fresh prior to use.

- Lysis Buffer: One protease inhibitor cocktail tablet (Roche Diagnostics, Indianapolis, IN) was added to 7 mL RIPA buffer. Solution stored at -20 °C prior to use.

- 40 mM IA Lysis Buffer: 9.25 μL IA stock solution added to 491 μL of lysis buffer. Solution prepared fresh prior to use.

AI.3 Redox Two-Dimensional Polyacrylamide Gel Electrophoresis (R2D-PAGE)

- 30% Acrylamide (37.5:1): 292 g acrylamide (EMD Chemicals, Gibbstown, NJ) and 8 g N'N'-methylenebisacrylamide (JT Baker, Phillipsburg, NJ) were dissolved in 600 mL water, and final volume was adjusted to 1 L with water. Solution filtered through a paper filter (Whatman, Mobile, Al) with a pore size of 11 μM prior to use to remove any undissolved material, poured in a light resistant container and stored at 4 °C prior to use.

- 1.5M Tris, pH 8.8: 181.5 g tris base (JT Baker) dissolved in 800 mL water, pH adjusted to 8.8 with 6 M HCl and final volume was adjusted to 1 L with water. Solution was stored at 4 °C prior to use.

- 0.5M Tris, pH 6.8: 6.0 g tris base dissolved in 80 mL water, pH adjusted to 6.8 with concentrated HCl and final volume was adjusted to 100 mL with water. Solution was stored at 4 °C prior to use.

- 10% SDS: 10 g SDS (JT Baker) dissolved in 100 mL water, and filtered through a paper filter (Whatman) with a pore size of 11 μM to remove any undissolved material. Solution stored at room temperature prior to use.

- 0.1% SDS: 1 part 10% SDS solution diluted in 99 parts water. Solution stored at room temperature prior to use.

- APS: 1 g APS (BDH, Toronto, ON) dissolved in 10 mL of water. Solution was stored at 4 °C prior to use.

- 10X Running Buffer: 29g Tris, 144 glycine (JT Baker, Phillipsburg, NJ), and 10 g SDS dissolved in 800 mL water, and final volume was adjusted to 1 L with water. Solution was stored at 4 °C prior to use.

- 1X Running Buffer: 1 part 10X running buffer diluted in 9 parts water. Solution prepared fresh prior to use.

- 2X Non-Reducing Sample Buffer: 1.933 g tris base, 8 g SDS, 0.1 g bromophenol blue (Bio-Rad, Hercules, Ca), and 20 mL glycerol (BDH, Toronto, ON) were dissolved in 120 mL water, pH adjusted to 6.8 with 6 M HCl and made to a final volume of 200 mL with water. Solution was filtered prior to use through a paper filter (Whatman),

with a pore size of 11 μM to remove any undissolved material and stored at -20 °C prior to use.

- 2X Sample Buffer: 1.933 g tris base, 8 g SDS, 0.1 g bromophenol blue (Bio-Rad), and 20 mL glycerol (BDH) were dissolved in 120 mL water, pH adjusted to 6.8 with 6 M HCl and made to a final volume of 190 mL with water. Solution was filtered prior to use to remove any undissolved material and stored at -20 °C. Solution prepared fresh prior to use by adding 5 parts β-Mercaptoethanol (Sigma) to 95 parts 2X Non-Reducing SDS Sample buffer.

- Agarose overlay solution: 0.2 g agarose (Bio-Rad) dissolved in 10 mL 1X running buffer. Solution prepared fresh and briefly boiled in microwave prior to use.

- Molecular Weight Marker: 0.25 μL low range silver stain SDS-PAGE Standard Ladder (Bio-Rad) mixed with 2.75 μL 2X SDS Sample Buffer. Sample prepared fresh and boiled for 5 min. prior to use.

- 100 mM DTT: 0.185 g DTT (Sigma) dissolved in 30 mL 2X SDS sample buffer. Sample prepared fresh prior to use.

- 40 mM IA 2X SDS Sample Buffer: 0.222 g IA dissolved in 30 mL 2X SDS Sample Buffer. Solution prepared fresh prior to use.

- 12.5% Gel Mixture: 100 mL of 12.5% gel mixture was prepared by mixing 41.6 mL 30% acrylamide mix, 31.9 mL water, 25 mL 1.5M Tris, pH 8.8, 1 mL 10% SDS solution, 500 μL APS, and 50 μL APS. Solution prepared fresh prior to casting gels.

- 4.0% Gel Mixture: 25 mL of 4% gel mixture was prepared by mixing 1.3 mL 30% acrylamide mix, 6.1 mL water, 2.5 mL 0.5M Tris, pH 6.8, 100 μL 10% SDS solution,

50 μL APS, and 10 μL TEMED (EMD Chemicals, Gibbstown, NJ). Solution prepared fresh prior to casting gels.

AI.4 Silver Staining

- Fixer: 500 mL methanol (EMD Chemicals), 50 mL acetic acid (EMD Chemicals) dissolved in 450 mL of water.

- Wash: 500 mL methanol dissolved 500 mL of water.

- Sensitizer: 0.2 g sodium thiosulphate (EMD Chemicals) dissolved in 1 L water. Solution prepared fresh and chilled on ice prior to use.

- Stain: 2 g silver nitrate (EMD Chemicals) dissolved in 1 L water. Solution prepared fresh and chilled on ice prior to use.

- Developer: 30 g sodium carbonate (EMD Chemicals), 0.5 mL 37% Formaldehyde (VWR, Westchester, PA), and 20 mL of sensitizer solution dissolved in 980 mL of water. Solution prepared fresh and chilled on ice prior to use.

- Stop: 50 mL acetic acid dissolved in 950 mL water.

- Storage: 10 mL acetic acid dissolved in 990 mL water

APPENDIX II: COPYRIGHT PERMISSION FROM PUBLISHER

Available online at: http://www.jbc.org/site/misc/Copyright_Permission.xhtml

These guidelines apply to the reuse of articles, figures, charts and photos in the *Journal of Biological Chemistry*, *Molecular & Cellular Proteomics* and the *Journal of Lipid Research*.

For authors reusing their own material:

Authors need **NOT** contact the journal to obtain rights to reuse their own material. They are automatically granted permission to do the following:

- Reuse the article in print collections of their own writing.
- Present a work orally in its entirety.
- Use an article in a thesis and/or dissertation.
- Reproduce an article for use in the author's courses. (If the author is employed by an academic institution, that institution also may reproduce the article for teaching purposes.)
- Reuse a figure, photo and/or table in future commercial and noncommercial works.
- Post a copy of the paper in PDF that you submitted via BenchPress.
- Only authors who published their papers under the "Author's Choice" option may post the final edited PDFs created by the publisher to their own/departmental/university Web sites.
- All authors may link to the journal site containing the final edited PDFs created by the publisher.

Please note that authors must include the following citation when using material that appeared in an ASBMB journal:

"This research was originally published in Journal Name. Author(s). Title. *Journal Name*. Year; Vol:pp-pp. © the American Society for Biochemistry and Molecular Biology."

For other parties using material for noncommercial use:

Other parties are welcome to copy, distribute, transmit and adapt the work — at no cost and without permission — for noncommercial use as long as they attribute the work to the original source using the citation above.

Examples of noncommercial use include:

- Reproducing a figure for educational purposes, such as schoolwork or lecture presentations, with attribution.
- Appending a reprinted article to a Ph.D. dissertation, with attribution.